Heterogeneous Cellular Networks With Energy and Spectral Efficient Techniques

Akbar, Sunila

Awarding institution:
King's College London

HETEROGENEOUS CELLULAR NETWORKS WITH ENERGY AND SPECTRAL EFFICIENT TECHNIQUES

SUNILA AKBAR

DOCTOR OF PHILOSOPHY

DEPARTMENT OF INFORMATICS
KING'S COLLEGE LONDON

2018

Acknowledgements

After thanking the Almighty "Allah" for blessing me with the strength to complete my doctoral studies, I would like to thank my supervisor Prof. Arumugam Nallanathan for the amazing opportunity he provided me with. His flexibility, encouragement, and dedication have pushed me far beyond my expectations. Thank you Sir, for everything; your knowledge, insightful guidance, unique perspective on novel research directions, and long lasting experience are irreplaceable assets for me.

My heartfelt thanks to Dr. Yansha Deng for her helpful advice and useful guidance related to my research. Her scientific inputs have helped me to overcome the difficulties of my research. She never hesitate to share great ideas and invaluable experiences with me.

In addition, I deeply appreciate Dr. Vasilis Friderikos and Dr. Reza Nakhai for their helpful guidance and useful advice during my progression panel meetings. I would also like to thank Prof Hamid Aghvami for always being welcoming to discuss my research. Special thanks to Prof George Karagiannidis and Dr. Maged Elkashlan for healthy criticism and invaluable suggestions that led to significant improvements in this thesis.

I would also like to thank my examiners: Prof. Timothy O'Farrell (The University of Sheffield) and Dr. Yi Ma (University of Surrey), for their invaluable comments and suggestions which have led to significant improvements in the presentation and quality of this thesis.

My stay at King's College would not have been so memorable without my mates at the Centre for Telecommunications Research. I am particularly thankful to Omar, Nasreen, Hessa, Sobhan, Fahad, Syed, Aravindh, Sagar, Hadi, Adnan, Hayder, Shabnam, Mohammed, Nadeem, Maria, Nneka, Firuz, and Sumayyah for all the cooperation and support extended to me.

I gratefully acknowledge Commonwealth Scholarship Commission in the UK, for awarding me the prestigious scholarship to pursue PhD.

Finally, I would like to dedicate this thesis the two most impactful persons in my life, my mother and my son. My mother's unconditional love and support have made me the person I am today. I will never be able to thank her enough for that. I am especially thankful to my son, Ahmed Hassan, for being the ultimate reason for finishing the PhD. Thank you Hassan, for sticking with me through all the good times and bad, and helping to keep me sane.

Table of Contents

Abstract

Owing to the dramatic increase in the smart devices' users in quest of high link capacity, the design of the next generation of wireless networks will necessarily have to consider spectral and energy efficiency as the key pillars. The future wireless heterogeneous cellular networks (HCNs), featuring planned base stations (BSs), overlaid with unplanned micro, pico and femto BSs, can provide substantial gains in throughput and user experience as compared to the conventional homogeneous networks. My research is focusing on developing analytical models for HCNs employing spectrum and energy efficient techinques using tools from stochastic geometry.

The first work is motivated to jointly support energy sustainability and high throughput performance by integrating simultaneous information and wireless power transfer (SWIPT) with HCNs. In this work, a tractable model for joint uplink (UL) and downlink (DL) transmission in a K-tier HCN with SWIPT is developed where the mobile users (MUs) decode information as well as harvest energy in the DL. The harvested energy is then utilized for UL information transmission. The analytical expressions for the DL average received power, the DL and UL outage probabilities and average ergodic rates are derived for the system design. The UL performance of a MU is shown to be improved by increasing the fraction of the DL received power for energy harvesting in the network, whereas the energy efficiency is shown to be improved with the increase in SBSs density.

The second work proposed a K-tier HCNs wherein the macrocell tier comprises half duplex (HD) BSs and the small cell tiers consist of full duplex (FD) BSs. In theory, FD data transmission is capable of doubling the spectral efficiency with the

same amount of energy compared to that of half-duplex (HD) system. The FD communication is considered at the small cell BSs only due to their low-powered nature and ease of deployment. The performance of the proposed HCNs is evaluated in terms of the DL and UL average ergodic rates which is shown to be improved as compared to the conventional HCNs where all tiers operate in HD mode.

An important challenge in HCNs with FD small cells is the decrease in coverage due to the increased interference from simultaneous DL and UL operations on the same band in FD mode. This motivates to consider massive multiuser multiple-input multiple-output (MIMO) at the macrocells, which is a promising wireless communication technology for improved coverage and cell edge performance. In the third work, HCNs with massive MIMO antennas at the macrocell BSs and FD small cell is studied. Since, UL power control further improves the coverage performance of the cell edge MUs and efficiently utilize their battery, distance proportional fractional power control has been considered as well. It is shown that the link reliability and area spectral efficiency of the network can be significantly leveraged by taking advantage of FD small cell BSs density and the number of antennas at the macrocell BSs.

At the end, according to the overall picture of the research conducted, the main conclusions together with some directions for the future work are presented.

List of Tables

List of Figures

List of Abbreviations

4G	Fourth Generation
5G	Fifth Generation
ADC	Analog-to-Digital-Converter
AS	Antenna Switching
AWGN	Additive White Gaussian Noise
BS	Base Station
CCDF	Complementary Cumulative Distribution Function
CSI	Channel State Information
CSIT	Channel State Information at the Transmitter
DSP	Digital Signal Processing
DL	Downlink
EH	Energy Harvesting
ER	Energy Receiver
e.g.	For example
FD	Full Duplex
FDD	Frequency Division Duplexing
HAP	Hybrid Access Point
HCN	Heterogeneous Cellular Network
HD	Half Duplex
HetNet	Heterogeneous Network
HPPP	Homogeneous Poisson Point Process
ID	Information Decoding
i.e.	that is

List of Abbreviations

IntRx	Integrated Receiver
M2M	Machine-to-Machine
MIMO	Multiple-Input Multiple-Output
MRP	Maximum Received Power
MRT	Maximum Ratio Transmission
MU	Mobile User
NBS	Nearest Base Station
PDF	Probability Density Function
PPP	Poisson Point Process
PS	Power Splitting
RF	Radio Frequency
RF-to-DC	Radio-Frequency-to-Direct-Current
RX	Receiver
SINR	Signal-to-Interference-plus-Noise Ratio
SISO	Single-Input Single-Output
SNR	Signal-to-Noise Ratio
SWIPT	Simultaneous Wireless Information and Power Transfer
TDD	Time Division Duplexing
TDMA	Time Division Multiple Access
TS	Time Switching
UL	Uplink
WPCN	Wireless Powered Communication Network
WPT	Wireless Power Transfer
w.r.t.	with respect to
ZFBF	Zero-Forcing Beamforming

List of Notations

$B_{(.)}[.,.]$	Incomplete Beta Function
${}_2F_1[.,.;.;.]$	Gauss Hypergeometric Function
$\Gamma(.)$	Gamma Function
$\gamma(.,.)$	Lower Incomplete Gamma Function
$W_{\lambda,\mu}(.)$	Whittaker Function

Chapter 1

Introduction

The upsurge growth of smart phones, netbooks, tablets, and machine-to-machine (M2M) communication devices along with the increasing popularity of cloud and Web 2.0 multimedia infotainment applications (e.g., Google, YouTube, Facebook) demand the fifth-generation (5G) system to be more spectrum efficient. This exponential growth of data traffic also threatens the rapid escalated energy consumption [7] and the resulting CO2 emissions, which evoke the rise of energy efficient technologies to improve the energy efficiency of wireless networks, and at the same time impose less detrimental effects on the environment [8]. It is estimated that 5G should have 1000 times higher mobile data volume per unit area [9], 10 to 100 times higher typical user data rate and number of connected devices, and 10 times longer battery life for low power devices [10].

To address the above challenges and meet the 5G system requirements, a dramatic change in the design of cellular architecture is needed. To achieve higher network capacity and increased spatial spectrum efficiency, traditional cellular systems are moving towards heterogeneous cellular networks (HCNs). The HCNs boost the network capacity through a better spatial resource reuse [11–13], where several classes of BSs, including microcell base stations (BSs), picocell BSs, and femtocell BSs, are distributed throughout the conventional macrocell network. In HCNs deployments, the overlaid macrocell provides a wide area coverage whereas the small cells are deployed in a more targeted manner to alleviate coverage dead zones, and more importantly, traffic hot zones [14]. In another direction, the advancements in energy harvesting technologies using radio frequency wireless power transfer (RF-WPT) have motivated the researchers to apply these for energy efficient wireless

communication systems [3, 15]. Unlike other harvesting techniques that depend on the environment, radio frequency harvesting can be predictable or on demand, and as such is better suited for supporting quality-of-service-based applications [16]. Alongside the developments, full duplex (FD) communications is widely considered as one of the promising techniques in 5G systems which can double the spectrum efficiency by simultaneous transmission and reception on the same frequency and time resource [4]. Moreover, massive multiple-input multiple-output (MIMO) is envisioned as a key technology for 5G wireless networks where the BSs equipped with hundreds of antennas simultaneously communicate with multiple mobile users (MUs) [17]. Massive MIMO enables fine-grained beamforming towards the MU that results in improved spectral and energy efficiency [18]. The work presented in this thesis develops stochastic geometry based analytical models for HCNs employing state-of-the-art spectrum and/or energy efficient RF-WPT, FD communications, and massive MIMO technologies [1].

This introductory chapter is divided into four sections. The first section provides a background on stochastic geometry modeling of HCNs, RF-WPT with emphasis on simultaneous wireless information and power transfer (SWIPT), FD communications, and massive MIMO. This section also highlights the research motivation of employing these techniques to the proposed network architectures. The second section presents the related works. In Section 1.3, the main contributions of the thesis are discussed. Finally, Section 1.4 presents the thesis organization.

1.1 Background

Stochastic Geometry Modeling of HCNs

A typical HCN utilizing a mix of macro, pico and femtocells is illustrated in Fig. 1.1. An immediate effect of the increasing heterogeneity and uncertainty of

[1] In this thesis, the focus is on evaluating the system performance in terms of spectral efficiency. The HCNs are considered with state-of-the-art technological solutions that promise reasonable power saving i.e., SWIPT and massive multiuser MIMO. Energy efficiency is presented and qunatified for SWIPT based HCNs in Chapter 3.

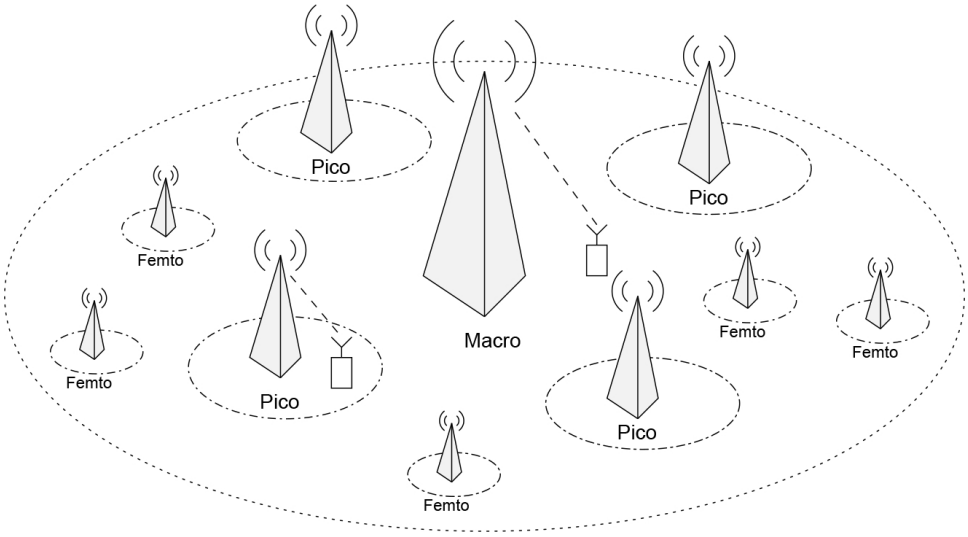

Figure 1.1: Illustration of a three-tier HCN [1].

current deployments on the study of cellular networks is that it has limited the applicability of classical cellular models based mainly on the regularity assumption of BS locations, such as deterministic grid-based models [19] and Wyner model [20], to HCNs. For instance, the hexagonal grid model in Fig. 1.2a is compared with the actual fourth generation (4G) deployment in a sprawling land-locked city in Fig. 1.2b [1]. The actual single tier deployment already deviates significantly from the deterministic grid model. The coverage footprints changes even dramatically with the addition of small cells in single tier network as shown in Fig. 1.3.

A new modeling approach based on stochastic geometry is now widely applied to capture the topological randomness of multi-tier HCNs, which leads to tractable and simple analytical results [21]. In [2], it was shown that the DL coverage probability for the Poisson point process (PPP) model provides a lower bound for the counterpart with actual 4G deployment. In stochastic geometry, the BS locations are modelled by a point process (PP) [22–25], which describes the random spatial patterns formed by points in euclidean space. Then, the analysis is conducted according to the properties of the selected PP. The performance of a specific realization of the cellular network at a specific geographical location is not the point of concern in stochastic geometry

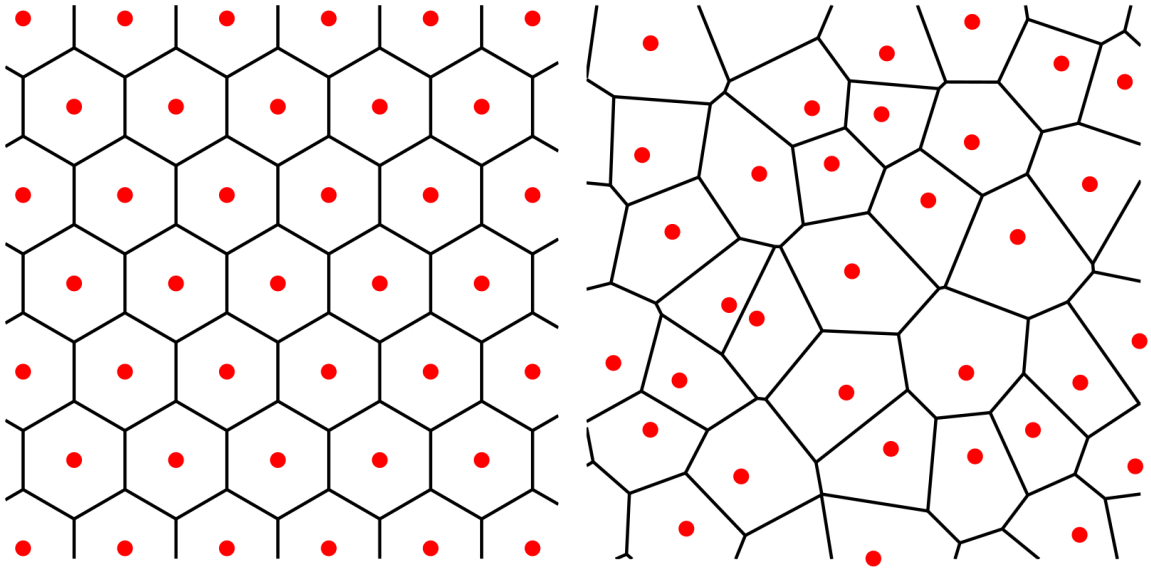

(a) Hexagonal Grid Model (b) Actual 4G Deployment

Figure 1.2: (a) Hexagonal grid model with the locations of macrocell BSs indicated by red circles [1]. (b) Coverage regions with macrocell BS locations drawn from an actual 4G deployment [2].

based analysis, rather, the average performance over all cellular network realizations is evaluated, which is denoted as spatially averaged performance. In this thesis tools from stochastic geometry are used to evaluate the system performance of K-tier HCNs in terms of Coverage/Outage Probability, Average Ergodic Rate, and/or Area Spectral Efficiency (ASE) of the network.

Energy Harvesting by Radio Frequency Wireless Power Transfer

Recently, there has been an upsurge of interest to integrate energy harvesting technologies into communication networks [3, 26–28]. Several studies have considered conventional renewable energy resources, such as solar, wind etc., and have investigated optimal resource allocation techniques for different objective functions and topologies. However, harvesting energy from conventional energy sources (e.g. solar, wind, ambient RF waves etc.) is not stable over time, location, and weather

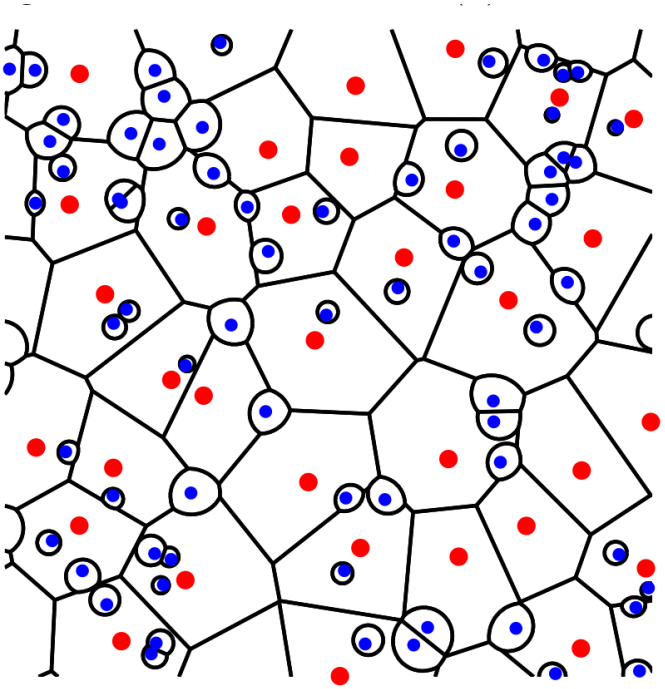

Figure 1.3: Coverage regions in a two tier HCNs with macrocell following the same locations as in Fig. 1.2a, and small cells (denoted by smaller circles) overlaid randomly [1].

conditions, therefore hard to satisfy the power demands of delay constrained wireless applications. Whereas, harvesting energy using wireless power transfer (WPT) provides stable and controllable energy, thus has motivated the researchers to apply it for energy efficient wireless communication systems. WPT can be implemented by three techniques, namely inductive coupling (short range), magnetic resonance coupling (mid range), and radio frequency wireless power transfer (RF-WPT) (long range). The applications of the first two techniques are quite limited, not only in terms of the transfer distance, but also due to the requirement of alignment and calibration of coils at both ends. RF-WPT can avoid these limitations, but comes at the cost of severe propagation loss over long transfer distance. In RF-WPT, the nodes charge their batteries from microwave energy over the air. The recent advances in antenna technologies and hardware production techniques have enabled much higher radio frequency (RF) power to be efficiently transferred to wireless devices.

Simultaneous Information and Power Transfer

With RF-WPT, information could also be concurrently transmitted using the same spectrum [29, 30]. Such a design paradigm is referred to as simultaneous wireless information and power transfer (SWIPT) that enjoys several advantages. First, transmitting information and energy in the same signal is more efficient in spectrum usage than transmitting them in orthogonal time or frequency channels [31]. Second, as compared to the traditional RF-WPT where the transmission of single tone (and its unintended harmonics) can interfere with communication links, SWIPT provides better interference control. Further, SWIPT offers a low cost option for sustainable systems with no requirement to modify hardware at the transmitter side [32].

One practical application of SWIPT is the wireless powered cellular networks (WPCNs) [33]. WPCNs have initiated a paradigm shift in designing cellular networks where the users harvest energy from the downlink (DL) for the uplink (UL) information transmission. In SWIPT based WPCNs, the users decode/transmit information as well as harvest energy in the DL for the UL information transmission. SWIPT thus can be a potential technique for spectrum and energy efficient 5G networks.

Full Duplex Communications

In half-duplex (HD) wireless communications systems, bidirectional communication between a pair of nodes is achieved with either frequency division duplexing (FDD) or time division duplexing (TDD). In FDD different frequency bands are used for the uplink (UL) and downlink (DL), whereas, in TDD, a single channel is shared in the time domain for both UL and DL. Such techniques however are not suitable to fulfil the envisioned requirements of next generation wireless systems [34]. Recently, increasing research has been conducted on FD communication, which allows transmitting and receiving data simultaneously, within the same frequency band [35]. In theory, FD data transmission is capable of doubling

the spectral efficiency of half-duplex (HD) system. However, FD has been previously regarded as hard to be realized in practice due to its high residual self-interference (SI) problem. Fortunately, the recent advances on SI cancellation, such as antenna separation schemes [36, 37], beamforming-based techniques [38–40], and digital circuit domain schemes [41, 42], have demonstrated the feasibility of FD transmission for short to medium range wireless communications.

Massive multiuser MIMO

Massive multiuser MIMO employs a large number of antennas at the BS to exploit the high antenna array gain. The large antenna array improves the throughput by enhancing the received signal power. Another advantage of massive multiuser MIMO lies in its potential to increase energy efficiency compared to a corresponding single-antenna system. It is shown in [4] that each single-antenna user in a massive multiuser MIMO system can scale down its transmit power proportional to the number of antennas at the BS with perfect channel state information (CSI) or to the square root of the number of BS antennas with imperfect CSI, to get the same performance as a corresponding single-input single-output (SISO) system. This leads to higher energy efficiency and is very important for future wireless networks where excessive energy consumption is a growing concern [5], [6]. Moreover, if adequate transmit power is available, then a massive multiuser MIMO system could significantly extend the coverage compared with a single antenna system due to superior interference mitigation [43]. The driving motivation of massive multiuser MIMO is thus to simultaneously and drastically increase data rates, coverage, and overall energy efficiency.

1.2 Related Works and Motivations

1.2.1 Energy Harvesting in WPCNs

Lately, energy harvesting in WPCNs has received considerable attention, where wireless devices harvest energy from the ambient RF signals in the wireless network. The work in [44] proposed *'harvest then transmit'* protocol in single-antenna WPCN, where MUs harvest energy in the DL for transmitting the UL information. The work in [45] studied the energy beamforming design with transmit power control to maximize the UL throughput performance in multi-antenna WPCN. The work in [31] highlighted the potential benefits of SWIPT in resource allocation algorithms and cognitive radio networks. Furthermore, WPCN designs are developed for user cooperation [46], FD network [47], and massive multiuser MIMO system [48].

In [49], RF signal transmitted by primary users was used to power the secondary users in cognitive radio network. In [50], the device to device (D2D) communication was powered by the energy harvested from the concurrent DL transmissions of the macro BSs. In [51], the power beacons (PBs) were deployed in the cellular network to power the MUs for the UL information transmission, but the deployment of dedicated PBs incur additional operation and maintenance costs. In [52], the UL transmission of MUs are powered by the ambient interference. However, it has been mentioned in [53] that harvesting energy from the non-dedicated ambient interference signals could be unstable and unreliable. Applying SWIPT in HCNs can provide stable and reliable energy for MUs by harvesting energy from the dedicated serving BS (similar to PBs), as well as from the DL interference signals at no extra cost. The densification of multi-tier HCNs will reduce the relative distance between BS and MU, which has the potential to fulfill the short range power transfer requirement reported in [53]. As such, the serving BS acts as a dedicated RF energy source, similar to power beacon in [51]. Meanwhile, due to the universal frequency reuse, the typical MU also endures high levels of interference from the nearby interfering BSs. These densely deployed interfering BSs are typically located close to the typical MU, acting as ambient RF

energy source for the MU [54].

A crucial factor in modeling the wireless powered HCNs is cell association which substantially affects the network performance [55]. The UL cell association in wireless powered HCNs has been studied in [53] and [52], where the MUs are powered by the harvested energy from the ambient RF signals. In [56], the UL cell association was based on nearest BS (NBS) cell association, while in [52], it was based on flexible cell association. However, the impact of different cell association schemes on the performance of WPCNs has not been studied in the literature. It is pointed out in [53], there are two types of user association designs for wireless powered HCNs: 1) DL based user association for maximizing the harvested energy, which increases the MUs transmit power; 2) UL based user association for minimizing the uplink path loss, which increases the received signal power at the serving BS [52, 56]. As such, the UL-DL decoupling access studied in [57–59] could be the promising approach to achieve both maximum downlink harvested energy and minimum uplink path-loss, however work is needed to have the concept of decoupled access in 5G. Motivated by these facts the proposed work evaluates the system performance of HCNs with SWIPT where the cell association is based on: 1) NBS and 2) MRP cell associations. The NBS cell association provides the lowest path loss in the UL information transmission, whereas, the conventional maximum received power (MRP) cell association enhances DL wireless power transfer at the MU of being associated with the BS that provides the maximum received power.

1.2.2 FD Communication and multiuser MIMO in Cellular Networks

FD-enabled wireless networks have been attracting growing interest, recently [60]. The performance gains brought by FD transmission in cellular networks have been studied in [61–63]. In [61], the ASE was derived for small cell networks with FD transmission, and the SI was shown to be dominant compared to the aggregate interference. Furthermore, the work in [62] proposed in-band α-duplex scheme in

multi-cell networks with FD operation in each cell, which allows a partial overlap between DL and UL frequency bands. The results in [62] demonstrated that the overlap parameter, α, can be optimized to achieve maximum FD gain. In [63], the cell association problem in multi-tier in-band FD networks was investigated. It is shown that the proposed decoupled cell association, where MUs can be served by different BSs in the UL and DL transmission, outperforms the coupled cell association in which MUs associate to the same BS in both DL and UL.

It has been noted in [64] that the biggest beneficiaries of FD technology might be the networks with relative low transmission power and short communication range [65–67], where the SI is more manageable as compared to the conventional high-power macro counterparts. FD transmission is shown to be a promising technique to improve the spectral efficiency of small cell wireless communications systems in [68]. Furthermore, it has been found in [69] that hybrid-duplex system where each tier operates either in HD or FD mode improves the heterogeneous network throughput. This inspires and motivates to investigate the feasibility and performance gains of FD small cells underlay HCNs, where the macro tier operates in HD mode.

In FD communication systems, each transmission potentially experiences higher interference from within the cell and from neighboring cells compared to the traditional HD cellular systems. The high interference in each direction raises several questions regarding the potential performance of FD operation in a cellular systems. As a consequence, FD systems not only cannot achieve their potential spectral efficiency gain, but can suffer from high outage probability. Mixed multi-cell systems [70–72], where only a given fraction of cells operate in FD mode, have been proposed in order to maintain the interference within a moderate level during FD operations. On the other hand, the work in [69] has shown that operating all BSs in FD or HD achieves higher throughput compared to the mixture of two modes. Besides, multiuser MIMO has been extensively investigated to enhance the spectral efficiency and reduce the interference by utilizing the spatial dimension [73]. The work in [74] presented the coverage probability and area spectral efficiency (ASE)

for the downlink (DL) MU in HCNs with multiuser MIMO using stochastic tools. The work in [74] was extended to [75], which studied the load balancing strategy, which maximizes the coverage probability. Considering HD multiuser MIMO at the macrocells will make up for the increased interference due to FD operation at small cells BSs. The study in Chapter 4 characterize the diverse interference issues due to the FD small cell transmissions, propose a theoretical framework to critically analyze system's performance, and compare with the conventional HCNs with HD SBSs.

1.2.3 Massive Multiuser MIMO and FD Communications in Cellular Networks

Massive multiuser MIMO is presented as one of three contributors to reaching higher spectral efficiencies in 5G systems, the others being advanced interference mitigation and densification using small cells [76]. Several recent studies focus on multiuser MIMO with a large numbers of antennas, where beamforming gains are so large that both intercell and intracell interference can be very low. Spectral efficiency can reach high values, like 100 b/s/Hz [77]. It is shown in [78] that small cell in-band wireless backhaul has the potential to increase the throughput of massive multiuser MIMO systems. The authors in [79] investigated the spectrum and energy efficiency of the massive MIMO-enabled FD cellular networks. In [80], the rate coverage probability of a massive multiuser MIMO-enabled wireless backhaul networks was evaluated, where each SBS can be configured with either in-band or out-of-band FD backhaul mode. In [81], the authors studied the joint in-band backhauling and interference mitigation problem in HCNs, which consists of a massive multiuser MIMO MBS overlaid with self-backhauled small cells. Note that the aforementioned studies have not considered the HCNs with only the SBSs in FD mode for comparatively controlled interference and massive multiuser MIMO at MBSs for boosting the coverage which would otherwise be reduced due to the increase in interference by FD small cells. The inspiration is to integrate the complementary benefits of massive multiuser MIMO and FD techniques in HCNs with massive

multiuser MIMO macro tier overlaid with a FD small cells. Massive multiuser MIMO MBSs not only ensure link reliability, but also reduce the radiated power, while FD SBSs fulfils the fast growing data demands.

Increasing the number of FD SBSs in HCNs to increase the overall throughput comes at the cost of a drop in coverage, as discussed in Section 1.2.2. It would be interesting to explore the trade-off between rate coverage probability and ASE of the HCNs, where massive multiuser MIMO are employed at the MBSs to compensate for the coverage reduction that results due to the increase in interference by FD SBSs with. The aim is to find the proportion of FD SBSs and number of massive multiuser antennas at MBSs such that some given constraints in terms of ASE or, alternatively, of coverage, can be met. The trade-off between the ASE and the link reliability was discussed in wireless ad-hoc networks [82–84]. In these networks, increasing the density of transmitters affects both link reliability and ASE, therefore the trade-off between them is essential to balance both aspects. The trade-off between the ASE and the coverage probability has been studied in massive multiuser MIMO HCNs [85] and a mixed multi-cell system composed of FD and HD small cells [72]. Most of the existing works investigated the ASE of FD networks while the coverage reduction is not taken into account.

Moreover, transmit power control in wireless cellular networks is used for the management of interference, energy, and connectivity. Fast UL power control has been an especially important feature in code division multiple access (CDMA) based networks [86–88]. The work on the use of power control in modern orthogonal frequency division multiple access (OFDMA) based networks has focused on evaluating performance of different power control algorithms for a given set of system parameters via intensive simulations [89, 90]. However, these studies utilize the standard regular hexagonal model for BS locations and the results are produced via simulation, which limits the scope to a limited set of possible design parameters. The works in [91, 92] modeled UL cellular networks with power control using tools from stochastic geometry. [91] derived UL coverage probability for a randomly chosen

MU with fractional power control, provided system design guidelines comparing DL and UL coverage, and evaluated transmit power utilization as a function of the power control parameters. They provided the tradeoff between using fractional power control to benefit cell-edge users and reducing overall power utilization by mobiles. In [92], the truncated channel inversion power control model accounted for limited transmit power of the MUs, per MU power control, and cutoff threshold for the power control. Motivated by the aforementioned studies, employing UL power control in the proposed HCNs in with FD SBSs in Chapter 5 can attain desirable coverage both in the DL and the UL by tuning the UL power control factor, where an increase in the UL power control factor increases the useful signal power at the serving SBS as well as the interference at other BSs and MUs.

1.3 Research Contents and Contributions

1.3.1 SWIPT in K-tier HCNs

In Chapter 3, a tractable model for joint DL and UL transmission of K-tier HCNs with SWIPT is developed for efficient spectrum and energy utilization. In the DL, the MUs with power splitting receiver architecture decode information and harvest energy based on SWIPT. While in the UL, the MUs utilize the harvested energy for information transmission. Since cell association greatly affects the energy harvesting in the DL, and the performance of wireless powered HCNs in the UL, therefore, the DL and the UL performance of a random MU in HCNs with NBS cell association is compared to that with maximum received power (MRP) cell association. The DL average received power for the MU with the NBS and the MRP cell associations is derived first. The system performance is then evaluated in terms of the outage probability and the average ergodic rate in the DL and the UL of a random MU in HCNs with the NBS and the MRP cell associations. The results show that increasing the small cell BS density, the BS transmit power, the time allocation factor, and the energy conversion efficiency, weakly affect the DL and UL performance of both cell

associations. However, the UL performance of both cell associations is shown to be improved by increasing the power splitting factor. Moreover, improvement in the energy efficiency is observed with the increase in SBSs density.

1.3.2 K-tier HCNs with FD Small Cells

In Chapter 4, a tractable model for DL and UL transmission in K-tier HCNs with HD multiuser MIMO at macrocell base stations (MBSs) and FD at small cell base stations (SBSs) is developed for spectrum efficiency. The small cells are a promising candidate for FD technology due to the low transmit power and lower cost for implementation compared with the macrocell counterpart. The analysis explicitly characterized the network interferences generating from the distributed FD SBSs and UL MUs for performance evaluation. To evaluate the spectral efficiency of the network, analytical expressions for the DL and UL average ergodic rate are derived. Numerical results investigate the impact of different parameters on the average ergodic rate in various scenarios. It is shown that applying FD technique at SBSs in HCNs with HD MBSs enhance the average ergodic rate of a random MU, compared to HCNs with HD MBSs and HD SBSs. Moreover, equipping large number of antennas at multiuser MIMO in macrocell enhance the average ergodic rate of a random MU in HCNs. The UL performance is shown to be improved by enhancing the self interference cancellation capability, increasing the density of FD SBSs, or decreasing the transmit power of FD SBSs.

1.3.3 Massive multiuser MIMO in K-tier HCNs with FD Small Cells and UL Power Control

In Chapter 5, HCNs with HD massive multiuser MIMO MBSs and FD SBSs is proposed to improve rate coverage and ASE. Employing massive multiuser MIMO at MBSs relax the coverage reduction that results due to the DL and UL interferences as well as the residual loop interference in FD small cells of HCNs. Distance-proportional

fractional power control is employed in the UL, which provides coverage improvement to the cell-edge MUs and efficient utilization of MUs battery. A tractable framework of the proposed system is presented, which allows to derive the expressions for the DL and the UL rate coverage probabilities, and the DL and the UL ASEs. The results revealed that equipping massive number of antennas at MBSs enhances the DL rate coverage probability, whereas increasing FD SBSs increases the DL and the UL ASEs. The results also demonstrate that by tuning the UL fractional power control, a desirable performance in both UL and DL can be achieved.

1.4 Thesis Organization

The remainder of this thesis is organized as follows. Chapter 2 introduces the background knowledge of this thesis. The technical contributions of this thesis are covered from Chapter 3 through 5. Specifically, Chapter 3 studies the DL and UL performance of K-tier HCNs with SWIPT. Exact and approximate expressions for the DL and UL outage probability and average ergodic rate experienced by a typical MU are derived using tools from stochastic geometry. Chapters 4, on another front, proposes FD small cells in K-tier HCNs to enhance the spectral efficiency where multiuser macrocell BSs operate in conventional HD mode. The network interferences generating from the distributed FD SBSs and UL MUs are characterized and the performance is evaluated in terms of the DL and UL average ergodic rates. In Chapter 5, the above model is presented with massive multiuser MIMO at MBSs for the improved coverage, and UL power control is used to enhance the coverage of cell edge MUs. The performance of the DL and the UL transmission of the HCNs is evaluated in terms of rate coverage probability and ASE. Finally the thesis is concluded and some interesting directions for future studies are pointed out in Chapter 6.

Chapter 2

Fundamental Concepts

This chapter provides the background knowledge for the technical works presented in the rest of the chapters. The basic fading channel characterization is first presented followed by the stochastic geometry modeling of wireless networks for a complete understanding of the technical works in Chapters 3, 4, and 5. The concept of SWIPT is explained in the next section, which is proposed for energy efficient HCNs in Chapter 3. FD Communications, multiuser MIMO, and massive multiuser MIMO are described in the last three sections of this chapter, which lay a solid foundation for the technical works in Chapters 4 and 5.

2.1 Characterization of Fading Channel

A fading channel is a communication channel in wireless communications, where the signal quality degrades from the transmitter to the receiver due to multipath propagation and shadowing. Fading channels are often classified into large scale and small scale fading.

2.1.1 Large Scale Fading

Large scale fading is the signal attenuation due to propagation over large distances and by the diffraction around large objects in the propagation path. Large scale fading is characterized by path loss and shadowing models. In this thesis, we consider only the path loss model since the shadowing is highly dependent on practical environment, such as trees, mountains and large buildings.

Path loss models simplify Maxwell's equations and vary in complexity and

accuracy. In this thesis, simplified path loss model is used which captures the main characteristics of path loss, given as

$$P_r = P_t K \left(\frac{d_0}{d} \right)^{\alpha}, \tag{2.1}$$

where P_r is the received power, P_t is the transmitted power, K is the constant that depends on the antenna characteristics and the free space path loss up to the reference distance d_0 between transmitter and receiver, and d is the distance between the transmitter and receiver.

2.1.2 Small Scale Fading

Small scale fading results from the presence of reflectors and scatterers in the propagation path that cause multiple versions of the transmitted signal to arrive at the receiver, each distorted in amplitude and phase as per the relationship between signal and channel parameters. The small scale fading can be classified into slow fading and fast fading [93] based on the multipath time delay spread [93]. **Coherence time** is defined to understand slow and fast fading, which is the minimum time required for the magnitude change of the signal to become uncorrelated from its previous value. If the symbol time duration is smaller than the coherence time, then we call it the slow fading. Conversely, we call it the fast fading. The slow fading is considered in this thesis where the amplitude and phase change through the propagation channel can be viewed as constant.

Small scale fading is also classified as flat fading and frequency-selective fading based on doppler spread, which depends on the frequency selectivity characteristic of fading channels [93]. **Coherence bandwidth** is defined to understand flat fading and frequency-selective fading, which is the approximate frequency interval over which two frequencies of a signal are likely to experience similar amplitude fading. In flat fading, the bandwidth of transmitted signal is much smaller than the coherence bandwidth, whereas in frequency-selective fading, the bandwidth of transmitted signal is bigger

than the coherence bandwidth.

Several multipath models have been developed to explain the observed statistical nature of a fading channels. In the following, Rayleigh fading and Nakagami-m fading used in this thesis are presented.

2.1.2.1 Rayleigh Fading

Rayleigh fading is a widely used multipath model in scenarios, where the signal may be considered to be scattered between the transmitter and receiver, such as cellular communication in a well built urban environment. It assumes that the magnitude of a signal varies randomly through the propagation according to the Rayleigh distribution [94]. The probability density function (PDF) of the Rayleigh fading channel $|h|^2$ is given by

$$f_{|h^2|}(\rho) = \frac{1}{\bar{\rho}} \exp\left(-\frac{\rho}{\bar{\rho}}\right) \tag{2.2}$$

where $\bar{\rho} = \mathbb{E}\left[|h|^2\right]$.

2.1.2.2 Nakagami-m Fading

Nakagami-m fading is a more general model for characterizing fading channels, which has the verstality in providing a good match to various experimentally obtained data [95]. In Nakagami-m fading, the channel power gain is Gamma distributed with fading severity parameters m, whose PDF is given as

$$f_{|h^2|}(\rho) = \frac{m^m \rho^{m-1}}{\Gamma(m)\bar{\rho}^m} \exp^{-\frac{m\rho}{\bar{\rho}}}, \tag{2.3}$$

where $\bar{\rho} = \mathbb{E}\left[|h|^2\right]$ and $\Gamma()$ is the Gamma function.

2.2 Stochastic Geometry Tools for Wireless Communications

Stochastic geometry allows to study the average behaviour over many spatial realizations of a network, where nodes follow specific probability distribution [96]. Lately, there has been growing interest in stochastic geometry to model different types of wireless networks, characterize their operation, and understand their behaviour [97]. In large-scale networks, where there exists high uncertainty on the locations and channels of wireless terminals, the stochastic geometry provides a simple and tractable approach to study the network behaviour. In some special cases, stochastic geometry based analysis can lead to closed-form expressions of the performance metrics of the system. These expressions enable the understanding of network operation and provide insights for the system design, which are often difficult to get from computationally intensive simulations. In the following, some basic concepts from stochastic geometry are introduced.

2.2.1 Point Processes

A point process (PP) is defined as a random collection of points residing in a measure space, which is the Euclidean space $\mathbb{R}^d$ for cellular networks [98]. It is mathematically defined as

$$\Phi = \{\mathbf{X}_i, i \in \mathbb{N}\} \tag{2.4}$$

where $\mathbf{X}_i$ is the random variable. Another way of defining point process is in terms of random counting measures, where the number of points falling in any set $\mathcal{S} \subset \mathbb{R}^2$ are counted, given as under

$$\Psi(\mathcal{S}) = \sum_{\mathbf{X}_i \in \Phi} \mathbb{1}(\mathbf{X}_i \in \mathcal{S}) \tag{2.5}$$

where $\Psi(\mathcal{S})$ is a random variable whose distribution depends upon Φ. In stochastic geometry based network analysis, the network is abstracted to a point process (PP), where the points represent the nodes located in a large geographical area. A matching PP is selected to model the positions of the nodes according to the network properties. Some of the important statistical measures of the PP are defined in the following.

Expectation Measure

Expectation measure is the mean of $\Psi(\mathcal{S})$ given as

$$\mu(\mathcal{S}) = \mathbb{E}[\Psi(\mathcal{S})] \tag{2.6}$$

Probability Generating functional PGFL

The PGFL of the PP with respect to (w.r.t.) a function f is defined as the mean of the product of the function's values at each point of the PP [98]

$$\mathcal{P}_{\Phi}(f) = \mathbb{E}\Big[\prod_{\mathbf{X}_i \in \Phi} f(\mathbf{X}_i)\Big] \tag{2.7}$$

In stochastic geometry based wireless network analysis, the PGFL is generally used to evaluate the Laplace transform of a interference I, which is usually an intermediate step in the characterization of signal-to-interference-plus-noise-ratio (SINR). The interference signal can be expressed as

$$I = \sum_{\mathbf{X}_i \in \Phi} g(\mathbf{X}_i) \tag{2.8}$$

where $g(\mathbf{X}_i)$ is the function that represents the interference signals from the interfering nodes of the network. In this case, its Laplace transform can be calculated as

$$\mathcal{L}_I(s) = \mathbb{E}\Bigg[\exp\Bigg(-\sum_{\mathbf{X}_i \in \Phi} s g(\mathbf{X}_i)\Bigg)\Bigg] = \mathbb{E}\Bigg[\prod_{\mathbf{X}_i \in \Phi} e^{-s g(\mathbf{X}_i)}\Bigg] \tag{2.9}$$

2.2.2 Poisson Point Processes

A Poisson point process (PPP) with expectation measure $\mu(.)$ is characterized by the following conditions

- If $\Psi(\mathcal{S})$ is Poisson distributed with mean $\mu(\mathcal{S})$ for every set $\mathcal{S}$.
- The random variables $\Psi(\mathcal{S}_1), ..., \Psi(\mathcal{S}_m)$ are independent for any m disjoint sets $\mathcal{S}_1, ..., \mathcal{S}_m$.

In this thesis, *homogeneous* Poisson point prcess (HPPP) is considered, which is a PPP with uniform intensity λ such that

$$\mu(\mathcal{S}) = \lambda \ell(\mathcal{S}) \tag{2.10}$$

where $\ell(\mathcal{S})$ is a Lebesgue measure (i.e. size) of $\mathcal{S}$. An important characteristic of of a HPPP is that conditioned on the number of points in $\mathcal{S}$, all the points are independently and uniformly distributed in $\mathcal{S}$. In the following, some important properties and statistical measures of HPPP are presented.

Campbell's Theorem

Campbell's theorem provides a key tool to convert a sum into a integral, therefore can be used to compute the expectation of a random variable of the interference signal I of the form (2.8). It states that

$$\mathbb{E}[I] = \mathbb{E}\left[\sum_{\mathbf{X}_i \in \Phi} f(\mathbf{X}_i)\right] = \int_{\mathbb{R}^d} \lambda f(\mathbf{x}) d\mathbf{x} \tag{2.11}$$

PGFL of a HPPP

The PGFL of a HPPP is used to convert an expectation of a product of the points in the PPP into a integral. It states that

$$\mathcal{P}_{\Phi}(f) = \mathbb{E}\left[\prod_{\mathbf{X}_i \in \Phi} f(\mathbf{X}_i)\right] = \exp\left(-\lambda \int_{\mathbb{R}^d} (1 - f(\mathbf{x}))d\mathbf{x}\right) \tag{2.12}$$

The Laplace transform of the interference signal (2.8) can be evaluated using PGFL.

Slivnyak's Theorem

Slivnyak's theorem states that for a PPP Φ, conditioning on a point at $\mathbf{x}$ does not change the distribution of the rest of the process because of the independence between all of the points of the PPP. Slivnyaks theorem is useful because it allows to add a point to the PPP at any feasible location, such as the origin or at a fixed distance from the origin, without changing its statistical properties

2.3 SWIPT

Recent advances in *rectennas* (rectifying antennas) for efficient radio-frequency-to-direct-current (RF-to-DC) conversion have enabled much higher RF power to be efficiently transferred and harvested by wireless devices. Besides, information could also be jointly transmitted with energy via the same waveform using SWIPT, which has shown to be more efficient in spectrum usage than transmitting information and energy separately in orthogonal waveforms [99, 100].

2.3.1 Rate Energy Trade-off

A practical SWIPT system involves rate-energy trade-off in both the transmitter and receiver designs to achieve balanced EH and ID performance. In Fig. 2.1, a SWIPT network with a multi-antenna hybrid access point (HAP) is shown that

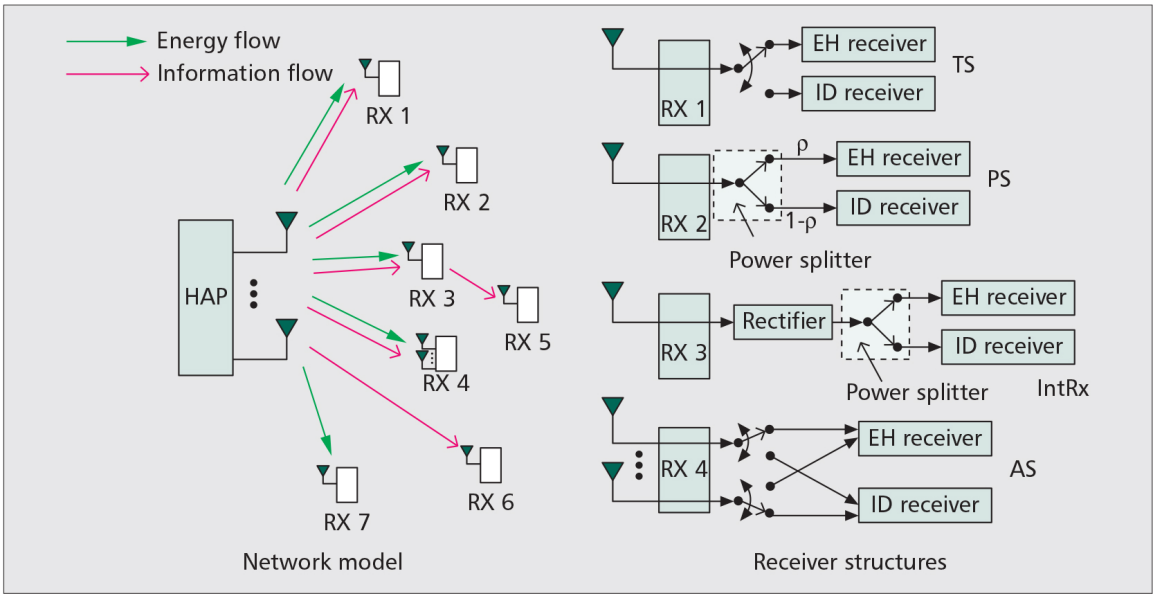

Figure 2.1: A SWIPT network model and practical receiver structures [3].

jointly transmits energy and information to multiple receivers, some of which only harvest energy or receive information, while some do both simultaneously. EH receivers are generally closer to the transmitter than ID receivers due to the different power sensitivities (e.g. -10 dBm for EH receivers vs. -60 dBm for ID receivers). The optimal waveforms for the information and energy transfer are fundamentally different, therefore the waveform design at the transmitter side need to follow a rate-energy trade-off for the balanced performance of SWIPT in terms of EH and ID.

2.3.2 Practical Receiver Structures

Fig. 2.1 illustrates some practical receiver structures, namely, time switching (TS), power splitting (PS), integrated ID/EH receiver (IntRx), and antenna switching (AS) [3].

Time Switching

The TS receiver architecture is shown as Rx 1 in Fig. 2.1, where the receiving antenna switches its operation periodically between the receive antenna for energy

harvesting (EH) and that for information decoding (ID) within each time slot. The time duration of energy/information transfer can be tuned to achieve different rate-energy trade-offs.

Power Splitting

The PS receiver architecture is shown as Rx 2 in Fig. 2.1, where the received signal at each antenna is split into two separate streams according to a power ratio $0 \leq \rho \leq 1$, where ρ times the received power is sent to the EH receiver and the other $(1-\rho)$ times the received power to the ID receiver. Adjusting ρ results in different rate-energy trade-offs.

Integrated Receiver

The IntRx receiver architecture is shown as Rx 3 in Fig. 2.1, where the RF front ends of the EH and ID receivers are combined, and the signal first converts into direct current (DC) and then splits into two streams for EH and ID. IntRx is superior than PS/TS receivers when more harvested energy is required, because active frequency down conversion is not performed [100].

Antenna Switching

The AS receiver architecture is shown as Rx 4 in Fig. 2.1, where the receiving antennas are divided into two groups with one group switched to ID and the other group to EH. It can be regarded as a special case of PS with ρ is being zero or one at each receiving antenna.

2.4 Power Consumption in SWIPT System

The power consumption of the SWIPT based OFDMA system with power splitting receiver architecture is formulated in [].

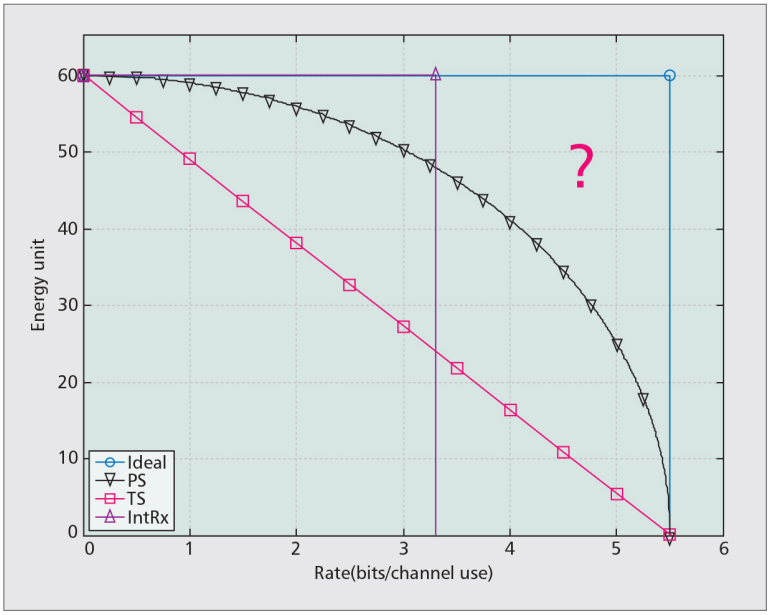

Figure 2.2: Comparison of rate-energy trade-offs of SWIPT receivers [3].

$$P_{consump.} = P_{C_T} + P_{C_R} + \epsilon P_t - \underbrace{P_{\mathrm{t}} \left| h_{b_{\widehat{k}} u_0} \right|^2 L_0 \left(\max \left\{ \left\| \boldsymbol{x}_{b_{\widehat{k}}, u_0} \right\|, d \right\} \right)^{-\ell_k}}_{I_{b_{\widehat{k}}}}$$
$$- \underbrace{\sum_{j=1}^{K} \sum_{b_j \in \Phi_j \setminus b_{\widehat{k}}} P_{\mathrm{t}, b_j} \left| h_{b_j u_0} \right|^2 L_0 \left(\max \left\{ \left\| \boldsymbol{x}_{b_j u_0} \right\|, d \right\} \right)^{-\ell_j}}_{I_{b_x}} \tag{2.13}$$

The comparisons of rate-energy trade-offs of SWIPT receivers in a point-to-point additive white Gaussian noise (AWGN) channel is shown in Fig. 2.2 [3]. The rate-energy region of the ideal receiver is a box. Similar is the observation for IntRx structure, where major amount of DC current is used for EH in contrast to ID as an optimal design. PS receiver is observed to have a strictly larger rate-energy region as compared to TS receiver. In Chapter 3, PS receiver is considered for SWIPT in HCNs.

2.5 FD Communications

In FD wireless communications, a device can transmit and receive signals wirelessly at the same time and in the same frequency band. The key challenge to implement FD communication is the large power difference between the self-interference created locally by a device's own wireless transmissions and the received signal of interest coming from a distant transmitting antenna. Recently, there has been tremendous progress towards SI cancellation techniques to achieve FD in both industry and academia.

2.5.1 SI Cancellation

There are several approaches to SI reduction for FD nodes, which can broadly classified into: wireless-propagation domain, analog-circuit domain, and digital domain approaches [4].

2.5.1.1 Wireless-Propagation Domain

In wireless-propagation domain cancellation techniques, the transmit chain is electromagnetically isolated from the receive chain, i.e., the self-interference is suppressed before it is reflected in the receive chain circuitry. Generally, this is accomplished by some combination of antenna directionality, cross-polarization, and transmit beamforming. The advantage of propagation domain is that the downstream receiver hardware does not need to process signals in detail with a large dynamic range.

2.5.1.2 Analog-Circuit Domain

In analog-circuit domain cancellation schemes, a copy of transmitted signal from a suitable location of the transmitter is tapped and subtracted (after proper gain, phase, and delay adjustment) from each receive antenna feed. Tapping the outgoing signal close to the antennas captures the presence of analog-domain non-idealities

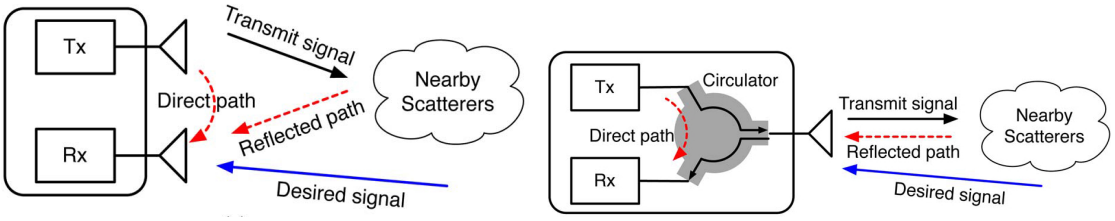

(a) Separate-Antenna Architecture. (b) Shared-Antenna Architecture.

Figure 2.3: Full Duplex Antenna Architectures [4].

e.g., oscillator phase-noise and amplifier distortion, whereas tapping the transmit signal in digital-domain, for subsequent use in analog-domain cancellation, facilitates sophisticated adaptive digital signal processing (DSP) techniques to reflected-path self-interference.

2.5.1.3 Digital Domain

In digital domain cancellation methods, the SI is cancelled after the analog-to-digital-converter (ADC) by applying sophisticated digital signal processing (DSP) techniques to the received signal, which makes the processing relatively easy. However, due to the fact that the ADCs dynamic-range limits the amount of SI reduction that is possible, a sufficient amount of the SI suppression must first be applied using the propagation-domain and/or analog-circuit-domain methods before the ADC.

2.5.2 FD Antenna Architectures

FD transmission can be realized at the access points through separated or shared antenna configurations [64].

2.5.2.1 Separate-Antenna

In the separate-antenna architecture, there is dedicated radiating antenna for transmission and dedicated sensing antenna for reception. Natural isolation between transmission and reception can be achieved from the sheer physical distance of the

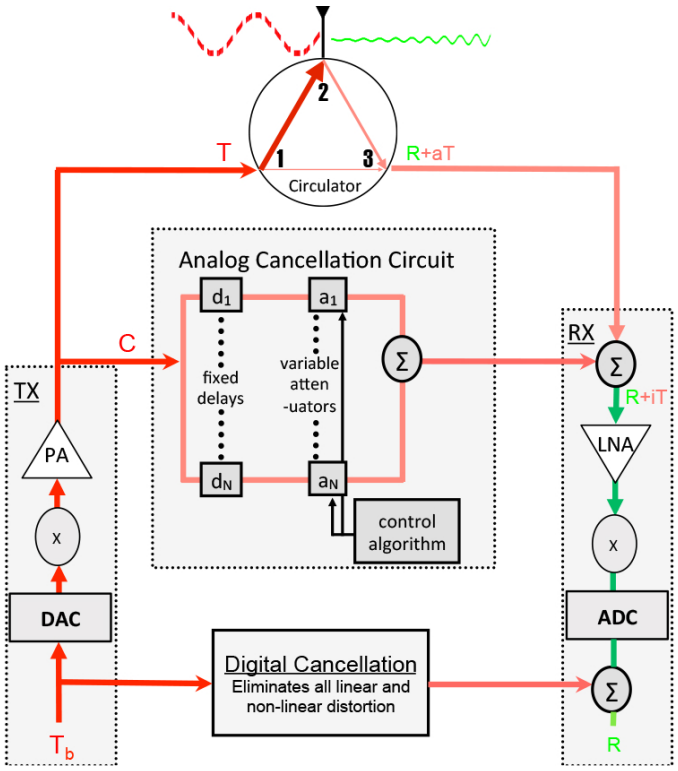

Figure 2.4: Block Diagram of Hybrid Analog and Digital SI Cancellation Design of FD Radio [5]. T (red) is the transmitting signal, R (green) is the intended receive signal.

antenna sets [101]. The advantage of separated antenna deployment is its relatively easy implementation, specifically for the large devices.

2.5.2.2 Shared-Antenna

In shared-antenna deployment, only one antenna set is used for both transmission and reception simultaneously. The received and transmitted signal are separated with the help of a circulator, which routes the transmitted signal from the transmitter to the shared-antenna and the received signal from the antenna to the receiver.

In terms of antenna usage, the efficiency of the shared-antenna configuration is higher than that of the separated one [102]. Besides, the shared-antenna configuration is a promising alternative for separated-antenna configuration in short range communications, where the transmit power is low and the antenna isolation

requirement is less rigorous compared with medium to long range communication [102]. Accordingly, in Chapter 4 and 5, shared-antenna architecture is assumed.

2.5.3 FD Design Example

Fig. 2.4 shows the block diagram of hybrid analog and digital SI cancellation design of FD radio, which can achieve 110 dB of cancellation and eliminates SI to the noise floor [5]. A single antenna is connected at port 2 of a 3 port device that provides limited isolation between port 1 and port 3 while letting signals pass through consecutive ports. The transmit signal is fed through port 1, which routes it to the antenna connected to port 2, while the received signal from the antenna is passed from port 2 through to port 3. The circulator cannot completely isolate port 1 and port 3, therefore the transmit signal leaks from port 1 to port 3 and causes interference to the received signal. The proposed analog cancellation circuit in [5] is trying to recreate a signal that matches the leaked interference signal for cancellation, where the transmit chain is tapped just before it goes to the circulator to obtain a small copy of the transmitted signal. The copy of the signal is then passed through a circuit which consists of parallel fixed lines of varying delays (essentially wires of different lengths) and tunable attenuators. The lines are then collected back and added up, and this combined signal is then subtracted from the signal on the receive path. In effect, the circuit is providing copies of the transmitted signal delayed by different fixed amounts and programmatically attenuated by different variable amounts so that the self-interference cancellation be maximized. In essence, the cancellation is viewed as a sampling and interpolation problem. The actual self-interference signal has a particular delay and amplitude that depends on the delay **d** and attenuation **a** through the circulator. The results have shown that the fixed delays in the cancellation circuit in Fig. 2.4 should be picked such that they straddle the delay of the self-interference signal through the circulator. In practice it is hard to know the precise value of **d** since it is a function of how the circuit is connected, but the range over which it varies can always be found and the fixed delays

outside of that range could be placed on either side. The digital cancellation stage eliminates any residual self interference. Assuming that analog cancellation provides 60dB, digital cancellation has to cancel the linear main signal component by another 50dB and non-linear components by another 20dB. The linear component consists of the main transmitted signal that is leaking over through the circulator after analog cancellation, as well as any delayed reflections of this signal from the environment, whereas the nonlinear component are created because radio circuits can take in an input signal x and create outputs that contain non-linear cubic and higher order terms such as x^3, x^5. These higher order signal terms have significant frequency content at frequencies close to the transmitted frequencies. In contrast to cancelling linear components, canceling nonlinear components calls for extra resources such as hardware, pilot overhead, and/ or computational complexity.

In summary, FD radio designs requires RF circuit and system design for anolog SI cancellation and digital signal processing for residual SI cancellation. The SI cancellation cannot be solved in any one domain alone, the solution requires understanding trade-offs in both the domains and architecting it appropriately which results in higher signalling overheads. In the foreseeable future, it is unlikely that mobile nodes are equipped with FD radios due to the cost and complexity of SI cancellation techniques. Considering this limitation, a typical deployment scenario will be the FD transmission between a FD BS and legacy HD nodes, where the BS assigns a subchannel to two different nodes, one for UL and the other for DL.

2.6 Multiple Antenna System

Multiple antennas equipped at the transmitter/receiver improves the wireless system performance by exploiting the spatial domain and utilizing the multipath effect [103–107]. In wireless communication systems, the diversity and signal-to-noise ratio (SNR) gains are achieved with multiple antennas as compared with the single antenna [108, 109]. The **diversity gain** is the increase in reliability by combining multiple received copies of transmitted signal. The **SNR gain** is the increase in

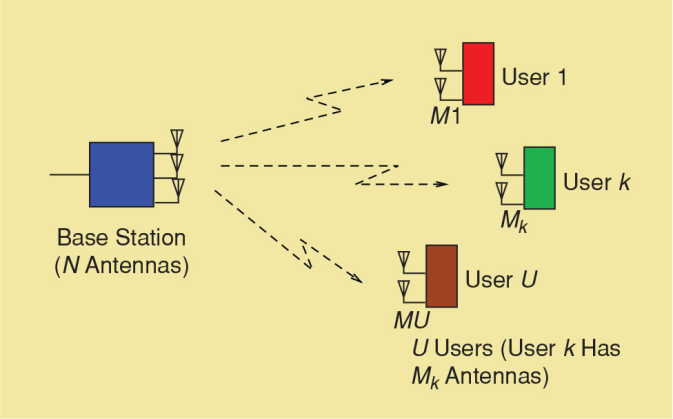

Figure 2.5: DL model of a multiuser MIMO network [6].

average received SNR by coherently combining the incoming/outgoing signals.

2.6.1 Multiuser MIMO

Multiuser MIMO has become an integral part of communications standards, such as 802.11 (WiFi), 802.16 (WiMAX), LTE, and is progressively being deployed throughout the world [110]. It allows multiple users to simultaneously access the same channel using the spatial degrees of freedom offered by MIMO, thereby enhances the system capacity. In spatial multiple access, the resulting multiuser interference is handled by the multiple antennas which in addition to providing per link diversity also give the degrees of freedom necessary for spatial separation of the users. Basic configuration of downlink multiuser MIMO systems is depicted in Fig. 2.5. The advantages of multiuser MIMO come at the cost of more expensive signal processing, the most substantial is to acquire channel state information at transmitter (CSIT) to properly serve the spatially multiplexed users [6].

The precoding algorithms for multiuser MIMO systems can be sub-divided into linear and nonlinear precoding, with nonlinear being the capacity achieving algorithms but are complex. The linear precoding approaches usually achieve reasonable performance with much lower complexity. Linear precoding techniques include maximum ratio transmission (MRT) [111] and zero-forcing beamforming

(ZFBF) [112]. Beamforming technique can focus energy toward a receiver by controlling the amplitude and phase of each antenna. In the following, ZFBF technique used for multiuser MIMO in Chapter 4 and massive multiuser MIMO in Chapter 5 of this thesis is presented.

Zero-forcing Beamforming

Zero-forcing precoding is a method of spatial signal processing by which the multiple antenna transmitter can nullify the multiuser interference signals. Instead of omnidirectional antennas where energy is sent in all directions, beamforming technique can focus energy toward users by controlling the amplitude and phase of each antenna. For a multiuser MIMO channel with N transmit antennas and M single antenna users, the signal before transmission is multiplied by a beamforming vector as

$$\mathbf{x}_{b_i,u_m^i} = \sum_{m=1}^{M} \frac{\hat{\mathbf{g}}_{b_i,u_m}}{\|\hat{\mathbf{g}}_{b_i,u_m}\|} s_{b_i,u_m^i}, \tag{2.14}$$

where $\hat{\mathbf{g}}_{b_i,u_m}$ is the estimate of the channel vector from the ith BS to mth user based on channel state information at the transmitter (CSIT) and $s_{b_i,u_m^i}, \mathbb{E}|s_{b_i,u_m^i}|^2 = 1$ is the source symbol for the mth user from the ith BS. Accordingly, the SNR at the typical m^*th user associated to the i^*th BS is given as

$$\text{SNR} = \frac{\frac{P}{M}\beta d_{b_{i^*},u_{m^*}^{i^*}}^{-\alpha} |\mathbf{g}_{b_{i^*},u_{m^*}^{i^*}} \mathbf{x}_{b_{i^*},u_{m^*}^{i^*}}|^2}{N_0}, \tag{2.15}$$

where P is the transmit power of the BS, β is the frequency dependant constant value, d is the distance between the m^*th user and the i^*th BS, $\mathbf{g}_{b_{i^*},u_{m^*}^{i^*}}$ is the respective channel vector, and $\mathbf{x}_{b_{i^*},u_{m^*}^{i^*}}$ is given in (2.14).

2.7 Massive multiuser MIMO

To achieve more dramatic gains as well as to simplify the required signal processing, massive multiuser MIMO systems have been proposed in [113, 114], where each BS is equipped with very large number of antennas, e.g., 100 or more. By equipping a BS with a large number of antennas, the effects of uncorrelated noise and small-scale fading are eliminated, the number of users per cell are independent of the size of the cell, and the required transmitted energy per bit vanishes. Furthermore, these benefits can be achieved by using simple linear signal processing approaches, such as matched filter (MF) precoding/detection in massive multiuser MIMO systems. For channel estimation, TDD mode is usually preferable with massive MIMO systems due to the high overhead and complexity associated with channel estimation under FDD mode. In TDD based massive MIMO transmission systems, pilot sequences are transmitted from users in the UL to estimate channels. There are many schemes for assigning pilot sequences to users in different cells, which should ideally be orthogonal. However, the number of orthogonal pilot sequences with a given period and bandwidth is limited, and the identical pilot sequences assigned to users in neighboring cells will interfere with each other causing pilot contamination. The pilot contamination poses a limit on the achievable rate in a massive MIMO system and several approaches were proposed to tackle that problem [115, 116]. In Chapter 5, no pilot contamination is assumed and perfect CSI is available at the BSs and the MUs.

Chapter 3

SWIPT in K-tier HCNs

3.1 Introduction

SWIPT has recently drawn significant interests for its dual use of radio signals to provide wireless data and energy access at the same time. In this chapter, a tractable model is developed for joint DL and UL transmission of K-tier HCNs with SWIPT to jointly support energy sustainability and high throughput performance in cellular networks. SWIPT is used in the DL transmission of HCNs where the MUs with no built-in power supply harvest energy and decode information. The MUs then utilize the harvested energy for information transmission in the UL. Since cell association greatly affects the energy harvesting in the DL and the performance of wireless powered HCNs in the UL, the DL and the UL performance of a random MU in HCNs with NBS cell association is compared to that with MRP cell association. The DL average received power for the MU with the NBS and the MRP cell associations is derived first and then the system performance is evaluated in terms of the outage probability and the average ergodic rate in the DL and the UL of a random MU in HCNs with the NBS and the MRP cell associations.

The remainder of the chapter is organized as follows. The system model of SWIPT in HCNs is presented in Section 3.2. In Section 3.3, the DL average received powers for the NBS and the MRP cell associations are derived. The network performance is then evaluated in terms of the DL and the UL outage probabilities, and the DL and the UL average ergodic rates for the NBS and the MRP cell association

in Section 3.4. Finally, the numerical results are discussed in Section 3.5 before the work is summarized in Section 3.6.

3.2 System Model

In this chapter, a conventional HCNs model is considered with K tiers of BSs spatially distributed in $\mathbb{R}^2$ as a HPPP Φ_j with spatial density λ_j, BS transmit power P_{t,b_j}, and path loss exponent ℓ_{j}, where $j = 1, \cdots, K$ is the index of the jth tier. The MUs are also modeled as an independent HPPP Φ_{u} with density λ_{u}. The MUs are assumed to have large storage battery which eliminates the randomness of instantaneous received power and provides fixed transmit power [51]. The jth tier BS and jth tier MU as are denoted as b_j, and u_j, respectively. The index of the tier with which a typical MU is associated is denoted as '$k \in \{1, \cdots, K\}$', and $b_{\widehat{k}}$ is the typical serving BS in the kth tier.

The channel path loss over the distance $\|\boldsymbol{x}\|$ is modelled as $L_0\|\boldsymbol{x}\|^{-\ell_j}$, where L_0 is the path loss at a reference distance of 1 m. The Rayleigh fading model with unit mean is considered to capture the random channel fluctuations, and the channel coefficients are assumed to be independent and identically distributed (i.i.d.) across all links. There is no intra-cell interference, where orthogonal multiple access is employed within a cell. The TDD mode is assumed. Furthermore, time division multiple access (TDMA) is considered, where several MUs share the same channel in different time slots, thus the BS transmit power is independent of the density of active MUs.

3.2.1 Transmission Block Structure

The transmission block structure is shown in Fig. 3.1, and the transmission block time is normalized as $T = 1$. A fraction of the block time αT is used for SWIPT, where α $(0 \leq \alpha \leq 1)$ is called the time allocation factor. The remaining portion of time $(1 - \alpha)T$ is used for the UL information transmission, which is powered by the

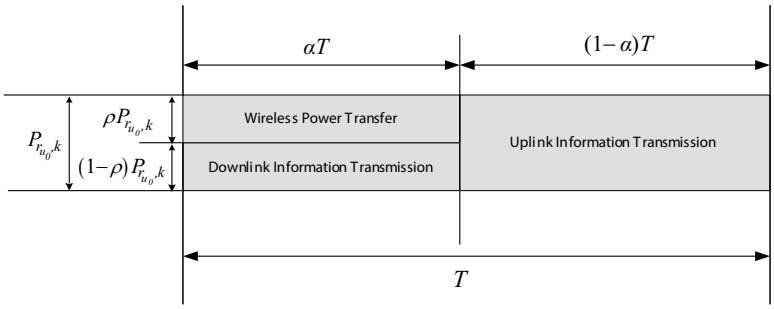

Figure 3.1: Transmission Frame Structure

energy harvested from the first αT time.

In the DL, the receiver with power splitting architecture splits the received signal for energy harvesting and information decoding. The DL received power at the typical user in the kth tier is assumed as $P_{\mathrm{r_{u_0,k}}}$, a fraction of which $\rho P_{\mathrm{r_{u_0,k}}}$ is used for energy harvesting, where ρ $(0 \leq \rho \leq 1)$ is called the power splitting factor. The remaining fraction of the received power $(1-\rho)P_{\mathrm{r_{u_0,k}}}$ is used for information decoding.

3.2.2 Cell Association

To ensure low path loss in the UL, the NBS cell association is considered. For a typical MU u_0 located at the origin, the location of the serving nearest BS in the kth tier, $\boldsymbol{x}_{b_{\widehat{k}}}$ is given as

$$\boldsymbol{x}_{b_{\widehat{k}}}\Big|_{\mathrm{NBS}} = \underset{\{\boldsymbol{x}\in\Phi_j\}_{j=1,\cdots,K}}{\operatorname{argmin}} \|\boldsymbol{x}\|, \tag{3.1}$$

where $\|\boldsymbol{x}\|$ denotes the Euclidean distance between a BS to the typical MU.

The performance of HCNs with the NBS cell association is compared to that with the MRP cell association. In the MRP cell asociation, the MU connects to the BS which offers the maximum (long term averaged) received power to the MU, i.e., small scale fading is ignored, as in [117]. For a typical MU u_0 located at the origin, the location of the serving BS in the kth tier that offers the maximum received power

to the typical MU, $\boldsymbol{x}_{b_{\widehat{k}}}$ is given as

$$\boldsymbol{x}_{b_{\widehat{k}}}\big|_{\mathrm{MRP}} = \underset{\{\boldsymbol{x}\in\boldsymbol{x}_{b_{\widehat{j}}}|_{\mathrm{MRP}}\}_{j=1,\cdots,K}}{\operatorname{argmax}} P_{\mathrm{t},b_j}\|\boldsymbol{x}\|^{-\ell_j}. \tag{3.2}$$

In (3.2), $\boldsymbol{x}_{b_{\widehat{j}}}$ represents the location of the BS in the jth tier that offers the maximum received power to the typical MU, given as

$$\boldsymbol{x}_{b_{\widehat{j}}}\big|_{\mathrm{MRP}} = \underset{\{\boldsymbol{x}\in\Phi_j\}_{j=1,\cdots,K}}{\operatorname{argmax}} P_{\mathrm{t},b_j}\|\boldsymbol{x}\|^{-\ell_j}, \tag{3.3}$$

where Φ_j denotes the position sets of BSs in the jth tier.

In the UL information transmission, the typical MU transmits information to the same serving BS of the HCN as in the current cellular networks [55].

3.2.3 Wireless Power Transfer

A short range propagation model [118] is used for wireless power transfer to avoid the singularity caused by proximity between BSs and MUs i.e., to ensure that the power received at the MU is finite [51]. The received power of a typical MU that is associated to the BS in the kth tier can be written as

$$P_{\mathrm{r}_{\mathrm{u}_0,\mathrm{k}}} = \underbrace{P_{\mathrm{t},b_{\widehat{k}}}\big|h_{b_{\widehat{k}}u_0}\big|^2 L_0\big(\max\big\{\big\|\boldsymbol{x}_{b_{\widehat{k}},u_0}\big\|,d\big\}\big)^{-\ell_k}}_{I_{b_{\widehat{k}}}} + \underbrace{\sum_{j=1}^{K}\sum_{b_j\in\Phi_j\setminus b_{\widehat{k}}} P_{\mathrm{t},b_j}\big|h_{b_ju_0}\big|^2 L_0\big(\max\big\{\big\|\boldsymbol{x}_{b_ju_0}\big\|,d\big\}\big)^{-\ell_j}}_{I_{b_x}}, \tag{3.4}$$

where $I_{b_{\widehat{k}}}$ is the useful signal, I_{b_x} is the intercell interference. In (3.4), $L_0\big(\max\big\{\big\|\boldsymbol{x}_{b_{\widehat{k}},u_0}\big\|,d\big\}\big)^{-\ell_k}$ represents the large scale fading between the jth tier BS to the typical MU, where L_0 is the path loss for a reference distance $r_0 = 1$, which is typically $(4\pi/\nu)^{-2}$, ν is the wavelength, $\big\|\boldsymbol{x}_{b_{\widehat{k}},u_0}\big\|$ is the distance between the serving BS and the typical MU, $d \geq 1$ is a constant used for short range propagation model

as defined above, and ℓ_k is the path loss exponent for the kth tier. In (3.4), $h_{b_{\widehat{k}}u_0}$ is the small-scale fading channel coefficient from the serving BS to the typical MU, which is assumed to be Rayleigh fading with unit mean. All the channels coefficients are assumed to be i.i.d. across all the links and follow an exponential distribution with unit mean. Note that more general fading/shadowing distributions can be accommodated as in [2] and many subsequent papers, but with a loss of tractability and without much change to the results and system design insights [98]. Similarly, $\left\|\boldsymbol{x}_{b_j u_0}\right\|$ is the distance between the jth tier BS and the typical MU and $h_{b_j u_0}$ is the small-scale fading interfering channel coefficient from the jth tier BS to the typical MU.

3.2.4 Downlink Information Transmission

In the DL information transmission, a fraction of the received power $(1-\rho)P_{\mathrm{r}_{\mathrm{u}_0,\mathrm{k}}}$ at the MU is used for information decoding in the αT time.

For the DL analysis, all point processes are shifted such that the typical MU is located at the origin. According to Slivnyak's theorem, the distribution of the shifted HPPPs remain the same as the original HPPPs with the same intensities [23]. The signal-to-interference-plus-noise ratio (SINR) of the DL information transmission is given by

$$SINR_k^{DL} = \frac{(1-\rho)\, P_{\mathrm{t},b_{\widehat{k}}} \left|h_{b_{\widehat{k}}u_0}\right|^2 L_0 \left\|\boldsymbol{x}_{b_{\widehat{k}}u_0}\right\|^{-\ell_k}}{(1-\rho)\sum\limits_{j=1}^{K}\sum\limits_{b_j\in\Phi_j\setminus b_{\widehat{k}}} P_{\mathrm{t},b_j}\left|h_{b_j u_0}\right|^2 L_0 \left\|\boldsymbol{x}_{b_j u_0}\right\|^{-\ell_j} + \sigma^2}, \tag{3.5}$$

where σ^2 is the noise power.

3.2.5 Uplink Information Transmission

In the UL information transmission, the MUs keep associated with the serving BSs that powered them in the first αT time, and use the harvested energy to transmit the UL information in the $(1-\alpha)T$ time.

The MUs are assumed to have large storage so that the randomness of instantaneous received power is suppressed and the large storage provides fixed average received power. The received energy converted into DC for the MU battery in the period αT is defined as $\eta\alpha T\rho\mathbb{E}\{P_{r_{u_0},k}\}$, where $0 < \eta < 1$ is the energy conversion efficiency. Thus, the signal power for UL information transmission in the period $(1-\alpha)T$ is given as $\phi\mathbb{E}\{P_{r_{u_0},k}\}$, where

$$\phi = \frac{\eta\rho\alpha}{(1-\alpha)} \tag{3.6}$$

For the UL analysis, Slivnyak's theorem is used to shift the points of HPPPs such that the serving BS $b_{\widehat{k}}$ is located at the origin. The UL SINR at the serving BS in the kth tier is given by

$$SINR_k^{UL} = \frac{\phi\mathbb{E}\{P_{r_{u_0},k}\}\left|h_{u_0,b_{\widehat{k}}}\right|^2 L_0\left\|\boldsymbol{x}_{u_0,b_{\widehat{k}}}\right\|^{-\ell_k}}{\sum\limits_{j=1}^{K}\sum\limits_{u_j\in\tilde{\Phi}_j\setminus u_0}\phi\mathbb{E}\{P_{r_{u_j},j}\}\left|h_{u_j,b_{\widehat{k}}}\right|^2 L_0\left\|\boldsymbol{x}_{u_j,b_{\widehat{k}}}\right\|^{-\ell_j}+\delta^2}, \tag{3.7}$$

where $h_{u_0,b_{\widehat{k}}}$ is the small-scale fading channel coefficient from the MU to its serving BS, $\left\|\boldsymbol{x}_{u_0,b_{\widehat{k}}}\right\|$ is the distance between the typical MU and the serving BS, $h_{u_j,b_{\widehat{k}}}$ is the small-scale fading interfering channel coefficient from the jth tier MU u_j to the serving BS, $\left\|\boldsymbol{x}_{u_j,b_{\widehat{k}}}\right\|$ is the distance between the jth tier MU and the serving BS, $\tilde{\Phi}_j$ denotes HPPP corresponding to the interfering MUs in the jth tier, δ^2 is the noise power, and ϕ is given in (3.6).

Based on the model defined in Section 3.2, the analytical expression for the average received power in the DL with the NBS and the MRP cell associations is derived first before evaluating the system performance.

3.3 Exact Analysis of Downlink Power Transfer

To determine the UL transmit power of a typical MU in the kth tier, the average received power at the typical MU with the NBS and the MRP cell associations is

derived in Lemma 3.3.1. and Lemma 3.3.2, respectively.

Lemma 3.3.1. *The average received power at the typical MU associated with the BS in the kth tier using NBS cell association is given by*

$$\mathbb{E}\left\{P_{r_{u_0},k}\right\}\big|_{\text{NBS}} = P_{t,b_{\tilde{k}}} L_0 (d^{-\ell_k}\chi_1 + \chi_2) + 2\pi L_0 \sum_{j=1}^{K} P_{t,b_j}\lambda_j \left(\chi_3 - \chi_4 + \chi_5\right), \tag{3.8}$$

where

$$\chi_1 = 1 - \exp\{\kappa d^2\}, \tag{3.9}$$

$$\chi_2 = \kappa^{\ell_k/4} d^{-\ell_k/2} \exp\left\{-\frac{1}{2}\kappa d^2\right\} W_{-\ell_k/2,1/2(1-\ell_k/2)}\left(\kappa d^2\right), \tag{3.10}$$

$$\chi_3 = \frac{\ell_j d^2}{2d^{\ell_j}(\ell_j - 2)}[1 - \exp\{-\kappa x^2\}], \tag{3.11}$$

$$\chi_4 = \frac{1}{2\kappa d^{\ell_j}}\gamma(2,\kappa), \tag{3.12}$$

$$\chi_5 = \frac{\pi\left(\sum_{j=1}^{K}\lambda_j\right)^{(3\ell_j-2)/4}}{\ell_j - 2} d^{-\ell_j/2+1} \exp\left\{-\frac{1}{2}\kappa x^2\right\} W_{(\ell_j-2)/4,\ell_j/4}(\kappa d^2), \tag{3.13}$$

and

$$\kappa = \pi \sum_{j=1}^{K} \lambda_j, \tag{3.14}$$

where $d \geq 1$ is a constant, defined in (3.4)*, $W_{\lambda,\mu}(.)$ is Whittaker function [119], and $\gamma(.,.)$ is lower incomplete gamma function [119].*

Proof. See Appendix A.1. □

Lemma 3.3.2. *The average received power at the typical MU associated with the BS in the kth tier using MRP cell association is given by*

$$\mathbb{E}\left\{P_{r_{u_0},k}\right\}\big|_{\text{MRP}} = \frac{P_{t,b_{\tilde{k}}} L_0}{\Upsilon_k}(d^{-\ell_k}\Xi_1 + \Xi_2) + \frac{2\pi L_0}{\Upsilon_k}\sum_{j=1}^{K} P_{t,b_j}\lambda_j \left(\Xi_3 + (\ell_j - 2)^{-1}\Xi_4\right), \tag{3.15}$$

where

$$\Xi_1 = \int_0^d x \exp\{-\sum_{j=1}^{K} \mu_{k,j} x^{2\ell_k/\ell_j}\} dx, \tag{3.16}$$

$$\Xi_2 = \int_d^{\infty} x^{-(\ell_k-1)} \exp\Big\{ -\sum_{j=1}^{K} \mu_{k,j} x^{2\ell_k/\ell_j} \Big\} dx, \tag{3.17}$$

$$\Xi_3 = \int_0^{\theta_{j,k}} \frac{x}{2d^{\ell_j}} \left(\frac{\ell_j d^2}{(\ell_j - 2)} - (\delta_{j,k}^{DL})^{2/\ell_j} x^{2\ell_k/\ell_j} \right) \exp\Big\{ -\sum_{j=1}^{K} \mu_{k,j} x^{2\ell_k/\ell_j} \Big\} dx, \tag{3.18}$$

$$\Xi_4 = \int_{\theta_{j,k}}^{\infty} \frac{x \exp\Big\{ -\sum\limits_{j=1}^{K} \mu_{k,j} x^{2\ell_k/\ell_j} \Big\}}{\left((\delta_{j,k}^{DL})^{1/\ell_j} x^{\ell_k/\ell_j}\right)^{\ell_j - 2}} dx, \tag{3.19}$$

$$\theta_{j,k} = d^{\ell_j/\ell_k} (\delta_{j,k}^{DL})^{-\ell_k}, \tag{3.20}$$

$$\Upsilon_k = \int_0^{\infty} r \exp\Big\{ -\sum_{j=1}^{K} \mu_{k,j} r^{2\ell_k/\ell_j} \Big\} dr, \tag{3.21}$$

$$\mu_{k,j} = \pi \lambda_j (\delta_{j,k}^{DL})^{2/\ell_j}, \tag{3.22}$$

and

$$\delta_{j,k}^{DL} = P_{\mathrm{t},b_j} / P_{\mathrm{t},b_k}. \tag{3.23}$$

where $d \geq 1$ is a constant, defined in (3.4).

Proof. See Appendix A.2. □

3.4 Performance Evaluations

The performance of the DL and the UL transmission of the HCNs is characterized by the outage probability, average ergodic rate, and energy efficiency.

3.4.1 Downlink Outage Probability

The DL outage probability is the probability that the instantaneous DL data rate of a randomly selected MU in HCNs is less than the target DL data rate. According to the law of total probability, the DL outage probability of a random MU in K-tier HCNs is given by [117]

$$P_{out}^{DL} = \sum_{k=1}^{K} \Lambda_k^{DL} P_{out,k}^{DL}, \tag{3.24}$$

where Λ_k^{DL} is the probability that a typical MU is associated with the kth tier, and $P_{out,k}^{DL}$ is the DL outage probability of the typical MU associated with the kth tier.

In (3.24), the probability that a typical MU is associated to the BS in the kth tier with the NBS cell association is given as [117]

$$\Lambda_k\big|_{\text{NBS}} = \left(1 + \frac{\sum_{j=1,j\neq k}^{K} \lambda_j}{\lambda_k}\right)^{-1}, \tag{3.25}$$

which means that a MU prefers to associate with a tier having higher BS density. Furthermore, the BS density of each tier is the only factor in determining the cell association in the NBS cell association model.

The probability that a typical MU is associated to the BS in the kth tier with the MRP cell association is given as [117]

$$\Lambda_k\big|_{\text{MRP}} = 2\pi\lambda_k \int_0^{\infty} r \exp\Big\{ - \sum_{j=1}^{K} \mu_{k,j} r^{2\ell_k/\ell_j} \Big\} dr, \tag{3.26}$$

where $\mu_{k,j}$ is given in (3.22). The tier association probability with MRP cell association indicates that a MU prefers to connect to a tier with higher BS density and BS transmit power. Moreover, the BS density is observed to be more dominant in determining $\Lambda_k\big|_{\text{MRP}}$ than BS transmit power because $\frac{2}{\ell} < 1(\ell > 2)$ both in practice and in the considered network model.

In (3.24), the DL outage probability for the typical MU at a distance $\left\|\boldsymbol{x}_{b_{\hat{k}},\text{u}_0}\right\|$

from its associated BS is defined using Shannon's channel capacity expression as

$$\begin{aligned} P_{out,k}^{DL}\left(\mathrm{R}_s\right) &= \mathbb{E}_{\left\|\boldsymbol{x}_{b_{\widehat{k}},\mathrm{u}_0}\right\|}\left[\Pr\left(\alpha \ln\left(1+SINR_k^{DL}\left(\left\|\boldsymbol{x}_{b_{\widehat{k}},\mathrm{u}_0}\right\|\right)\right) \leq \mathrm{R}_s\right)\right] \\ &= \mathbb{E}_{\left\|\boldsymbol{x}_{b_{\widehat{k}},\mathrm{u}_0}\right\|}\left[\Pr\left(SINR_k^{DL}\left(\left\|\boldsymbol{x}_{b_{\widehat{k}},\mathrm{u}_0}\right\|\right) \leq \beta\right)\right], \end{aligned} \tag{3.27}$$

where R_s is the rate threshold, and

$$\beta = \mathrm{e}^{\mathrm{R}_s/\alpha} - 1. \tag{3.28}$$

Shannon's channel capacity formula assumes the additive noise is Gaussian and that coded trasmission is employed with codewords drawn from a Gaussian codebook. In (3.27), the formula is extended to include interference as well which should also be Gaussian. Therefore, it is assumed that each transmitter randomly selects its transmitted symbol from a Gaussian constellation with unit variance. Accordingly, the baseband aggregate interference signal is Gaussian conditioned on the PPP, which validates lumping the aggregate interference with the noise term. That is, treating interference as noise, the instantaneous SINR in (3.5) is analogous to the SNR in Shannon's channel capacity theorem.

3.4.1.1 General Case

In this section the general result for the DL outage probability of a typical MU associated with the BS in the kth tier is presented from which the special result for interference-limited case will follow.

Theorem 3.4.1. *The DL outage probability of a typical MU associated with the BS in the kth tier using NBS cell association is derived as*

$$P_{out,k,NBS}^{DL}\left(\mathrm{R}_s\right) = 1 - 2\kappa \int_0^{\infty} x \exp\Big\{ -\sigma^2\beta\Omega_k^{DL}x^{\ell_k} - \sum_{j=1}^{K}\pi\lambda_j\Big(\vartheta_{k,j}+x^2\Big)\Big\}dx, \tag{3.29}$$

where

$$\vartheta_{k,j} = \mho_{k,j}^{2/\ell_j} \int_{\mho_{k,j}^{-2/\ell_j} x^2}^{\infty} \frac{1}{1+z^{\ell_j/2}} dz, \tag{3.30}$$

$$\Omega_k^{DL} = \big((1-\rho) P_{t,b_{\widehat{k}}} L_0\big)^{-1}, \tag{3.31}$$

and

$$\mho_{k,j} = \beta \delta_{j,k}^{DL} x^{\ell_k}, \tag{3.32}$$

where κ, β, and $\delta_{j,k}^{DL}$ are given in (3.14), (3.28), *and* (3.23), *respectively.*

Proof. See Appendix A.3. □

Theorem 3.4.2. *The DL outage probability of a typical MU associated with the BS in the kth tier using MRP cell association is derived as*

$$P_{out,k,MRP}^{DL}(\mathrm{R}_s) = 1 - \frac{1}{\Upsilon_k} \int_0^{\infty} x \exp\Big\{ -\sigma^2 \beta \Omega_k^{DL} x^{\ell_k} - \sum_{j=1}^{K} \pi \lambda_j \Big(\varpi_{k,j} + \big(\delta_{j,k}^{DL}\big)^{2/\ell_j} x^{2\ell_k/\ell_j} \Big) \Big\} dx, \tag{3.33}$$

where

$$\varpi_{k,j} = \mho_{k,j}^{2/\ell_j} \int_{\beta^{-2/\ell_j}}^{\infty} \frac{1}{1+z^{\ell_j/2}} dz, \tag{3.34}$$

Υ_k, β, $\delta_{j,k}^{DL}$, Ω_k^{DL}, and $\mho_{k,j}$ are given in (3.21), (3.28), (3.23), (3.31), *and* (3.32), *respectively.*

Proof. See Appendix A.4. □

3.4.1.2 Interference-Limited Case, Equal Path Loss Exponents $\{\ell_j\} = 4$

In HCNs with high transmit power BSs, the interference dominates the noise. The thermal noise can therefore be neglected in the rest of this section.

Corollary 3.4.1. *With $\{\ell_j\} = 4$ and $\sigma^2 = 0$, the DL outage probability of a typical MU associated with the kth tier using NBS cell association is derived as*

$$P^{DL}_{out,k,NBS}(R_s) = 1 - \frac{\kappa}{\sum\limits_{j=1}^{K} \pi\lambda_j \left(\sqrt{\beta\delta^{DL}_{j,k}} \arctan\left\{\sqrt{\beta\delta^{DL}_{j,k}}\right\} + 1\right)} \tag{3.35}$$

where κ, β, and $\delta^{DL}_{j,k}$ are given in (3.14), (3.28), *and* (3.23), *respectively.*

Corollary 3.4.2. *With $\{\ell_j\} = 4$ and $\sigma^2 = 0$, the DL outage probability of a typical MU associated with the kth tier using MRP cell association is derived as*

$$P^{DL}_{out,k,MRP}(R_s) = 1 - \frac{\sum\limits_{j=1}^{K} \lambda_j \sqrt{\delta^{DL}_{j,k}}}{\sum\limits_{j=1}^{K} \lambda_j \sqrt{\delta^{DL}_{j,k}} \left(\left(\sqrt{\beta} \arctan\left\{\sqrt{\beta}\right\}\right) + 1\right)} \tag{3.36}$$

where β and $\delta^{DL}_{j,k}$ are given in (3.28) *and* (3.23), *respectively.*

The expressions in (3.35) and (3.36) are in closed-form. The DL outage probability in the interference-limited scenario is found to be independent of the power splitting factor ρ. This is due to the fact that the term $(1-\rho)$ in the $SINR^{DL}_k$ expression in (3.5) cancels out with $\sigma^2 = 0$.

3.4.2 Downlink Average Ergodic Rate

The DL average ergodic rate of a K tier HCNs measures the spectral efficiency of HCNs in the DL. The DL average ergodic rate of a random MU in the K-tier HCNs is given by

$$R^{DL} = \sum_{k=1}^{K} \Lambda^{DL}_k R^{DL}_k, \tag{3.37}$$

where R^{DL}_k is the DL average ergodic rate of a typical MU associated with the kth tier and Λ^{UL}_k is given in (3.25) for the NBS cell association, and in (3.26) for the MRP cell association, respectively.

In (3.37), the DL average ergodic rate for a typical MU at a distance $\left\|\boldsymbol{x}_{b_{\widehat{k}},\mathrm{u}_0}\right\|$ from its associated BS in the kth tier is defined as

$$R_k^{DL} = \mathbb{E}_{\left\|\boldsymbol{x}_{b_{\widehat{k}},\mathrm{u}_0}\right\|}\left[\mathbb{E}_{SINR_k^{DL}}\left[\alpha \ln\left(1+SINR_k^{DL}\left(\left\|\boldsymbol{x}_{b_{\widehat{k}},\mathrm{u}_0}\right\|\right)\right)\right]\right]. \tag{3.38}$$

3.4.2.1 General Case

In this section, the general result for the DL average ergodic rate of a typical MU associated with the kth tier is presented followed by the special result for the interference-limited scenario.

Theorem 3.4.3. *The DL average ergodic rate of a typical MU associated with the kth tier using NBS cell association is derived as*

$$\begin{aligned} R_{k,NBS}^{DL} =& 2\kappa \int_0^\infty \int_0^\infty x \exp\Big\{ -\sigma^2(\mathrm{e}^{t/\alpha}-1)\Omega_k^{DL} x^{\ell_k} - \sum_{j=1}^{K} \pi\lambda_j \Big(\left((\mathrm{e}^{t/\alpha}-1)\delta_{j,k}^{DL} x^{\ell_k}\right)^{2/\ell_j} \\ & \int_{\left((\mathrm{e}^{t/\alpha}-1)\delta_{j,k}^{DL} x^{\ell_k}\right)^{-2/\ell_j} x^2}^{\infty} \frac{1}{1+z^{\ell_j/2}} dz - x^2 \Big) \Big\} dt dx, \end{aligned} \tag{3.39}$$

where Ω_k^{DL} and $\delta_{j,k}^{DL}$ are given in (3.31) *and* (3.23)*, respectively.*

Proof. See Appendix A.5. □

Theorem 3.4.4. *The DL average ergodic rate of a typical MU associated with the kth tier using MRP cell association is derived as*

$$\begin{aligned} R_{k,MRP}^{DL} =& \frac{1}{\Upsilon_k} \int_0^\infty \int_0^\infty x \exp\Big\{ -\sigma^2(\mathrm{e}^{t/\alpha}-1)\Omega_k^{DL} x^{\ell_k} - \sum_{j=1}^{K} \pi\lambda_j \Big(\left((\mathrm{e}^{t/\alpha}-1)\delta_{j,k}^{DL} x^{\ell_k}\right)^{2/\ell_j} \\ & \int_{(\mathrm{e}^{t/\alpha}-1)^{-2/\ell_j}}^{\infty} \frac{1}{1+z^{\ell_j/2}} dz + \left(\delta_{j,k}^{DL}\right)^{2/\ell_j} x^{2\ell_k/\ell_j} \Big) \Big\} dt dx, \end{aligned} \tag{3.40}$$

where Ω_k^{DL} and $\delta_{j,k}^{DL}$ are given in (3.31) *and* (3.23)*, respectively.*

Proof. See Appendix A.6. □

3.4.2.2 Interference-Limited Case, Equal Path Loss Exponents $\{\ell_j\} = 4$

In the following, the DL average ergodic rate of a typical MU associated with the kth tier in HCNs is presented for the interference-limited scenario.

Corollary 3.4.3. *With $\{\ell_j\} = 4$ and $\sigma^2 = 0$, the DL average ergodic rate of a typical MU associated with the kth tier using NBS cell association is derived as*

$$R_{k,NBS}^{DL} = \int_0^{\infty} \frac{\kappa}{\sum_{j=1}^{K} \pi\lambda_j \left(\sqrt{\left(\mathrm{e}^{t/\alpha}-1\right)\delta_{j,k}^{DL}} \arctan\left\{\sqrt{\left(\mathrm{e}^{t/\alpha}-1\right)\delta_{j,k}^{DL}}\right\} + 1\right)} dt, \quad (3.41)$$

where κ and $\delta_{j,k}^{DL}$ are given in (3.14) *and* (3.23)*, respectively.*

Corollary 3.4.4. *With $\{\ell_j\} = 4$ and $\sigma^2 = 0$, the DL average ergodic rate of a typical MU associated with the kth tier using MRP cell associations is derived as*

$$R_{k,MRP}^{DL} = \int_0^{\infty} \frac{\sum_{j=1}^{K} \lambda_j \sqrt{\delta_{j,k}^{DL}}}{\sum_{j=1}^{K} \lambda_j \sqrt{\delta_{j,k}^{DL}} \left(\left(\sqrt{\left(\mathrm{e}^{t/\alpha}-1\right)} \arctan\left\{\sqrt{\left(\mathrm{e}^{t/\alpha}-1\right)}\right\}\right) + 1\right)} dt, \quad (3.42)$$

where $\delta_{j,k}^{DL}$ is given in (3.23)*.*

In these corollaries, the double integral in Theorem 3.4.3 and 3.4.4 is simplified to a single integral. The DL average ergodic rate in the interference-limited scenario is found to be independent of the power splitting factor due to the fact that with $\sigma^2 = 0$, the term $(1-\rho)$ disappears in the $SINR_k^{DL}$ expression given in (3.5).

In the following, the UL performance of the HCNs is presented which reflects the DL energy harvesting efficiency of SWIPT with the NBS and the MRP cell associations. The UL performance is characterized in terms of the UL outage probability and the UL average ergodic rate.

3.4.3 Uplink Outage Probability

The UL outage probability is the probability that the instantaneous UL data rate at the serving BS in HCNs is less than the target UL data rate. The UL outage probability in HCNs is given by

$$P_{out}^{UL} = \sum_{k=1}^{K} \Lambda_k^{UL} P_{out,k}^{UL}, \tag{3.43}$$

where Λ_k^{UL} is given in (3.25) for the NBS cell association, and in (3.26) for the MRP cell association, and $P_{out,k}^{UL}$ is the UL outage probability of a typical MU associated with the kth tier.

In (3.43), the UL outage probability for a typical MU at a distance $\left\|\boldsymbol{x}_{\mathrm{u}_0,b_{\widehat{k}}}\right\|$ from its associated BS is defined as

$$\begin{aligned} P_{out,k}^{UL}\left(\mathrm{R}_s\right) &= \mathbb{E}_{\left\|\boldsymbol{x}_{b_{\widehat{k}},\mathrm{u}_0}\right\|}\left[\Pr\left((1-\alpha)\ln\left(1+SINR_k^{UL}\left(\left\|\boldsymbol{x}_{b_{\widehat{k}},\mathrm{u}_0}\right\|\right)\right)\leq \mathrm{R}_s\right)\right] \\ &= \mathbb{E}_{\left\|\boldsymbol{x}_{b_{\widehat{k}},\mathrm{u}_0}\right\|}\left[\Pr\left(SINR_k^{UL}\left(\left\|\boldsymbol{x}_{b_{\widehat{k}},\mathrm{u}_0}\right\|\right)\leq \Psi\right)\right]. \end{aligned} \tag{3.44}$$

where

$$\Psi = \mathrm{e}^{\mathrm{R}_s/(1-\alpha)} - 1. \tag{3.45}$$

3.4.3.1 General Case

In the following, the general result for the UL outage probability of a typical MU associated with the kth tier is derived.

Theorem 3.4.5. *The UL outage probability of a typical MU associated with the kth*

tier using NBS cell association is derived as

$$P^{UL}_{out,k,NBS}\left(\mathrm{R}_s\right) = 1 - 2\kappa \int_0^{\infty} x \exp\left\{ -\sigma^2 \Psi \Omega_k^{UL} x^{\ell_k} - \sum_{j=1}^{K} \left(\zeta_{k,j}^{UL} x^{\frac{2\ell_k}{\ell_j}} \Psi^{\frac{2}{\ell_j}} + \pi \lambda_j x^2 \right) \right\} dx, \tag{3.46}$$

where

$$\Omega_k^{UL} = \left(\phi \mathbb{E}\{P_{r_{\mathrm{u}_0},k}\} L_0\right)^{-1}, \tag{3.47}$$

$$\zeta_{k,j}^{UL} = \pi \lambda_j \left(\delta_{j,k}^{UL}\right)^{\frac{2}{\ell_j}} \Gamma\left(1 + \frac{2}{\ell_j}\right) \Gamma\left(1 - \frac{2}{\ell_j}\right), \tag{3.48}$$

$$\delta_{j,k}^{UL} = \frac{\mathbb{E}\left[P_{r_{\mathrm{u}_j},j}\right]}{\mathbb{E}\left[P_{r_{\mathrm{u}_0},k}\right]}, \tag{3.49}$$

and Ψ *is given in* (3.45).

Proof. The proof follows similar steps to Theorem 3.4.1. □

Theorem 3.4.6. *The UL outage probability of a typical MU associated with the kth tier using MRP cell association is derived as*

$$P^{UL}_{out,k,MRP}\left(\mathrm{R}_s\right) = 1 - \frac{1}{\Upsilon_k} \int_0^{\infty} x \exp\left\{ -\sigma^2 \Psi \Omega_k^{UL} x^{\ell_k} - \sum_{j=1}^{K} \left(\zeta_{k,j}^{UL} x^{\frac{2\ell_k}{\ell_j}} \Psi^{\frac{2}{\ell_j}} + \mu_{k,j} x^{2\ell_k/\ell_j} \right) \right\} dx, \tag{3.50}$$

where Ψ, Ω_k^{UL}, $\zeta_{k,j}^{UL}$, *and* $\mu_{k,j}$ *are given in* (3.45), (3.47), (3.48), *and* (3.22) *respectively.*

Proof. The proof follows similar steps to Theorem 3.4.2. □

3.4.3.2 Interference-Limited Case, Equal Path Loss Exponents $\{\ell_j\} = 4$

In the following, the UL outage probability of a typical MU associated with the kth tier is presented for the interference-limited case.

Corollary 3.4.5. *With $\{\ell_j\} = 4$ and $\delta^2 = 0$, the UL outage probability of a typical MU associated with the kth tier using NBS cell association is derived as*

$$P^{UL}_{out,k,NBS}(R_s) = 1 - \frac{\kappa}{\sum_{j=1}^{K} \pi\lambda_j \left(\frac{\pi}{2}\sqrt{\delta^{UL}_{j,k}\Psi} + 1\right)}, \tag{3.51}$$

where κ, $\delta^{UL}_{j,k}$, and Ψ are given in (3.14), (3.49), *and* (3.45), *respectively.*

Corollary 3.4.6. *With $\{\ell_j\} = 4$ and $\delta^2 = 0$, the UL outage probability of a typical MU associated with the kth tier using MRP cell association is derived as*

$$P^{UL}_{out,k,MRP}(R_s) = 1 - \frac{\sum_{j=1}^{K} \lambda_j \sqrt{\delta^{DL}_{j,k}}}{\sum_{j=1}^{K} \lambda_j \left(\frac{\pi}{2}\sqrt{\delta^{UL}_{j,k}\Psi} + \sqrt{\delta^{DL}_{j,k}}\right)}, \tag{3.52}$$

where $\delta^{DL}_{j,k}$, $\delta^{UL}_{j,k}$, and Ψ are given in (3.23), (3.49), *and* (3.45), *respectively.*

The UL outage probabilities for the NBS and the MRP cell associations are found to be independent of the energy conversion efficiency and the power splitting factor. This can be explained by the fact that the term $\phi = \frac{\eta\rho\alpha}{(1-\alpha)}$ in (3.7) cancels out with $\delta^2 = 0$.

3.4.4 Uplink Average Ergodic Rate

The UL average ergodic rate of a random MU in K-tier HCNs is given by

$$R^{UL} = \sum_{k=1}^{K} A^{UL}_k R^{UL}_k, \tag{3.53}$$

where R^{UL}_k is the UL average ergodic rate of a typical MU associated with the kth tier and Λ^{UL}_k is given in (3.25) for the NBS cell association, and in (3.26) for the MRP cell association, respectively.

In (3.53), the UL average ergodic rate of a random MU located at a distance

$\left\|\boldsymbol{x}_{\mathrm{u}_0,b_{\widehat{k}}}\right\|$ from its associated BS in the kth tier is defined as

$$R_k^{UL} = \mathbb{E}_{\left\|\boldsymbol{x}_{\mathrm{u}_0,b_{\widehat{k}}}\right\|}\left[\mathbb{E}_{SINR_k^{UL}}\left[(1-\alpha)\ln\left(1+SINR_k^{UL}\left(\left\|\boldsymbol{x}_{\mathrm{u}_0,b_{\widehat{k}}}\right\|\right)\right)\right]\right]. \tag{3.54}$$

3.4.4.1 General Case

The general result for the UL average ergodic rate of a random MU associated with the BS in kth tier is presented in the following theorems.

Theorem 3.4.7. *The UL average ergodic rate of a random MU associated with the BS in kth tier using NBS cell association is derived as*

$$R_{k,NBS}^{UL} = 2(1-\alpha)\kappa \int_0^\infty \int_0^\infty \frac{x}{1+t} \exp\left[-\delta^2 \Omega_k^{UL} t x^{\ell_k} - \sum_{j=1}^{K} \left(\zeta_{k,j}^{UL} t^{\frac{2}{\ell_j}} x^{\frac{2\ell_k}{\ell_j}} + \pi \lambda_j x^2 \right) \right] dx dt, \tag{3.55}$$

where κ, Ω_k^{UL}, and $\zeta_{k,j}^{UL}$ are given in (3.14), (3.47), *and* (3.48), *respectively.*

Proof. The proof follows similar steps to Theorem 3.4.3. □

Theorem 3.4.8. *The UL average ergodic rate of a random MU associated with the BS in kth tier using MRP cell association is derived as*

$$R_{k,MRP}^{UL} = \frac{(1-\alpha)}{\Upsilon_k} \int_0^\infty \int_0^\infty \frac{x}{1+t} \exp\left[-\delta^2 \Omega_k^{UL} t x^{\ell_k} - \sum_{j=1}^{K} \left(\zeta_{k,j}^{UL} t^{\frac{2}{\ell_j}} x^{\frac{2\ell_k}{\ell_j}} + \mu_{k,j} x^{2\ell_k/\ell_j} \right) \right] dx dt, \tag{3.56}$$

Proof. The proof follows similar steps to Theorem 3.4.4. □

3.4.4.2 Interference-Limited Case, Equal Path Loss Exponents $\{\ell_j\} = 4$

The UL average ergodic rate of a typical MU associated with the kth tier for the interference-limited network is presented in the following corollaries.

Corollary 3.4.7. *With $\{\ell_j\} = 4$ and $\delta^2 = 0$, the UL average ergodic rate of a typical*

MU associated with the kth tier using NBS cell association is derived as

$$R_{k,NBS}^{UL} = \int_0^{\infty} \frac{(1-\alpha)\kappa}{(1+t)\sum_{j=1}^{K} \pi\lambda_j \left(\frac{\pi}{2}\sqrt{\delta_{j,k}^{UL} t}+1\right)} dt, \tag{3.57}$$

where κ and $\delta_{k,j}^{UL}$ are given in (3.14) *and* (3.49)*, respectively.*

Corollary 3.4.8. *With $\{\ell_j\} = 4$ and $\delta^2 = 0$, the UL average ergodic rate of a typical MU associated with the kth tier using MRP cell association is derived as*

$$R_{k,MRP}^{UL}(R_s) = \int_0^{\infty} \frac{(1-\alpha)\sum_{j=1}^{K} \lambda_j \sqrt{\delta_{j,k}^{DL}}}{(1+t)\sum_{j=1}^{K} \lambda_j \left(\frac{\pi}{2}\sqrt{\delta_{j,k}^{UL} t}+\sqrt{\delta_{j,k}^{DL}}\right)} dt, \tag{3.58}$$

where $\delta_{j,k}^{DL}$ and $\delta_{j,k}^{UL}$ are given in (3.23) *and* (3.49)*, respectively.*

In the interference-limited scenario, the UL average ergodic rate does not depend on the energy conversion efficiency and the power splitting factor with the NBS and the MRP cell associations. This can be seen in (3.7) that with $\delta^2 = 0$, the term $\phi = \frac{\eta\rho\alpha}{(1-\alpha)}$ cancels out and $SINR_k^{UL}$ becomes independent of η and ρ.

In the following, the global (GL) performance of the HCNs is presented which reflects the impact of power splitting factor on the overall (DL+UL) performance. The GL performance is characterized in terms of the GL average ergodic rate.

3.4.5 Global Average Ergodic Rate

The GL average ergodic rate of a random MU in K tier HCNs is defined as the sum of the DL average ergodic rate and the UL average ergodic rate, as follows

$$R^{GL} = R^{DL} + R^{UL}, \tag{3.59}$$

where R^{DL} and R^{UL} are given in (3.37) and (3.53), respectively. The GL average ergodic rate is defined to find the optimal power splitting factor ρ^* that maximizes

the GL average ergodic rate. The evaluation for the exact expression of ρ^* turns out to be intractable, therefore, we numerically evaluate the optimal ρ^* that maximizes R^{GL} in the numerical results.

3.4.6 Energy Efficiency

The energy efficiency of transmitting one MU data stream in K-tier HCNs is defined as the total average number of bits successfully conveyed to the typical MU in the DL per Joule consumed energy and is given by

$$EE = \sum_{k=1}^{K} \Lambda_k^{DL} \frac{R_k^{DL}}{P_k^{total}}, \tag{3.60}$$

where P_k^{total} is the total power consumption in each channel use of the kth tier given as

$$P_k^{total} = P_k^0|_T + P_k^0|_R + \frac{P_k}{\epsilon_k} - \phi \mathbb{E}\left\{P_{r_{u_0},k}\right\}, \tag{3.61}$$

where $P_k^0|_T$ is the static hardware power consumption of the BS in the kth tier, $P_k^0|_R$ is the total circuit power consumption at the MU, ϵ_k is the efficiency of the power amplifier, and $\mathbb{E}\left\{P_{r_{u_0},k}\right\}$ is the average received power as derived in Lemma 3.3.1 and 3.3.2, for the NBS and the MRP cell association, respectively. In (3.61), ϕ is given in (3.6).

3.5 Numerical Results

In this section, the system performance with the NBS cell association is compared to that with the MRP cell association in terms of the DL outage probability, the DL average ergodic rate, the UL outage probability, and the UL average ergodic rate. The DL outage probability, the DL average ergodic rate, the UL outage probability, and the UL average ergodic rate for the NBS cell association are plotted using (3.29), (3.46), (3.39), and (3.55), respectively. The DL outage probability, the DL average

ergodic rate, the UL outage probability, and the UL average ergodic rate for the MRP cell association are plotted using (3.33), (3.40), (3.50), and (3.56), respectively. The analytical results are validated by Monte Carlo simulations, where the BSs and the MUs are deployed according to the proposed model for a two-tier HCN. In all the figures, the path loss is assumed to be $L_0 = -38.5$ dB at 1 meter, and the path loss exponents are $\ell_1 = 3.8$ and $\ell_2 = 3.5$. The thermal noise power at the MU and the BS are fixed as $\sigma^2 = \delta^2 = -104$ dB for 10 MHz bandwidth. Unless otherwise stated, the time allocation factor $\alpha = 0.5$ and the power splitting factor $\rho = 0.5$. The circuit power consumed by information decoding is ignored. For energy receiver, the RF to DC conversion efficiency is assumed to be 50 % i.e., $\eta = 0.5$ and all the MUs have the same η. Moreover, the processing power in the UL is ignored [120] except for the energy efficiency evaluation in Section 3.5.5.

3.5.1 Effect of Picocell BSs Density and BS Transmit Power

In this subsection, the effect of the density of picocell BSs and the transmit power at the BSs on the DL outage probability, the DL average ergodic rate, the UL outage probability, and the UL average ergodic rate of a random MU in HCNs with the NBS and the MRP cell associations is examined. In Figs. 3.2, 3.3, 3.4, and 3.5, we set $\lambda_1 = 10^{-3}$ and $R_s = 0.5$ nats/s/Hz.

Downlink Performance: Fig. 3.2 (a) and Fig. 3.2 (b) compare the impact of the density of picocell BSs λ_2 and the BS transmit power $P_{t,b}$ of each tier on the DL outage probability with the NBS cell association $P^{DL}_{out,NBS}(R_s)$, to the DL outage probability with the MRP cell association $P^{DL}_{out,MRP}(R_s)$, respectively. Fig. 3.3 (a) and Fig. 3.3 (b) compare the impact of the density of picocell BSs λ_2 and the BS transmit power of each tier on the DL average ergodic rate with the NBS cell association R^{DL}_{NBS}, to the DL aveargе ergodic rate with the MRP cell association R^{DL}_{MRP} respectively.

With the increase of λ_2, $P^{DL}_{out,NBS}$ and R^{DL}_{NBS} improve due to the increase in signal strength at the MU from the nearest serving BS. Interestingly, the increase in λ_2 does not have a significant affect on $P^{DL}_{out,MRP}$ and R^{DL}_{MRP} at both tiers. It is also

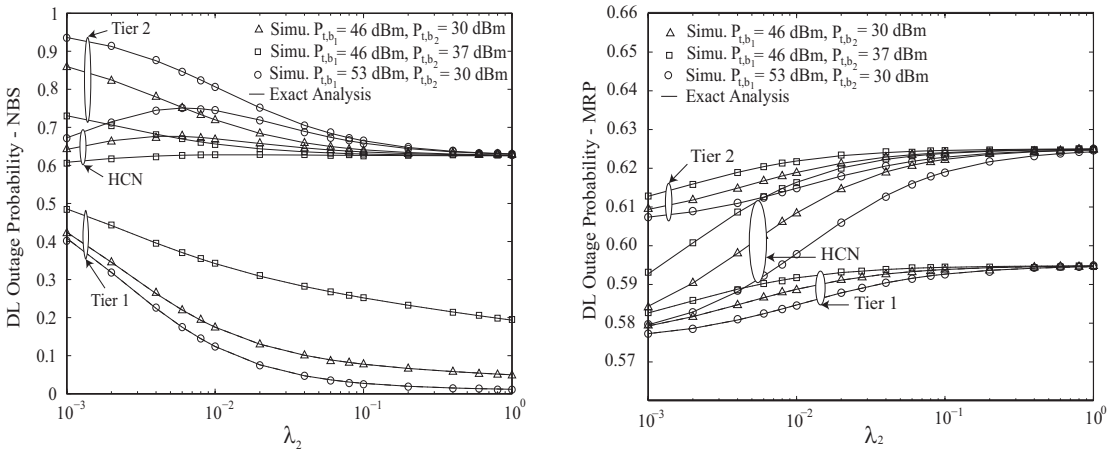

(a) DL outage probability with the NBS cell association.

(b) DL outage probability with the MRP cell association.

Figure 3.2: Impact of picocell BS density and BS transmit power on the DL outage probability in a two-tier HCN.

observed that $P^{DL}_{out,NBS}$, R^{DL}_{NBS}, $P^{DL}_{out,MRP}$, and R^{DL}_{MRP} of a random MU in HCNs are approximately the same with the increase in λ_2.

With the increase of $P_{t,b}$ in the kth tier, $P^{DL}_{out,NBS}(R_s)$ and R^{DL}_{NBS} of the kth tier improve, while that of other tiers degrade. This is due to the increased signal power at the MUs in the kth tier, and the increased interference at the MUs of the other tiers. Surprisingly, the increase in $P_{t,b}$ of the kth tier slightly affects $P^{DL}_{out,MRP}(R_s)$ and R^{DL}_{MRP} of both the tiers. Furthermore, it is shown that $P^{DL}_{out,NBS}(R_s)$, R^{DL}_{NBS}, $P^{DL}_{out,MRP}(R_s)$, and R^{DL}_{MRP} of a random MU in HCNs cannot be greatly improved by increasing $P_{t,b}$.

Uplink Performance: Fig. 3.4 (a) and Fig. 3.4 (b) show the effect of picocell BS density λ_2 and the BS transmit power $P_{t,b}$ on the UL outage probability with the NBS $P^{UL}_{out,NBS}(R_s)$, to the UL outage probability with the MRP cell association $P^{UL}_{out,MRP}(R_s)$, respectively. Fig. 3.5 (a) and Fig. 3.5 (b) compare the impact of the density of picocell BSs λ_2 and the BS transmit power of each tier on the UL average ergodic rate with the NBS cell association R^{UL}_{NBS}, to the UL aveargе ergodic rate with the MRP cell association R^{UL}_{MRP}, respectively.

Increasing λ_2 improves $P^{UL}_{out,NBS}(R_s)$ and R^{UL}_{NBS} due to the increased harvested

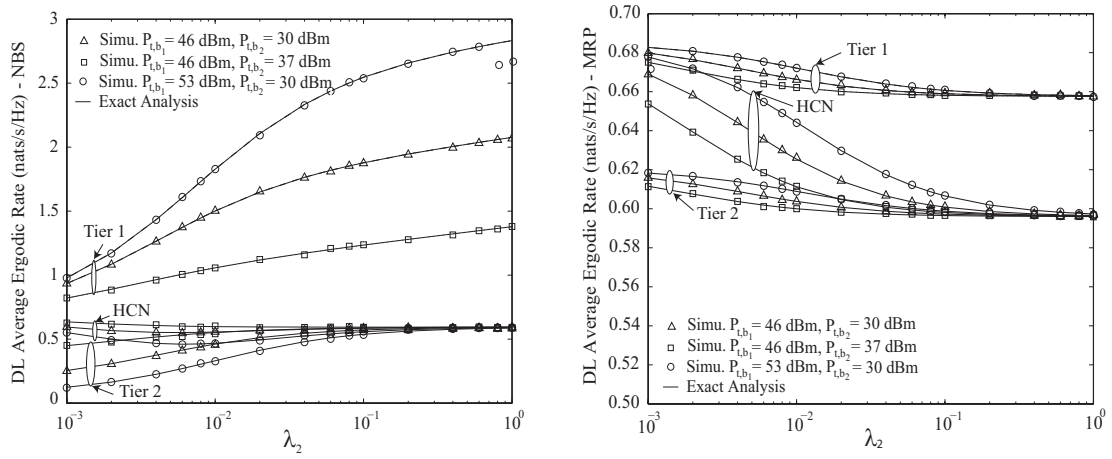

(a) DL average ergodic rate with the NBS cell association.

(b) DL average ergodic rate with the MRP cell association.

Figure 3.3: Impact of picocell BS density and BS transmit power on the DL average ergodic rate in a two-tier HCN.

energy from the serving nearest BS and the decreased path loss. However, increasing λ_2 to a certain value degrades $P^{UL}_{out,NBS}(R_s)$ and R^{UL}_{NBS} of the macrocell MUs due to the dominant effect of the increased interference from the macrocell MUs with increased transmit power. In contrast, for the MRP cell association, the increase in λ_2 degrades $P^{UL}_{out,MRP}(R_s)$ and R^{UL}_{MRP} of both the tiers due to the dominant effect of higher interference from the large number of other picocell MUs. Furthermore, $P^{DL}_{out,NBS}(R_s)$, R^{DL}_{NBS}, $P^{DL}_{out,MRP}(R_s)$, and R^{DL}_{MRP} are slightly affected by increasing λ_2.

The increase in $P_{t,b}$ in the kth tier improves $P^{UL}_{out,NBS}(R_s)$ and R^{UL}_{NBS} in the kth tier and degrades that in other tiers. The low path loss results in the increased signal power at the BS of its own tier, and the increased interference at the BS of the other tier. The opposite holds true for the MRP cell association, i.e., increasing the BS transmit power in the kth tier degrades $P^{UL}_{out,MRP}(R_s)$ and R^{UL}_{MRP} of the kth tier while improves that of other tiers. This is because increasing the BS transmit power in the kth tier results in the increased distance between the MU and the associated BS of the kth tier as opposed to the decrease of the distance between the MU and the associated BS of the other tiers as in (A.6). Increasing BS transmit power only slightly effects $P^{UL}_{out,NBS}(R_s)$, R^{UL}_{NBS}, $P^{UL}_{out,MRP}(R_s)$, and R^{UL}_{MRP} of a random MU in

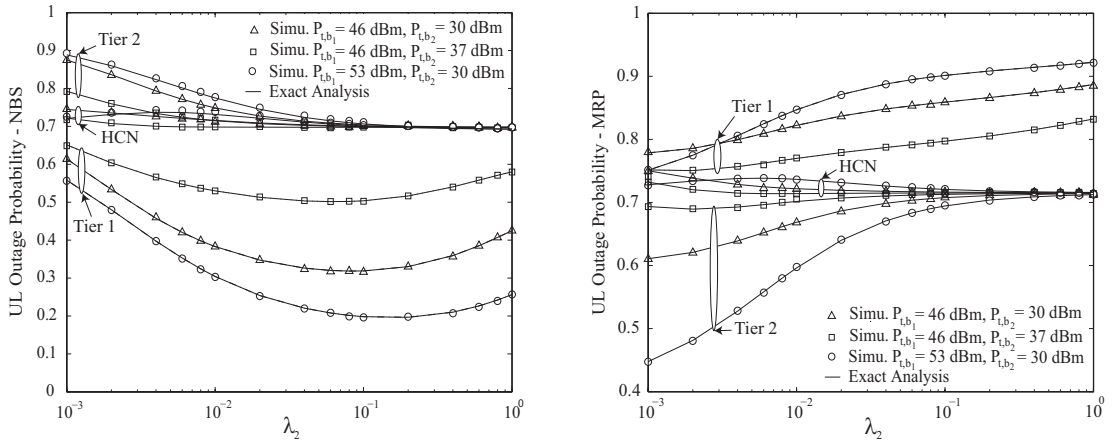

(a) UL outage probability with the NBS cell association.

(b) UL outage probability with the MRP cell association.

Figure 3.4: Impact of picocell BS density and BS transmit power on the UL outage probability in a two-tier HCN.

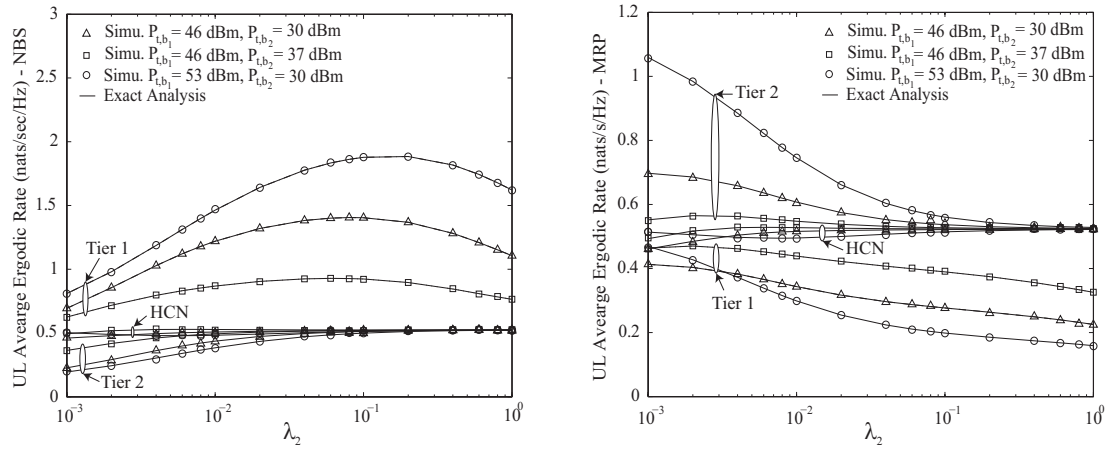

(a) UL average ergodic rate with the NBS cell association.

(b) UL average ergodic rate with the MRP cell association.

Figure 3.5: Impact of picocell BS density and BS transmit power on the UL average ergodic rate in a two-tier HCN.

HCNs.

3.5.2 Effect of Time Allocation Factor, and Power Splitting Factor on the DL and the UL performance

In this subsection, the effect of the time allocation factor and the power allocation factor on the DL and UL outage probability and average ergodic rate of a random MU in HCNs with the NBS and the MRP cell associations is examined. In Fig. 6, we set $\lambda_1 = 10^{-3}$, $\lambda_2 = 2 \times 10^{-3}$, $P_{t,b_1} = 46$ dBm, and $P_{t,b_2} = 37$ dBm.

Fig. 3.6 (a) examines the impact of the time allocation factor α and the power splitting factor ρ on the DL and the UL outage probability of a random MU in HCNs with the NBS and the MRP cell associations. Fig. 3.6 (b) examines the impact of α and ρ on the DL and the UL average ergodic rate of a random MU in HCNs with the NBS and the MRP cell associations. With the increase of α, the DL outage probabilities, $P^{DL}_{out,NBS}(R_s)$ and $P^{DL}_{out,MRP}(R_s)$, and the DL average ergodic rates, R^{DL}_{NBS} and R^{DL}_{MRP}, improve due to allocating large fraction of time to the DL transmission. For the UL performance, first we observe that with the increase in α, the UL outage probabilities, $P^{UL}_{out,NBS}(R_s)$ and $P^{UL}_{out,MRP}(R_s)$, and the UL average ergodic rates, R^{UL}_{NBS} and R^{UL}_{MRP}, improve and then degrade. This is because for small α, the noise plays a dominant role in the $SINR^{UL}_k$ as shown in (3.7), thus the $SINR^{UL}_k$ increases with increasing α. However, for large α, the degradation of the $P^{UL}_{out,NBS}(R_s)$, R^{UL}_{NBS}, $P^{UL}_{out,MRP}(R_s)$, and R^{UL}_{MRP} is due to allocating a large fraction of time to the DL transmission than to the UL transmission. Interestingly, with the increase of ρ, the DL performance of a random MU in HCNs remains almost unchanged. This is because, with high density of high transmit power BSs, the interference plays a dominant role in the $SINR^{DL}_k$ in (5) and as such the thermal noise is ignored. However, the UL performance of a random MU in HCNs improves by increasing ρ. Transmitting the UL information using a larger fraction of the DL average received power results in the improved UL performance.

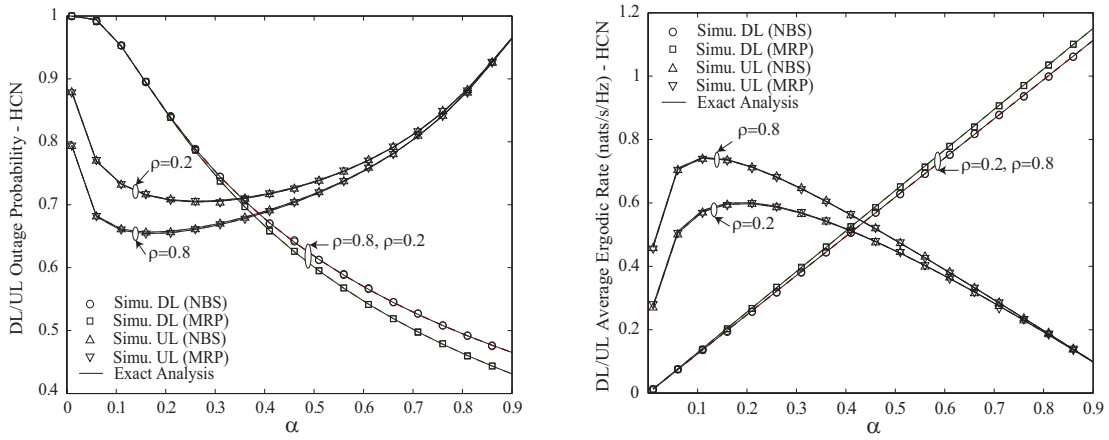

(a) DL/UL outage probability.

(b) DL/UL average ergodic rate.

Figure 3.6: Impact of time allocation factor and power splitting factor on the DL/UL performance in a two-tier HCN.

3.5.3 Effect of Rate Threshold on the DL and the UL performance

Fig. 3.7 compares the DL and the UL outage probability of a random MU in HCNs with the NBS to that with the MRP cell association. In Fig. 3.7, $\lambda_1 = 10^{-3}$, $\lambda_2 = 2 \times 10^{-3}$, $P_{t,b_1} = 46$ dBm, and $P_{t,b_2} = 37$ dBm. In Fig. 3.7, the horizontal axis represents the rate threshold R_s in nats/sec/Hz.

The DL outage probability of a random MU in HCNs with the MRP cell association is narrowly better than that with the NBS cell association. This is due to the lower aggregate interference in the $SINR_k^{DL}$ with the MRP cell association than that with the NBS cell association. The UL outage probability a random MU in HCNs with the NBS cell association is comparable to that with the MRP cell association.

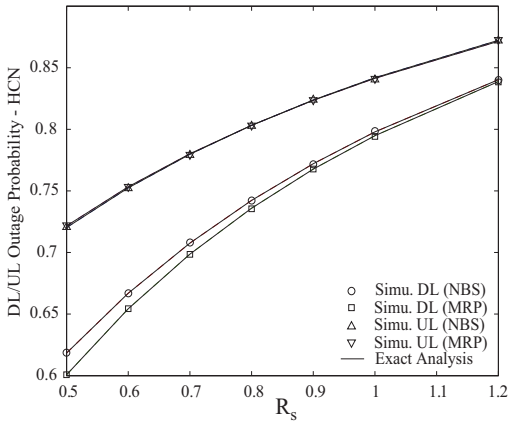

Figure 3.7: Impact of rate threshold on the DL/UL outage probability in a two-tier HCN.

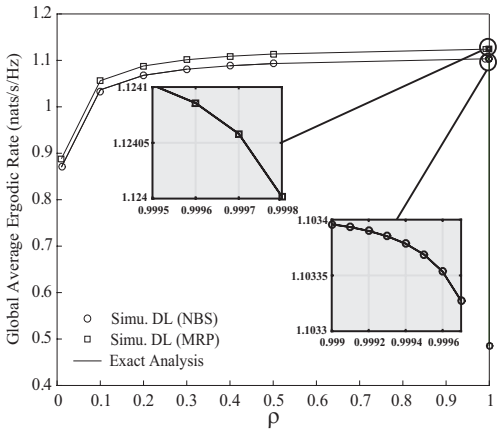

Figure 3.8: Impact of power splitting factor on the GL average ergodic rate in a two-tier HCN.

3.5.4 Effect of Power Splitting Factor on the Global Average Ergodic Rate

Fig. 3.8 examines the impact of power splitting factor ρ on the GL average ergodic rate for the NBS and MRP cell associations using (3.59). In Fig. 3.8, we set $\lambda_1 = 10^{-3}$, $\lambda_2 = 2 \times 10^{-3}$, $P_{t,b_1} = 46$ dBm, and $P_{t,b_2} = 37$ dBm.

It is observed that the GL average ergodic rate first increases, then decreases with increasing ρ. The increasing trend is due to the increase in the UL average ergodic rate. The sudden decrease is due to the decrease in the DL average ergodic rate. We observe that the optimal power splitting factor ρ^*, that maximizes the GL average ergodic rate, occurs near one, i.e., $\rho^*_{NBS} = 0.999$ and $\rho^*_{MRP} = 0.9995$. Moreover, the improvement in the GL average ergodic rate for $\rho = 0.4$ to the optimal ρ^* is observed to be very small, which reveals that the optimal operation region for ρ is [0.4, 0.999].

3.5.5 Effect of Picocell BSs Density and BS Transmit Power on the Energy Efficiency

Fig. 3.9 examines the impact of picocell BS density λ_2 and BS transmit power on the energy efficiency for the NBS and MRP cell associations using (3.60). In Fig. 3.9, the macrocell BS density $\lambda_1 = 10^{-3}$, the static hardware power consumption at the BSs of both the tiers as $P_k^0|_T = 30$ dBm, the total circuit power consumption at the MU $P_k^0|_R = 20$ dBm, and the power amplifier efficiency $\epsilon_k = 6.28$ as considered in the SWIPT based network in [121].

The energy efficiency is shown to be improved with the increase in number of small cell BSs density with both the cell associations as the average received power is increased with the increase in λ_2 resulting in the decrease of the power consumption in (3.61). Furthermore, it is observed that energy efficiency decreases with the increase of BS transmit power of each tier. This is due to the fact that average ergodic rate is observed to be almost constant with the increase in BS transmit power of each tier as shown in Fig. 3.3 (a) and Fig. 3.3 (b), whereas the power consumption increases as in (3.61). The energy efficiency in HCNs with the NBS cell association is slightly better than with the MRP cell association due to slightly better DL average ergodic rate with the NBS cell association as shown in Fig. 3.3 (a) and Fig. 3.3 (b).

Note that the proposed work is a baseline model with single antennas and by equipping the BSs with multiple number of antennas will largely improve the received power in (3.61) which will increase the energy efficiency. Massive MIMO antennas can be used at the BSs for forming sharp energy beams towards MUs to achieve better efficiency [3]. Moreover, the advancements in the areas of lower power electronics and displays (e.g., reflective displays) will further decrease the power consumption of mobile devices and improves the energy efficiency.

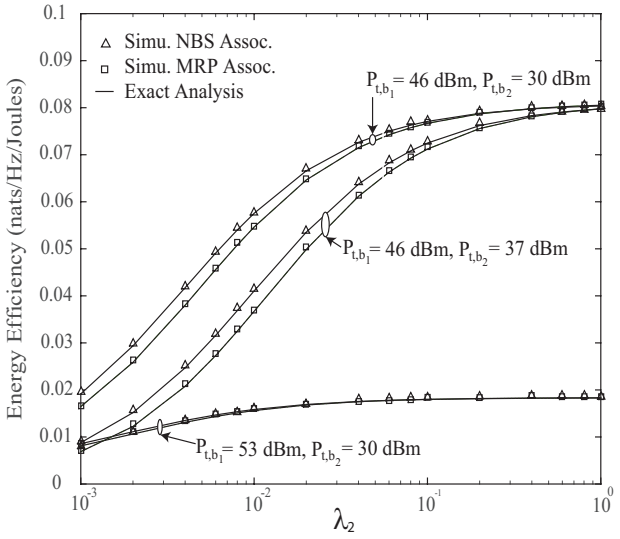

Figure 3.9: Impact of picocell BSs density and BS transmit power on the energy efficiency in a two-tier HCNs.

3.6 Chapter Summary

In this chapter, a tractable analytical model of K-tier HCNs with SWIPT is presented, where the MUs harvest energy and decode information simultaneously in the DL, and the harvested energy at the MU is then utilized for information transmission in the UL. The analytical expressions for the DL average received power at a random MU with the NBS and the MRP cell associations are derived to demonstrate the effect of harvested energy on the UL information transmission. The DL and the UL performance is evaluated in terms of the outage probability and the average ergodic rate of a random MU in HCNs with the NBS and the MRP cell associations. The DL and UL performance of the NBS cell association is comparable to that of the conventional MRP cell association despite the fact that the UL path loss in the NBS cell association is low. Owing to its simple implementation with low system overheads, the NBS cell association sounds an optimal choice. It is shown that although the harvested energy at the MU can be increased by deploying more small cell BSs and increasing the BS transmit power, the UL performance of a random

MU in HCNs with the NBS and the MRP cell associations can not be improved. Nevertheless, the UL performance of a random MU can be improved by increasing the power splitting factor. Furthermore, the energy efficiency is shown to be improved with the increase in SBSs density and degraded with the increase in BS transmit power of each tier. With the advancements in WPT and interference cancellation, HCNs with SWIPT prove to be promising candidates for 5G systems.

Chapter 4

K-tier HCNs with FD Small Cells

4.1 Introduction

In this chapter, the DL and the UL transmission in K-tier HCNs with FD small cell base stations (SBSs) is investigated for improved spectrum efficiency.

FD communication has emerged as an attractive solution for increasing the network throughput by allowing DL and UL transmissions in the same spectrum. In theory, FD data transmission is capable of doubling the spectral efficiency of HD system. Though the gains of FD systems can be easily foreseen, practical implementations of such FD systems pose many challenges and a lot of technical problems still need to be solved before its actual deployment on a system level. The crucial barrier in implementing full-duplex systems resides is the SI from the transmit antennas to receive antennas at a wireless transceiver. More explicitly, the radiated power in the DL interferes with its own desired received signals in the UL. Fortunately, the recent advances on SI cancellation, such as antenna separation schemes [36], beamforming-based techniques [38], and digital circuit domain schemes [41], have demonstrated the feasibility of FD transmission for short to medium range wireless communications.

In this chapter, the FD operation is considered only at the SBSs as operating all the BSs in FD mode is likely to erode the performance gain of the FD communication since simultaneous DL and UL operation on the same band brings increased interference, and thus reduced coverage. Inspired by the work in [69], where making

different tiers operate in different duplex modes in heterogeneous networks enhances the network throughput, the HCNs is considered, where only small cells operate in FD mode, and the macrocells operate in HD mode. Small cell systems are considered to be especially suitable for deployment of FD technology due to low transmit powers, short transmission distances and low mobility [68]. In the considered HCNs, multiuser MIMO is assumed at the MBSs which aims to reduce the interference as well as to increase spectral efficiency by utilizing the spatial dimension [122]. A tractable framework of the proposed system is presented, which allows to derive analytical expressions for the DL and the UL average ergodic rates.

The remainder of the chapter is organized as follows. In Section 4.2, the system model of HCNs with multiuser MIMO at the MBSs and FD operation at the SBSs is presented. The DL and UL average ergodic rates are derived in Section 4.3. The performance comparison of the proposed model with that of the conventional HCNs is presented in Section 4.4. Finally, numerical results are discussed in Section 4.5 before the paper is summarized in Section 4.6.

The notations commonly used throughout in this chapter are presented in Table 4.1.

4.2 System Model

This chapter considers K-tier HCNs, where the MBSs and the SBSs are spatially located in $\mathbb{R}^2$, following HPPP, $\Phi_{b^{\mathrm{M}}}$ and Φ_{b^k} with intensity $\lambda_{b^{\mathrm{M}}}$ and λ_{b^k} $(k = 2, \cdots, K)$, respectively. Multiuser MIMO is considered at the MBSs, where each BS is equipped with N antennas, serving U_{M} MUs, and operates in HD mode. Each SBS is equipped with single antenna, and is transmitting and receiving at the same time in FD mode [123, 124]. All the MUs have single antenna and operate in HD mode. In this work, the DL performance of the macrocell is considered, while the SBSs have transmissions in the DL and UL simultaneously due to the FD operation. The performance of the UL transmission of MBSs can be easily analyzed following the proposed method of this work. In HCNs with FD small cells, the DL and UL

Table 4.1: Frequent Notations for HCNs with FD Small Cells

Notation	Definition
P_{M}	Transmit power of MBS
P_k	Transmit power of kth tier SBS
P_u	Transmit power of the MU
α_{M}	Path loss exponent for Macrocell
α_k	Path loss exponent for kth tier small cell
β	Frequency dependent constant value
$h_{R_{SI},k}$	Residual self interfering channel of a kth tier BS
N_o	Noise power

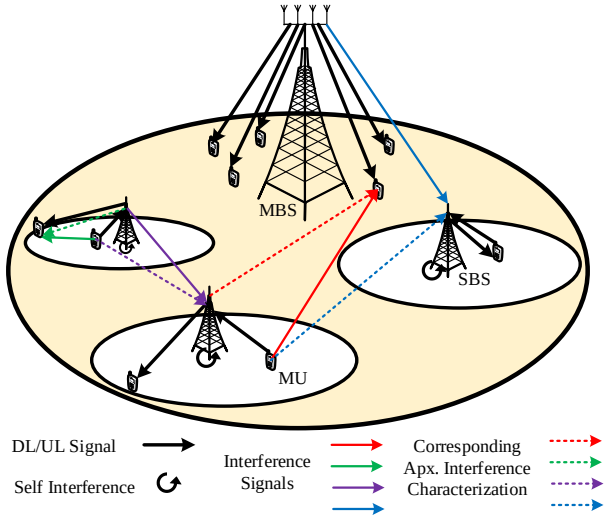

Figure 4.1: Example cells of the proposed HCNs with HD multiuser MIMO MBS and FD SBSs and the interference characterizations.

small cell transmissions occur simultaneously by reusing the spectrum of the DL macrocell transmissions due to the full frequency reuse in HCNs [125]. The network is assumed to be fully-loaded, such that each MBS has U_{M} active MUs [74, 75], and each SBS serves one active DL MU and one active UL MU in each time instant [63], as shown in Fig. 4.1. Accordingly, the intensity of the active DL MUs in HCNs is

$\lambda_u^{\mathrm{DL}} = (U_M \lambda_{b^M} + \sum_{k=2}^{K} \lambda_{b^k})$, whereas the active UL MUs are modeled by an independent HPPP Φ_{u^k} with intensity $\lambda_{u^k}^{\mathrm{UL}} = \lambda_{b^k}$. The analysis is performed at a typical MU, which is assumed to be at the origin.

The channel path loss over the distance $|x|$ is modelled as $\beta|x|^{-\alpha}$, where β is the frequency dependent constant value and α is the path loss exponent. The channels are assumed to be independent and identically distributed (i.i.d.) quasi-static Rayleigh fading. The TDD mode is considered, where channel reciprocity can be exploited which allows a BS to estimate its DL channels from the UL training signals sent by the MUs. Therefore, the resulting number of training signals scales linearly with the number of MUs, and is independent of the number of antennas in contrast to frequency division duplexing (FDD). We consider time division multiple access (TDMA), where several MUs share the same channel in different time slots, thus the BS transmit power is independent of the density of active MUs, and there is no intra-cell interference in each cell. In a snap of time, each MBS can serve U_{M} MUs and each FD SBS serves one DL and one UL MU per channel.

4.2.1 SI Cancellation for FD Small Cells

The SBS in FD mode receives self-interference from its transmitted signal, and performs SI cancellation to combat it. Since, the amount of SI depends on the transmit power of the SBS, the residual SI power after SI cancellation is defined as [38, 41]

$$P_{R_{SI}}(P_k) = P_k |h_{R_{SI},k}|^2, \tag{4.1}$$

where $h_{R_{SI},k}$ is the residual self interfering channel of a kth tier BS, and $h_{R_{SI},k}$ is characterized according to the cancellation algorithms. For instance, using digital-domain cancellation algorithms, $h_{R_{SI},k}$ can be modeled as $h_{R_{SI},k} = h_{S,k} - \hat{h}_{S,k}$, where $h_{S,k}$ and $\hat{h}_{S,k}$ are the self-interfering channel and its estimate channel, respectively [38, 41]. In [126], $h_{R_{SI},k}$ is regarded as a constant value with $|h_{R_{SI},k}|^2 = \sigma_e^2$

for the estimation error variance σ_e^2. However, modeling $h_{R_{SI},k}$ is still challenging for other cancellation techniques, such as analog-domain schemes [5, 67, 127–129], propagation-domain schemes [130], and combined schemes of different domains [131]. The parametrization of the SI cancellation capability in (4.1) can make the analysis more generic. Therefore, in our analysis, we consider, a constant value for $h_{R_{SI},k}$ [1], given as

$$|h_{R_{SI},k}|^2 = 10^{L_{dB,k}/10}, \tag{4.2}$$

where $L_{dB,k}$ is the ratio between the residual self-interference after interference cancellation and the transmit power at the kth tier BS as defined in [69].

4.2.2 Cell Association

To obtain the strongest received signal, the maximum received power cell association rule is considered in the DL transmission, where the DL MU connects to the BS, which provides the maximum long-term average received power [117]. The average received power at a typical DL MU connected to the MBS m ($m \in \Phi_{b^{\mathrm{M}}}$) is expressed as

$$P_{r,\mathrm{M}} = G_a \frac{P_{\mathrm{M}}}{U_{\mathrm{M}}} \beta \left| X_{m,u^{\mathrm{M}}} \right|^{-\alpha_{\mathrm{M}}}, \tag{4.3}$$

where the small-scale fading channel power gain between the typical DL macrocell MU and its serving MBS in zero-forcing beamforming (ZFBF) transmission, $g_{o,u_0^{\mathrm{M}}} \sim \Gamma\left(N - U_{\mathrm{M}} + 1, 1\right)$, is approximated as the array gain $G_a = N - U_{\mathrm{M}} + 1$ for $(1 < U_M < N)$ [43].

The average received power at a DL MU that is connected to the kth tier SBS

[1] The analysis can be easily extended to the case of random $h_{R_{SI},k}$. For instance, once the probability density function (PDF) of $h_{R_{SI},k}$ is available for a certain SI cancellation algorithm, we can average the analytical results derived in the paper over the distribution of $h_{R_{SI},k}$.

b^k ($b^k \in \Phi_{b^k}$), is expressed as

$$P_{r,b^k} = P_k \beta \left(\left| X_{b^k,u^k} \right| \right)^{-\alpha_k}. \tag{4.4}$$

For the UL transmission, the MUs can only associate with the FD SBSs. The MU is assumed to associate to the SBS that offers the strongest average received power.

Based on the cell association model, the set of interfering MUs and FD SBSs may correlate. However, to maintain model tractability, the set of interfering MUs is assumed to be independent of the set of interfering FD SBSs as in [61, 132].

4.2.3 SINR Models

4.2.3.1 DL SINR of a Macrocell MU

The SINR for a typical DL macrocell MU u_0^{M} located at the origin is given as

$$\mathrm{SINR}_{\mathrm{M}}^{\mathrm{DL}} = \frac{\frac{P_{\mathrm{M}}}{U_{\mathrm{M}}} \beta g_{o,u_0^{\mathrm{M}}} \left| X_{o,u_0^{\mathrm{M}}} \right|^{-\alpha_{\mathrm{M}}}}{\underbrace{I_{\mathrm{M},u_0^{\mathrm{M}}} + I_{S,u_0^{\mathrm{M}}} + I_{u_{ul}^s,u_0^{\mathrm{M}}}}_{I_{u_0^{\mathrm{M}}}} + N_0}, \tag{4.5}$$

where $g_{o,u_0^{\mathrm{M}}} \sim \Gamma\left(N - U_{\mathrm{M}} + 1, 1\right)$ is the small-scale fading channel power gain between the typical DL macrocell MU and its serving MBS, and $\left| X_{o,u_0^{\mathrm{M}}} \right|$ is the distance between the typical DL macrocell MU and its serving MBS. In (4.5), $I_{\mathrm{M},u_0^{\mathrm{M}}}$, $I_{S,u_0^{\mathrm{M}}}$, and $I_{u_{ul}^s,u_0^{\mathrm{M}}}$ are the interferences from the other MBSs, the SBSs, and the UL small cell MUs given as

$$I_{\mathrm{M},u_0^{\mathrm{M}}} = \sum_{x \in \Phi_b^{\mathrm{M}} \setminus o} \frac{P_{\mathrm{M}}}{U_{\mathrm{M}}} h_{x,u_0^{\mathrm{M}}} \beta \left| X_{x,u_0^{\mathrm{M}}} \right|^{-\alpha_{\mathrm{M}}}, \tag{4.6}$$

$$I_{S,u_0^{\mathrm{M}}} = \sum_{j=2}^{K} \sum_{y \in \Phi_b^j} P_j h_{y,u_o^{\mathrm{M}}} \beta \left| X_{y,u_0^{\mathrm{M}}} \right|^{-\alpha_j}, \tag{4.7}$$

and

$$I_{u_{ul}^s,u_0^{\mathrm{M}}} = \sum_{j=2}^{K} \sum_{z\in\Phi_u^j} P_u h_{z,u_0^{\mathrm{M}}} \beta \left| X_{z,u_0^{\mathrm{M}}} \right|^{-\alpha_j}, \tag{4.8}$$

respectively. In (4.6), (4.7), and (4.8), $h_{x,u_0^{\mathrm{M}}} \sim \Gamma\left(U_{\mathrm{M}},1\right)$, $h_{y,u_0^{\mathrm{M}}} \sim \exp\left(1\right)$, and $h_{z,u_0^{\mathrm{M}}} \sim \exp\left(1\right)$ denote the small-scale fading channel power gains from the MBSs to the typical DL macrocell MU, from the SBSs to the typical DL macrocell MU, and from the UL small cell MUs to the typical DL macrocell MU, respectively, and their corresponding distances are denoted as $\left|X_{x,u_0^{\mathrm{M}}}\right|$, $\left|X_{y,u_0^{\mathrm{M}}}\right|$, and $\left|X_{z,u_0^{\mathrm{M}}}\right|$, respectively.

4.2.3.2 DL SINR of a Small Cell MU

The SINR for a typical DL small cell MU u_0^k located at the origin can be written as

$$\mathrm{SINR}_k^{\mathrm{DL}} = \frac{P_k g_{o,u_0^k} \beta \left| X_{o,u_0^k} \right|^{-\alpha_k}}{I_{\mathrm{M},u_0^k} + I_{S,u_0^k} + I_{u_{ul}^s,u_0^k} + N_0}, \tag{4.9}$$

where g_{o,u_0^k} is the small-scale fading channel power gain between the typical DL small cell MU and its serving SBS, and $\left|X_{o,u_0^k}\right|$ is the distance between the typical DL small cell MU and its serving SBS. In (4.9), I_{M,u_0^k}, I_{S,u_0^k}, and $I_{u_{ul}^s,u_0^k}$ are the interference from the other MBSs, the SBSs, and the UL small cell MUs, which are given as

$$I_{\mathrm{M},u_0^k} = \sum_{x\in\Phi_b^{\mathrm{M}}} \frac{P_{\mathrm{M}}}{U_{\mathrm{M}}} h_{x,u_0^k} \beta \left| X_{x,u_0^k} \right|^{-\alpha_{\mathrm{M}}}, \tag{4.10}$$

$$I_{S,u_0^k} = \sum_{j=2}^{K} \sum_{y\in\Phi_b^j\setminus o} P_j h_{y,u_0^k} \beta \left| X_{y,u_0^k} \right|^{-\alpha_j}, \tag{4.11}$$

and

$$I_{u_{ul}^s,u_0^k} = \sum_{j=2}^{K} \sum_{z \in \Phi_u^j} P_u h_{z,u_0^k} \beta \left| X_{z,u_0^k} \right|^{-\alpha_j}, \tag{4.12}$$

respectively. In (4.10), $h_{x,u_0^k} \sim \Gamma\left(U_{\mathrm{M}}, 1\right)$ denotes the small-scale fading channel power gain between the MBSs and the typical DL small cell MU. The distances between the typical DL small cell MU and the MBSs, the other small cell MU, and the UL small cell MU are denoted as $\left|X_{x,u_0^k}\right|$, $\left|X_{y,u_0^k}\right|$, and $\left|X_{z,u_0^k}\right|$, respectively.

4.2.3.3 UL SINR of a Small Cell MU

The UL SINR for a typical SBS b_0^k located at the origin can be written as

$$\mathrm{SINR}_k^{\mathrm{UL}} = \frac{P_u g_{o,b_0^k} \beta \left| X_{o,b_0^k} \right|^{-\alpha_k}}{P_{R_{SI}}(P_k) + I_{\mathrm{M},b_0^k} + I_{S,b_0^k} + I_{u_{ul}^s,b_0^k} + N_0}, \tag{4.13}$$

where ρ_k is the receiver sensitivity of the serving SBS, $g_{o,b_0^k} \sim \exp\left(1\right)$ is the small-scale fading channel power gain between the typical UL small cell MU and its serving SBS, $\left|X_{o,\mathrm{b}_0^k}\right|$ is the corresponding distance, and $P_{R_{SI}}(P_k)$ is the residual SI power after performing cancellation given in (4.1). In (4.13), I_{M,b_0^k}, I_{S,b_0^k}, and $I_{u_{ul}^s,b_0^k}$ are the interference from the MBSs, the other SBSs, and the other UL small cell MUs given as

$$I_{\mathrm{M},b_0^k} = \sum_{x \in \Phi_b^{\mathrm{M}}} \frac{P_{\mathrm{M}}}{U_{\mathrm{M}}} h_{x,b_0^k} \beta \left| X_{x,b_0^k} \right|^{-\alpha_{\mathrm{M}}}, \tag{4.14}$$

$$I_{S,b_0^k} = \sum_{j=2}^{K} \sum_{y \in \Phi_b^j \setminus b_0^k} P_j h_{y,b_0^k} \beta \left| X_{y,b_0^k} \right|^{-\alpha_j}, \tag{4.15}$$

and

$$I_{u_{ul}^s,b_0^k} = \sum_{j=2}^{K} \sum_{z \in \Phi_u^j \setminus o} P_u h_{z,b_0^k} \beta \left| X_{z,b_0^k} \right|^{-\alpha_j}, \tag{4.16}$$

respectively. In (4.14), $h_{x,b_0^k} \sim \Gamma(U_{\mathrm{M}}, 1)$ denotes the small-scale fading channel power gain between the typical UL small cell MU and the MBSs. The distances between the typical SBS and the MBSs, the other SBSs, and the other UL small cell MUs are denoted as $\left|X_{x,b_0^k}\right|$, $\left|X_{y,b_0^k}\right|$, and $\left|X_{z,b_0^k}\right|$, respectively.

4.2.4 Interference Characterization

Characterizing the interference in proposed HCNs is the key challenge in evaluating the system performance. The reason is the difficulty to obtain exact characteristics of the interference from the UL small cell MUs to the DL macrocell MU, $I_{u_{ul}^s,u_0^{\mathrm{M}}}$ in (8), the interference from the UL small cell MUs to the DL small cell MU, $I_{u_{ul}^s,u_0^k}$ in (12), the interference from the MBSs in the DL to the SBSs in the UL, I_{M,b_0^k} in (14), and the interference from the SBSs in the DL to the SBSs in the UL, I_{S,b_0^k} in (15). We characterize the interferences as shown in Fig. 4.1 using similar approximation as in [69]. For instance, to characterize $I_{u_{ul}^s,\mathrm{u}_0^{\mathrm{M}}}$, we consider a DL macrocell MU located at $\mathbf{a}$, its serving MBS located at $\mathbf{b}$, a FD SBS located at $\mathbf{c}$, and its associated UL MU at $\mathbf{c}+\mathbf{N}(\mathbf{c})$, where $\mathbf{N}(\mathbf{c})$ is the relative location of small cell MU to its serving SBS at $\mathbf{c}$ in the UL. Generally, the distance between DL macrocell MU $\mathbf{a}$ and FD SBS $\mathbf{c}$ is greater than the distance between $\mathbf{c}+\mathbf{N}(\mathbf{c})$ and $\mathbf{c}$, i.e., $\|\mathbf{a}-\mathbf{c}\| \gg \|\mathbf{N}(\mathbf{c})\|$. Therefore, we assume that the distance between macrocell MU at $\mathbf{a}$ and UL small cell MU at $\mathbf{c}+\mathbf{N}(\mathbf{c})$ can be approximated as the distance between a macrocell MU at $\mathbf{a}$ and the SBS at $\mathbf{c}$.

Similarly, to characterize $I_{u_{ul}^s,u_0^k}$, we assume the distance between a typical DL small cell MU and the UL small cell MU can be approximated as the distance between a typical DL small cell MU and the interfering SBS. This assumption holds true due to the reason that the distance between a typical DL small cell MU and the interfering FD SBS is greater than the distance between the FD SBS and its associated UL small cell MU. Likewise, we characterize the interferences I_{M,b_0^k} and I_{S,b_0^k}.

4.3 Performance Evaluation

In order to measure the spectral efficiency of the network, the performance of the K-tier HCNs is evaluated in terms of DL and UL average ergodic rates. Since a typical MU can associate with at most one tier, the performance of each tier as well as per tier association probability determine the overall performance of HCNs in the DL and the UL as per the law of total probability. To facilitate the analysis, we first present the per tier association probability.

DL Cell Association

Lemma 4.3.1. *The probability that a typical MU is associated with the MBS is given as*

$$\Lambda_{\mathrm{M}} = 2\pi\lambda_{b^{\mathrm{M}}} \int_0^{\infty} r \exp\Big\{ -\pi\lambda_{b^{\mathrm{M}}} r^2 - \pi \sum_{j=2}^{K} \lambda_{\mathrm{b^j}} \left(\frac{P_j}{\Psi P_{\mathrm{M}}}\right)^{2/\alpha_j} r^{2\alpha_{\mathrm{M}}/\alpha_j} \Big\} \mathrm{dr}, \tag{4.17}$$

where

$$\Psi = \frac{N - U_{\mathrm{M}} + 1}{U_{\mathrm{M}}}. \tag{4.18}$$

Proof. Please refer to Appendix B.1. □

The PDF of the distance $|X_{o,\mathrm{M}}|$ between the typical MU and its associated MBS is presented in the following lemma.

Lemma 4.3.2. *The PDF of the distance between a typical MU and its serving MBS is given by*

$$f_{|X_{o,\mathrm{M}}|}(x) = \frac{2\pi\lambda_{b^{\mathrm{M}}}}{\Lambda_{\mathrm{M}}} x \exp\left\{ -\pi\lambda_{b^{\mathrm{M}}} x^2 - \pi \sum_{j=2}^{K} \lambda_{b^j} \left(\frac{P_j}{\Psi P_{\mathrm{M}}}\right)^{2/\alpha_j} x^{2\alpha_{\mathrm{M}}/\alpha_j} \right\}, \tag{4.19}$$

where Ψ and Λ_{M} are given in (4.18) *and* (4.17)*, respectively.*

Proof. Please refer to Appendix B.2. □

The probability that a typical MU is associated with the kth tier SBS and the PDF of the distance $|X_{o,k}|$ between the typical DL MU and its serving SBS is presented in the following lemmas.

Lemma 4.3.3. *The probability that a typical MU is associated with the kth tier SBS is given as*

$$\Lambda_k^{\mathrm{DL}} = 2\pi\lambda_{b^k} \int_0^{\infty} r \exp\Big\{ -\pi \sum_{j=2}^{K} \lambda_{b^j} (P_j r^{\alpha_k}/P_k)^{2/\alpha_j} - \pi\lambda_{b^{\mathrm{M}}} \left(\frac{P_{\mathrm{M}}\Psi}{P_k}\right)^{2/\alpha_{\mathrm{M}}} r^{2\alpha_k/\alpha_{\mathrm{M}}} \Big\} \mathrm{dr}, \tag{4.20}$$

where Ψ *is given in* (4.18).

Proof. The proof follows analogous steps to Lemma 4.3.1. □

Lemma 4.3.4. *The PDF of the distance between a typical MU and its serving kth tier SBS is given by*

$$f_{|X_{o,k}|}(x)\,|_{DL} = \frac{2\pi\lambda_{b^k}}{\Lambda_k^{\mathrm{DL}}} x \exp\left\{ -\pi \sum_{j=2}^{K} \lambda_{b^j} (P_j x^{\alpha_{\mathrm{k}}}/P_k)^{2/\alpha_j} - \pi\lambda_{b^{\mathrm{M}}} \left(\frac{P_{\mathrm{M}}\Psi}{P_k}\right)^{2/\alpha_M} x^{2\alpha_k/\alpha_{\mathrm{M}}} \right\}, \tag{4.21}$$

where Ψ *and* Λ_k^{DL} *are given in* (4.18) *and* (4.20)*, respectively.*

Proof. The proof follows analogous steps to Lemma 4.3.2. □

UL Cell Association

In the UL transmission, a typical MUs can only associate with the FD SBS that offers the maximum average received power. The probability that a typical MU is associated with the kth tier SBS is given as [117]

$$\Lambda_k^{\mathrm{UL}} = 2\pi\lambda_{b^k} \int_0^{\infty} r \exp\Big\{ -\sum_{j=2}^{K} \pi\lambda_j (P_j/P_k)^{2/\alpha_j} r^{2\alpha_k/\alpha_j} \Big\} dr. \tag{4.22}$$

4.3.1 DL Average Ergodic Rate

In this section, the DL average ergodic rate of a typical MU in K-tier HCNs is derived. The DL average ergodic rate of a random MU in the K-tier HCNs is given by

$$R^{\mathrm{DL}} = \Lambda_{\mathrm{M}} R_{\mathrm{M}} + \sum_{k=2}^{K} \Lambda_k^{\mathrm{DL}} R_k^{\mathrm{DL}}, \tag{4.23}$$

where Λ_{M} and Λ_k^{DL} are given in (4.17) and (4.20), respectively, R_{M} is the DL average ergodic rate between a typical MU and its serving MBS, and R_k^{DL} is the DL average ergodic rate between a typical MU and its serving SBS.

In (4.23), the DL average ergodic rate between a typical MU and its serving MBS is defined as

$$R_{\mathrm{M}} = \mathbb{E}_{\left|X_{o,u_0^{\mathrm{M}}}\right|}\left[\mathbb{E}_{\mathrm{SINR}_{\mathrm{M}}^{\mathrm{DL}}}\left[\ln\left(1+\mathrm{SINR}_{\mathrm{M}}^{\mathrm{DL}}\left(\left|X_{o,u_0^{\mathrm{M}}}\right|\right)\right)\right]\right], \tag{4.24}$$

where $\mathrm{SINR}_{\mathrm{M}}^{\mathrm{DL}}$ is given in (4.5) and γ^{DL} is given as

$$\gamma^{\mathrm{DL}} = \mathrm{e}^{\gamma_R^{\mathrm{DL}}} - 1. \tag{4.25}$$

In (4.25), γ_R^{DL} is the DL rate threshold. Similarly, the DL average ergodic rate of typical MU at a distance $\left|X_{o,u_0^k}\right|$ from its associated SBS in the kth tier is defined as

$$R_k^{\mathrm{DL}} = \mathbb{E}_{\left|X_{o,u_0^k}\right|}\left[\mathbb{E}_{\mathrm{SINR}_k^{\mathrm{DL}}}\left[\ln\left(1+\mathrm{SINR}_k^{\mathrm{DL}}\left(\left|X_{o,u_0^k}\right|\right)\right)\right]\right], \tag{4.26}$$

where $\mathrm{SINR}_{\mathrm{k}}^{\mathrm{DL}}$ and γ_R^{DL} are given in (4.9) and (4.25), respectively.

Theorem 4.3.1. *The DL average ergodic rate of a typical MU associated with the*

MBS is derived as

$$R_{\mathrm{M}} = \frac{2\pi\lambda_{\mathrm{b^M}}}{\Lambda_{\mathrm{M}}} \int_0^{\infty}\int_0^{\infty} \left(\frac{x}{\tau+1}\right) \sum_{n=0}^{N-U_M} \frac{(x^{\alpha_M})^n}{n!(-1)^n} \sum \frac{n!}{\prod_{l=1}^{n} m_l (l!)^{m_l}} \kappa(x) \prod_{l=1}^{n} \left(\psi^{(l)}(x,\tau)\right)^{m_l} d\tau dx, \tag{4.27}$$

where

$$\kappa(x,\tau) = \exp\left\{ -\frac{\tau U_{\mathrm{M}} x^{\alpha_M} N_0}{P_{\mathrm{M}}\beta} - \zeta\left(\frac{\tau U_{\mathrm{M}} x^{\alpha_M}}{P_{\mathrm{M}}\beta}\right) - \pi\lambda_{b^{\mathrm{M}}} x^2 - \pi \sum_{j=2}^{K} \lambda_{b^k} \left(\frac{P_j}{\Psi P_{\mathrm{M}}}\right)^{\frac{2}{\alpha_j}} x^{\frac{2\alpha_{\mathrm{M}}}{\alpha_j}} \right\}, \tag{4.28}$$

$\sum_{n}$ *is over all n-tuples of non-negative integers* $(m_1, ..., m_n)$ *that satisfy the constraint* $\sum_{l=1}^{n} l\,.\,m_l = n$, Ψ *is given in* (4.18), Λ_{M} *is given by* (4.17), *and* $\zeta(.)$, $\psi^{(1)}(x,\tau)$, *and* $\psi^{(l)}(x,\tau)$ *are given as*

$$\begin{aligned}\zeta(s) =& 2\pi\lambda_{b^M} \sum_{\nu=1}^{U_M} \binom{U_M}{\nu} \left(\frac{P_M}{U_M}\beta\right)^{\nu} s^{\nu} \frac{\left(-s\frac{P_M}{U_M}\beta\right)^{-\nu+\frac{2}{\alpha_M}}}{\alpha_M} B_{\left(-s\frac{P_M}{U_M}\beta x^{-\alpha_M}\right)}\left[\nu - \frac{2}{\alpha_M}, 1 - U_M\right] \\ &+ \sum_{j=2}^{K} \pi\lambda_j \left\{ 2sP_j\beta \frac{D_j^M(x)^{2-\alpha_j}}{\alpha_j - 2} {}_2F_1\left[\frac{\alpha_j - 2}{\alpha_j}, 1; 2 - \frac{2}{\alpha_j}; -sP_j\beta(D_j^M(x))^{-\alpha_j}\right] + (sP_u\beta)^{\frac{2}{\alpha_j}} \right. \\ &\left. \Gamma\left(1 + \frac{2}{\alpha_j}\right)\Gamma\left(1 - \frac{2}{\alpha_j}\right) \right\},\end{aligned}$$

$$\begin{aligned}\psi^{(1)}(x,\tau) =& -\frac{\gamma^{\mathrm{DL}} U_M x^{\alpha_M} N_0}{P_M\beta} - 2\pi\lambda_{b^M} U_M \tau \frac{x^{2-\alpha_M}}{\alpha_M - 2} {}_2F_1\left[\frac{\alpha_M - 2}{\alpha_M}, U_M + 1; 2 - \frac{2}{\alpha_M}; -\tau\right] \\ &- \sum_{j=2}^{K} \pi\lambda_j \left\{ 2 \times \frac{\tau U_M P_j}{P_M} \frac{D_j^M(x)^{2-\alpha_j}}{\alpha_j - 2} {}_2F_1\left[\frac{\alpha_j - 2}{\alpha_j}, 2; 2 - \frac{2}{\alpha_j}; -\frac{\tau U_M P_j x^{\alpha_M}}{P_M}\right.\right. \\ &\left.\left. (D_j^M(x))^{-\alpha_j}\right] + x^{\alpha_M} \left(\frac{\tau U_M P_u x^{\alpha_k}}{P_M}\right)^{\frac{2}{\alpha_j}} \frac{2}{\alpha_j} \Gamma\left(1 + \frac{2}{\alpha_j}\right)\Gamma\left(1 - \frac{2}{\alpha_j}\right) \right\},\end{aligned}$$

and

$$\psi^{(l)}(x,\tau) = 2\pi\lambda_{b^M}\frac{(U_M+l-1)!}{(U_M-1)!}(-\tau)^{\frac{2}{\alpha_M}}\frac{\left(x^{\alpha_M}\right)^{-l+\frac{2}{\alpha_M}}}{\alpha_M}B_{(-\tau)}\left[l-\frac{2}{\alpha_M},1-U_M-l\right]+\sum_{j=2}^{K}\pi\lambda_j$$
$$\left\{2l!\left(-\frac{\tau U_M P_j}{P_M}\right)^{\frac{2}{\alpha_M}}\frac{\left(x^{\alpha_M}\right)^{-l+\frac{2}{\alpha_M}}}{\alpha_M}B_{\left(-\frac{\tau U_M P_j x^{\alpha_M}}{P_M}\left(D_j^M(x)\right)^{-\alpha_M}\right)}\left[l-\frac{2}{\alpha_M},-l\right]\right.$$
$$\left.+x^{-\alpha_M}\left(\frac{\tau U_M P_u x^{\alpha_k}}{P_M}\right)^{\frac{2}{\alpha_j}}\prod_{i=0}^{l-1}\left(\frac{2}{\alpha_j}-i\right)\Gamma\left(1+\frac{2}{\alpha_j}\right)\Gamma\left(1-\frac{2}{\alpha_j}\right)\right\}.$$

In (4.29) *and* (4.29), $D_j^{\mathrm{M}}(x)$ *is the distance between the closest interfering BS of the* j*th tier and the typical macrocell MU given as*

$$D_j^{\mathrm{M}}(x)=\left(\frac{P_j}{\Psi P_{\mathrm{M}}}\right)^{\frac{1}{\alpha_j}}x^{\frac{\alpha_{\mathrm{M}}}{\alpha_j}}, \tag{4.29}$$

where Ψ *is given in* (4.18).

Proof. Please refer to Appendix B.3. □

Theorem 4.3.2. *The DL average ergodic rate of a typical MU associated with the* k*th tier SBS is derived as*

$$R_k^{\mathrm{DL}}=\frac{2\pi\lambda_{\mathrm{b^k}}}{\Lambda_{\mathrm{k}}^{DL}}\int_0^{\infty}\int_0^{\infty}\left(\frac{x}{\tau+1}\right)\exp\left\{-\frac{\tau x^{\alpha_k}N_0}{P_k\beta}-\Xi(x,\tau)-\pi\sum_{j=2}^{K}\lambda_{\mathrm{b^j}}\left(\frac{P_j x^{\alpha_{\mathrm{k}}}}{P_k}\right)^{\frac{2}{\alpha_{\mathrm{j}}}}\right.$$
$$\left.-\pi\lambda_{\mathrm{b^M}}\left(\frac{P_{\mathrm{M}}\Psi}{P_{\mathrm{k}}}\right)x^{2\alpha_{\mathrm{k}}/\alpha_{\mathrm{M}}}\right\}d\tau dx, \tag{4.30}$$

where Ψ, Λ_k^{DL}, *and* τ *are given in* (4.18), (4.20), *and* (4.25), *respectively. In* (4.30),

$\Xi(x,\tau)$ is given as

$$\Xi(x,\tau) = 2\pi\lambda_{b^M}\sum_{\nu=1}^{U_M}\binom{U_M}{\nu}\left(\frac{\tau x^{\alpha_k}P_M}{P_k U_M}\right)^{\nu}\frac{\left(-\frac{\tau x^{\alpha_k}P_M}{P_k U_M}\right)^{-\nu+\frac{2}{\alpha_M}}}{\alpha_M}B_{\left(-\frac{\tau x^{\alpha_k}P_M}{P_k U_M}\left(D_M^k(x)\right)^{-\alpha_M}\right)}\left[\nu-\frac{2}{\alpha_M},1-U_M\right]+\sum_{j=2}^{K}\pi\lambda_j\left\{2\tau x^{\alpha_k}\frac{P_j}{P_k}\frac{\left(D_j^k(x)\right)^{2-\alpha_j}}{(\alpha_j-2)}{}_2F_1\left[\frac{\alpha_j-2}{\alpha_j},1;2-\frac{2}{\alpha_j};-\frac{\tau P_j}{P_k}(D_j^k(x))^{\alpha_k-\alpha_j}\right]+\left(\frac{\tau P_u x^{\alpha_k}}{P_k}\right)^{\frac{2}{\alpha_j}}\Gamma\left(1+\frac{2}{\alpha_j}\right)\Gamma\left(1-\frac{2}{\alpha_j}\right)\right\},$$

where $D_{\mathrm{M}}^k(x)$ is the distance between the closest interfering MBS and the typical small cell MU, and $D_j^k(x)$ is the distance between the closest interfering BS in the jth tier and the typical small cell MU, given as

$$D_{\mathrm{M}}^k(x) = \left(\frac{\Psi P_{\mathrm{M}}}{P_k}\right)^{\frac{1}{\alpha_{\mathrm{M}}}} x^{\frac{\alpha_k}{\alpha_{\mathrm{M}}}}, \tag{4.31}$$

and

$$D_j^k(x) = \left(\frac{P_j}{P_k}\right)^{\frac{1}{\alpha_j}} x^{\frac{\alpha_k}{\alpha_j}}. \tag{4.32}$$

In (4.31), *Ψ is given in* (4.18).

Proof. Please refer to Appendix B.4. □

In the following, we present the UL performance metrics which reflect the effect of the self-IC, the density of SBSs, and the transmit power of SBSs on the UL performance in the HCNs. We characterize the UL performance in terms of the UL average ergodic rate.

4.3.2 UL Average Ergodic Rate

In this section, we derive the UL average ergodic rate using

$$R^{\mathrm{UL}} = \sum_{k=2}^{K} \Lambda_k^{\mathrm{UL}} R_k^{\mathrm{UL}}, \tag{4.33}$$

where Λ_k^{UL} is given in (4.22), and C_k^{UL} is the UL rate coverage probability between a typical MU and its serving SBS defined as

$$R_k^{\mathrm{UL}} = \mathbb{E}_{\left|X_{o,b_0^k}\right|}\left[\mathbb{E}_{\mathrm{SINR}_k^{\mathrm{UL}}}\left[\ln\left(1+\mathrm{SINR}_k^{\mathrm{UL}}\left(\left|X_{o,b_0^k}\right|\right)\right)\right]\right], \tag{4.34}$$

where $\mathrm{SINR}_{\mathrm{k}}^{\mathrm{UL}}$ is given in (4.13) and γ^{UL} is given as

$$\gamma^{\mathrm{UL}} = \mathrm{e}^{\gamma_R^{\mathrm{UL}}} - 1, \tag{4.35}$$

and γ_R^{UL} is the UL rate threshold.

Theorem 4.3.3. *The UL average ergodic rate of a typical MU associated with the kth tier SBS is derived as*

$$R_k^{\mathrm{UL}} = \frac{2\pi\lambda_{b^k}}{\Lambda_k^{UL}} \int_0^{\infty}\int_0^{\infty} \left(\frac{x}{\tau+1}\right) \exp\Big\{ - \frac{\tau x^{\alpha_k}(N_0 + P_k|h_{R_{SI},k}|^2)}{P_u\beta} - \Upsilon(x,\tau) - \sum_{j=2}^{K}\pi\lambda_j (P_j/P_k)^{2/\alpha_j} x^{2\alpha_k/\alpha_j}\Big\} d\tau dx, \tag{4.36}$$

where Λ_k^{UL} *and* $|h_{R_{SI},k}|^2$ *are given in* (4.22) *and* (4.2)*, respectively. In* (4.36)*,* $\Upsilon(x,\tau)$ *is given as*

$$\Upsilon(x,\tau) = 2\pi\lambda_{b^M} \sum_{\nu=1}^{U_M} \binom{U_M}{\nu} \left(\frac{\tau x^{\alpha_k} P_M}{P_u U_M \alpha_M}\right) \frac{\Gamma\left(\nu - \frac{2}{\alpha_M}\right)\Gamma\left(U_M - \nu + \frac{2}{\alpha_M}\right)}{\Gamma(U_M)} + \sum_{j=2}^{K}\pi\lambda_j \left(\frac{\tau x^{\alpha_k}}{P_u}\right)^{\frac{2}{\alpha_j}} \Gamma\left(1+\frac{2}{\alpha_j}\right)\Gamma\left(1-\frac{2}{\alpha_j}\right)\left\{(P_j)^{\frac{2}{\alpha_j}} + (P_u)^{\frac{2}{\alpha_j}}\right\}.$$

Proof. The proof follows analogous steps to Theorem 1. □

4.4 Performance Comparison with the Conventional HD HCNs

In order to compare the performance of the proposed HCNs with FD SBSs with that of the conventional HD HCNs with HD SBSs, the average ergodic rate of a random MU in HCNs is defined as

$$R = R^{\mathrm{DL}} + R^{\mathrm{UL}}, \tag{4.37}$$

where R^{DL} and R^{UL} are given in (4.23) and (4.33), respectively. Furthermore, we define the average ergodic rate of FD small cell MUs as

$$R_{\mathrm{SBS}} = R^{\mathrm{DL}}_{\mathrm{SBS}} + R^{\mathrm{UL}}, \tag{4.38}$$

where $R^{\mathrm{DL}}_{\mathrm{SBS}}$ and R^{UL} are given in (4.23) and (4.33), respectively.

4.5 Numerical Results

In this section, we investigate the system performance in the DL and the UL in terms of the average ergodic rate of HCNs with multiuser MIMO antennas at the MBSs and FD operation at the SBSs. We plot the DL average ergodic rate and the UL average ergodic rate using (4.23) and (4.33), respectively. We validate the accuracy of the derived expressions for a two-tier HCNs with network radius $A_n = \pi(1000)^2$ km^2 consisting of HD macrocells with density $\lambda_{b^{\mathrm{M}}}$ and FD small cells with density λ_{b^2}, via Monte Carlo simulations. The interference approximations in Section 4.2.4 are not made in the simulation. The simulation is repeated and averaged over 10,000 iterations. The results presented in the figures of this section validate the accuracy of our approach to characterize the interferences and show that the assumptions made have a minor effect on the accuracy of the proposed analytical model. Unless specified, the parameter values used in this section are listed in Table 4.2.

Table 4.2: Parameter Values unless specified for HCNs with FD Small Cells

Parameter	Value	Parameter	Value
$\lambda_{b^{\mathrm{M}}}$	5×10^{-5}	λ_{b^2}	$20\lambda_{b^{\mathrm{M}}}$
P_{M}	40 dBm	P_2	33 dBm
P_u	23 dBm	U_M	5
α_{M}	3.5	α_2	4
N_0	-100 dBm	$P_k h_{LI}$	0

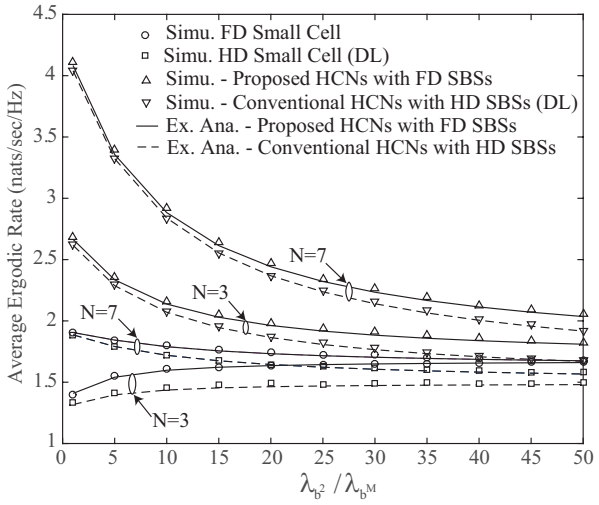

Figure 4.2: Average Ergodic Rate in a two-tier HCNs with $U_M = 2$.

4.5.1 Performance comparison of the proposed HCNs with the conventional HCNs

In Fig. 4.2, the average ergodic rate of the proposed HCNs with HD MBSs and FD SBSs is compared with that of the conventional HCNs with HD MBSs and HD SBSs. The average ergodic rate of a small cell MU in the proposed HCNs is plotted using (4.38), and that in the conventional HCNs using R_{SBS}^{DL} in (4.38) with no UL interference from the MUs, i.e., $I_{u_{ul}^s, u_0^k} = 0$ in (4.9). The average ergodic rate of a random MU in the proposed HCNs is plotted using (4.37), and that in the conventional HCNs R^{DL} in (4.37) with no UL interference from the MUs, i.e.,

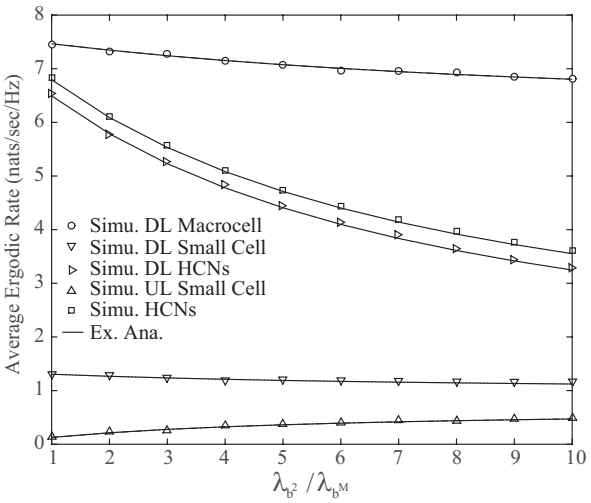

Figure 4.3: Average Ergodic Rate in a two-tier HCNs with $N = 10$.

$I_{u_{ul}^s,\mathrm{u}_0^M} = 0$ in (4.5) and $I_{u_{ul}^s,u_0^k} = 0$ in (4.9).

The average ergodic rate of a small cell MU in the proposed HCNs is observed to be higher than that in the conventional HCNs for larger λ_{b^2}. Similarly, the average ergodic rate of a random MU in the proposed HCNs is shown to be higher than that in the conventional HCNs. It is shown that the average ergodic rate improves with the increase in N due to antenna array gain. Furthermore, with the higher N, the average ergodic rate of a small cell MU and a random MU in HCNs decreases with the increase in λ_{b^2} both in the proposed and the conventional HCNs. This is due to the increased interference from the SBSs. However, with the smaller N, the average ergodic rate of small cell MU increases with the increase of λ_{b^2} both in the proposed and conventional HCNs. The smaller antenna array gain with smaller N implies larger number of MUs to be associated to the SBSs. Therefore, increasing the number of SBSs results into increased average ergodic rate of a small cell MU.

4.5.2 Impact of number of SBSs on the DL and UL average ergodic rate

Fig. 4.3 examines the effect of $\lambda_{b^2}/\lambda_{b^M}$ on the DL and UL average ergodic rate using (4.23) and (4.33), respectively. It can be observed that with the increase of $\lambda_{b^2}/\lambda_{b^M}$, the DL average ergodic rate of a typical macrocell MU, small cell MU, and random MU in HCNs decreases. This is due to the increased interference from the large number of SBSs. The UL average ergodic rate in small cells is observed to be increased with the increase in $\lambda_{b^2}/\lambda_{b^M}$. This is due to the reason that with large number of SBSs, the distance between the active MU and its serving SBS becomes smaller, which enhances the received power at the SBS. The average ergodic rate of a random MU in HCN is plotted by (4.37), which is shown to decrease with the increase of SBSs. The reason is the dominant effect of decreased DL aveage ergodic rate of both the tiers.

4.5.3 Impact of SI cancellation capability with different SBS density and SBS transmit power on the UL average ergodic rate

Fig. 4.4 plots the UL average ergodic rate versus SI cancellation capability L_{dB} using (4.33). As expected, an increase in the L_{dB} increases the UL average ergodic rate of the small cell MU. The increase of the density of SBSs increases the UL average ergodic rate of the small cell due to the decreased distance between the MU and the SBS. However, with the increase of the SBS transmit power, the UL average ergodic rate decreases due to the increase in SI.

4.6 Chapter Summary

In this chapter, a tractable model for multiuser MIMO in HCNs with FD small cells is presented. Relying on stochastic geometry, the analytical expressions for the

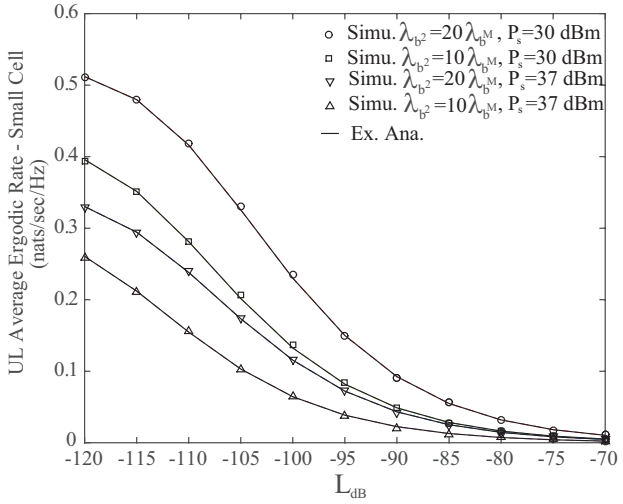

Figure 4.4: Uplink Average Ergodic Rate in a two-tier HCNs with parameters $\lambda_{b^2} = 10\lambda_{b^M}$.

DL average ergodic rate for macrocell and small cell MUs, and the UL average ergodic rate of small cell MU are derived. It is shown that the average ergodic rate of a typical MU in the proposed HCNs with FD SBSs outperforms that in conventional HCNs with HD SBSs. The average ergodic rate of the network is shown to be improved with increasing the number of antennas at the MBSs. It is observed that the UL average ergodic rate of FD small cells improves with the decreased SBS transmit power. Furthermore, increasing the number of FD SBSs results into improved UL performance but degraded DL performance.

Chapter 5

Massive Multiuser MIMO in K-tier HCNs with FD Small Cells and UL Power Control

5.1 Introduction

Alike in Chapter 4, the benefits brought by FD SBSs in HCNs for higher spectrum efficiency continues to be exploited in this chapter. The FD small cells have the potential of enhancing the spectral efficiency of the network, however, they also increase the interference due to the simultaneous DL and UL transmission on the same band which decreases coverage [72]. In order to compensate this cost, a simple solution is to employ massive multiuser MIMO at the BSs. It was shown in [43] that large scale MIMO system could be the preferred route compared to the network MIMO towards interference mitigation in multicell networks. In addition, it is found in [133] that the energy efficiency in multiuser MIMO is achieved in a massive multiuser MIMO setup wherein hundreds of antennas are deployed to serve relatively many users using regularized zero-forcing precoding. Towards this end, combining massive multiuser MIMO and small cells has shown to greatly improve the total power consumption of the network in [134]. However, due to the facts that: 1) a more powerful SI cancellation scheme is required to make FD MIMO systems feasible, and 2) the residual interference at each receive chain increase linearly with the number of antennas [135], massive multiuser MIMO is considered only at the MBSs. For the proposed HCNs, massive antennas at MBSs ensure coverage over large areas, while SBSs act as capacity-drivers [136]. Moreover, distance-proportional fractional power control is employed in the UL for: 1) mitigating the near-far problem that occurs

when a BS cannot decode the signals of cell-edge MUs due to the much greater received power (and thus interference) caused by intracell MUs, and 2) improving battery utilization of the MU [91, 92].

The performance of the DL and the UL transmission of the proposed HCNs is evaluated in terms of rate coverage probability and ASE. Most of the existing work investigates the spectral efficiency while decrease in coverage probability is not taken into account as a metric to assess the system. In this chapter, the ASE vs. coverage trade-off of the proposed HCNs is investigated as adjusting the number of antennas at MBSs with massive multiuser MIMO and the FD SBS densities affect both the link reliability and ASE of the HCNs. The aim is to find the system parameters such that some given constraints in terms of ASE or, alternatively, of rate coverage, can be achieved.

The rest of the paper is organized as follows. In Section 5.2, the system model of HCNs with massive multiuser MIMO at the MBSs and FD operation at the SBSs is discussed. In Section 5.3, the cell association model is presented and the rate coverage probability and ASE both in the DL and the UL are derived. The performance comparison of the proposed HCNs with FD SBSs with the conventional HCNs with HD SBSs is presented in Section 5.4. Finally, numerical results are discussed in Section 5.5 before the paper is summarized in Section 5.6.

The notations commonly used throughout the paper are presented in Table 5.1.

5.2 System Model

In this chapter, a K-tier HCNs is considered, where the MBSs and the SBSs are spatially located in $\mathbb{R}^2$, following HPPP, $\Phi_{b^{\mathrm{M}}}$ and Φ_{b^k} with intensity $\lambda_{b^{\mathrm{M}}}$ and λ_{b^k} ($k = 2, \cdots, K$), respectively. Massive multiuser MIMO is assumed at the MBSs, where each BS is equipped with N antennas, serving U_{M} MUs ($1 < U_{\mathrm{M}} \ll N$), and operates in HD mode. Each SBS is equipped with single antenna, and is transmitting and receiving at the same time in FD mode [123, 124]. All the MUs have single antenna and operate in HD mode. In this work, the focus is on the DL performance

Table 5.1: Frequent Notations for Massive MIMO in HCNs with FD Small Cells

Notation	Definition
P_{M}	Transmit power of MBS
P_k	Transmit power of kth tier SBS
ρ_k	Receiver's sensitivity at the kth tier SBS
ϵ	UL power control factor
α_{M}	Path loss exponent for Macrocell
α_k	Path loss exponent for kth tier small cell
G_a	Array gain of MBS antenna
β	Frequency dependent constant value
$h_{R_{SI},k}$	Residual self interfering channel of a kth tier BS
N_o	Noise power

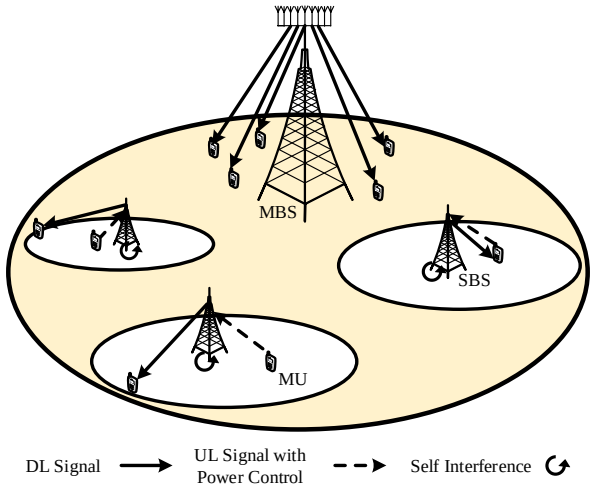

Figure 5.1: Example cells of the proposed HCNs with HD massive multiuser MIMO MBS and FD SBSs.

of the macrocell without pilot contamination, while the SBSs have transmissions in the DL and UL simultaneously due to the FD operation. The performance of the UL transmission of MBSs can be easily analyzed following the proposed method of our work. In HCNs with FD small cells, the DL and UL small cell transmissions occur

simultaneously by reusing the spectrum of the DL macrocell transmissions due to the full frequency reuse in HCNs [125]. The network is assumed to be fully-loaded, such that each MBS has U_{M} active MUs [74, 75], and each SBS serves one active DL MU and one active UL MU in each time instant [63], as shown in Fig. 5.1. Accordingly, the intensity of the active DL MUs in HCNs is $\lambda_u^{\mathrm{DL}} = (U_M \lambda_{b^M} + \sum_{k=2}^{K} \lambda_{b^k})$, whereas the active UL MUs are modeled by an independent HPPP Φ_{u^k} with intensity $\lambda_{u^k}^{\mathrm{UL}} = \lambda_{b^k}$. The analysis will be performed at a typical MU, which is assumed to be at the origin.

The channel path loss over the distance $|x|$ is modelled as $\beta|x|^{-\alpha}$, where β is the frequency dependent constant value and α is the path loss exponent. The channels are modeled as independent and identically distributed (i.i.d.) quasi-static Rayleigh fading. The TDD mode is assumed, where channel reciprocity can be exploited and allows a BS to estimate its DL channels from UL pilots sent by the MUs. Therefore, the resulting number of pilots scales linearly with the number of MUs, and is independent of the number of antennas in contrast to FDD. The TDMA is assumed, where several MUs share the same channel in different time slots, thus the BS transmit power is independent of the density of active MUs, and there is no intra-cell interference in each cell. In a snap of time, each MBS can serve U_{M} MUs and each FD SBS serves one DL and one UL MU per channel.

5.2.1 BS and MU Transmit Power Allocation

Each MBS and SBS transmit with fixed power, P_{M} and P_k, respectively. To limit the UL interference and reduce the overall power consumption of MUs, distance-proportional fractional power control [91] is employed in the UL, where the MU at a distance d from the associated SBS adjusts its transmit power to compensate large-scale fading given as

$$P_u = \rho_k \beta^{-\epsilon} d^{\epsilon \alpha_j}, \tag{5.1}$$

where $0 \leq \epsilon \leq 1$, is the power control factor, and ρ_k is the receiver sensitivity of the kth tier SBS.

5.2.2 Massive multiuser MIMO

Each MBS transmit U_{M} data streams using linear zero-forcing ZFBF with the equal transmit power allocation [43], thus the uncorrelated intra-cell interference is suppressed. Sophisticated channel estimation design with sufficient training information that guarantees perfect CSI [137] is assumed. In the training phase, each MU sends a pre-assigned orthogonal pilot sequence to the MBS, which is perfectly estimated by the MBS without pilot contamination, therefore the perfect channel state information is available at the BSs and MUs. The non-pilot contamination assumption is valid when the pre-assigned pilot sequences used in different macrocells are orthogonal to each other [138]. The maximum number of MUs per MBS depends on the dimension of the UL pilot field. Accordingly, the number of channel vectors that can be estimated and for which the DL precoder can be designed is determined. In the proposed model, the number of MU served by each MBS is assumed to be fixed.

5.2.3 SI Cancellation for FD Small Cells

The SBS in FD mode receives self-interference from its transmitted signal, and performs SI cancellation to combat it. Since, the amount of SI depends on the transmit power of the SBS, the residual SI power after SI cancellation is defined as [38, 41]

$$P_{R_{SI}}(P_k) = P_k |h_{R_{SI},k}|^2, \tag{5.2}$$

where $h_{R_{SI},k}$ is the residual self interfering channel of a kth tier BS, and $h_{R_{SI},k}$ is characterized according to the cancellation algorithms. In this chapter, a constant

value for $h_{R_{SI},k}$ is considered, similar as in Chapter 4, i.e.,

$$|h_{R_{SI},k}|^2 = 10^{L_{dB,k}/10}, \tag{5.3}$$

where $L_{dB,k}$ is the ratio between the residual self-interference after interference cancellation and the transmit power at the kth tier BS as defined in [69].

5.2.4 Cell Association

To obtain the strongest received signal, the maximum received power cell association rule is considered in the DL transmission, where the DL MU connects to the BS, which provides the maximum long-term average received power [117]. The average received power at a typical DL MU connected to the MBS m ($m \in \Phi_{b^{\mathrm{M}}}$) is expressed as

$$P_{r,\mathrm{M}} = G_a \frac{P_{\mathrm{M}}}{U_{\mathrm{M}}} \beta \left| X_{m,u^{\mathrm{M}}} \right|^{-\alpha_{\mathrm{M}}}, \tag{5.4}$$

where the array gain G_a of ZFBF transmission is $N - U_{\mathrm{M}} + 1$ [43].

The average received power at a DL MU that is connected to the kth tier SBS b^k ($b^k \in \Phi_{b^k}$), is expressed as

$$P_{r,b^k} = P_k \beta \left(\left| X_{b^k,u^k} \right| \right)^{-\alpha_k}. \tag{5.5}$$

For the UL transmission, the MUs can only associate with the FD SBSs. Considering that the HD UL MU associated to the nearest BS can maximize the UL signal-to-interference-plus-noise ratio (SINR) [63], the nearest BS cell association is considered in the UL.

Based on the cell association model, the set of interfering MUs and FD SBSs may correlate. However, to maintain model tractability, the set of interfering MUs is assumed to be independent of the set of interfering FD SBSs as in [61, 132].

5.2.5 SINR Models

5.2.5.1 DL SINR of a Macrocell MU

With massive multiuser MIMO at the MBSs, the SINR for a typical DL macrocell MU u_0^{M} located at the origin is given as

$$\mathrm{SINR}_{\mathrm{M}}^{\mathrm{DL}} = \frac{P_{\mathrm{M}}\beta\left|X_{o,u_0^{\mathrm{M}}}\right|^{-\alpha_{\mathrm{M}}}}{\underbrace{I_{\mathrm{M}_{m\mathrm{M}},u_0^{\mathrm{M}}} + I_{S,u_0^{\mathrm{M}}} + I_{u_{ul}^s,u_0^{\mathrm{M}}}}_{I_{u_o^{\mathrm{M}}}\big|_{m\mathrm{M}}} + N_0}, \tag{5.6}$$

where the massive multiuser MIMO gain, $N - U_{\mathrm{M}} + 1$, and the impact of equal power allocation per backhaul stream (i.e., the denominator of MBS's transmit power $\frac{P_{\mathrm{M}}}{U_{\mathrm{M}}}$) have been incorporated in (5.23). In (5.6), $I_{\mathrm{M}_{m\mathrm{M}},u_0^{\mathrm{M}}}$, $I_{S,u_0^{\mathrm{M}}}$, and $I_{u_{ul}^s,u_0^{\mathrm{M}}}$ are the interferences from the other MBSs, the SBSs, and the UL small cell MUs, given as

$$\begin{aligned} I_{\mathrm{M}_{m\mathrm{M}},u_0^{\mathrm{M}}} &= \sum_{x\in\Phi_b^{\mathrm{M}}\setminus o} \frac{P_{\mathrm{M}}}{U_M}\beta h_{x,u_o^M}\left|X_{x,u_0^{\mathrm{M}}}\right|^{-\alpha_{\mathrm{M}}} \\ &\overset{(a)}{\approx} \sum_{x\in\Phi_b^{\mathrm{M}}\setminus o} P_{\mathrm{M}}\beta\left|X_{x,u_0^{\mathrm{M}}}\right|^{-\alpha_{\mathrm{M}}} \end{aligned} \tag{5.7}$$

$$I_{S,u_0^{\mathrm{M}}} = \sum_{j=2}^{K}\sum_{y\in\Phi_b^j} P_j h_{y,u_o^{\mathrm{M}}}\beta\left|X_{y,u_0^{\mathrm{M}}}\right|^{-\alpha_j}, \tag{5.8}$$

and

$$I_{u_{ul}^s,u_0^{\mathrm{M}}} = \sum_{j=2}^{K}\sum_{z\in\Phi_u^j} \rho_j\beta^{-\epsilon}|R_{z,b_z}|^{\epsilon\alpha_j} h_{z,u_0^{\mathrm{M}}}\beta\left|X_{z,u_0^{\mathrm{M}}}\right|^{-\alpha_j}, \tag{5.9}$$

respectively. In (5.7), $\left|X_{x,u_0^{\mathrm{M}}}\right|$ is the distance between the interfering MBS and the typical macrocell MU, and the approximation in (a) results due to the fact that with the large number of U_{M}, i.e., $(1 < U_{\mathrm{M}} \ll N)$, the small scale channel fading vanishes by the channel hardening effect as in [80]. In (5.8) and (5.9), $h_{y,u_0^{\mathrm{M}}} \sim \exp(1)$ and $h_{z,u_0^{\mathrm{M}}} \sim \exp(1)$ denote the small-scale fading channel power gains from the SBSs to

the typical DL macrocell MU and from the UL small cell MUs to the typical DL macrocell MU, respectively, and their corresponding distances are denoted as $\left|X_{y,u_0^{\mathrm{M}}}\right|$ and $\left|X_{z,u_0^{\mathrm{M}}}\right|$, respectively. In (5.9), $\rho_j \beta^{-\epsilon} |R_{z,b_z}|^{\epsilon\alpha_j}$ is the transmit power of the UL MU at a distance of $|R_{z,b_z}|$ from its serving SBS, where ρ_j is the receiver sensitivity at the SBS of the jth tier and ϵ is the power control factor.

5.2.5.2 DL SINR of a Small Cell MU

The SINR for a typical DL small cell MU u_0^k located at the origin can be written as

$$\mathrm{SINR}_k^{\mathrm{DL}} = \frac{P_k g_{o,\mathrm{u}_0^{\mathrm{k}}} \beta \left|X_{o,u_0^k}\right|^{-\alpha_k}}{I_{\mathrm{M}_{m\mathrm{M}},u_0^k} + I_{S,u_0^k} + I_{u_{ul}^s,u_0^k} + N_0}, \tag{5.10}$$

where g_{o,u_0^k} is the small-scale fading channel power gain between the typical DL small cell MU and its serving SBS, and $\left|X_{o,u_0^k}\right|$ is the distance between the typical DL small cell MU and its serving SBS. In (5.10), $I_{\mathrm{M}_{m\mathrm{M}},u_0^k}$, I_{S,u_0^k}, and $I_{u_{ul}^s,u_0^k}$ are the interference from the MBSs, the other SBSs, and the UL small cell MUs, which are given as

$$I_{\mathrm{M}_{m\mathrm{M}},u_0^k} \overset{(a)}{\approx} \sum_{x \in \Phi_b^{\mathrm{M}} \setminus o} P_{\mathrm{M}} \beta \left|X_{x,u_0^k}\right|^{-\alpha_{\mathrm{M}}} \tag{5.11}$$

$$I_{S,u_0^k} = \sum_{j=2}^{K} \sum_{y \in \Phi_b^j \setminus o} P_j h_{y,u_0^k} \beta \left|X_{y,u_0^k}\right|^{-\alpha_j}, \tag{5.12}$$

and

$$I_{u_{ul}^s,u_0^k} = \sum_{j=2}^{K} \sum_{z \in \Phi_u^j} \rho_j \beta^{-\epsilon} |R_{z,b_z}|^{\epsilon\alpha_j} h_{z,u_0^k} \beta \left|X_{z,u_0^k}\right|^{-\alpha_j}, \tag{5.13}$$

respectively. In (5.11), $\left|X_{x,u_0^k}\right|$ is the distance between the DL small cell MU and the MBSs and the approximation in (a) results as the small scale fading factor vanishes due to channel hardening effect. The distances between the typical DL small cell MU and the other SBSs, and the UL small cell MU are denoted as $\left|X_{y,u_0^k}\right|$ and $\left|X_{z,u_0^k}\right|$,

respectively.

5.2.5.3 UL SINR of a Small Cell MU

The UL SINR for a typical SBS b_0^k located at the origin can be written as

$$\mathrm{SINR}_k^{\mathrm{UL}} = \frac{\rho_k g_{o,b_0^k} \beta^{1-\epsilon} \left| X_{o,b_0^k} \right|^{\alpha_k(\epsilon-1)}}{P_{R_{SI}}(P_k) + I_{\mathrm{M}_{m\mathrm{M}},b_0^k} + I_{S,b_0^k} + I_{u_{ul}^s,b_0^k} + N_0}, \tag{5.14}$$

where ρ_k is the receiver sensitivity of the serving SBS, $g_{o,b_0^k} \sim \exp(1)$ is the small-scale fading channel power gain between the typical UL small cell MU and its serving SBS, $\left| X_{o,\mathrm{b}_0^k} \right|$ is the corresponding distance, and $P_{R_{SI}}(P_k)$ is the residual SI power after performing cancellation given in (5.2). In (5.14), $I_{\mathrm{M}_{m\mathrm{M}},b_0^k}$ I_{S,b_0^k}, and $I_{u_{ul}^s,b_0^k}$ are the interference from the MBSs, the other SBSs, and the other UL small cell MUs given as

$$I_{\mathrm{M}_{m\mathrm{M}},b_0^k} \overset{(a)}{\approx} \sum_{x \in \Phi_b^{\mathrm{M}} \setminus o} P_{\mathrm{M}} \beta \left| X_{x,b_0^k} \right|^{-\alpha_{\mathrm{M}}} \tag{5.15}$$

$$I_{S,b_0^k} = \sum_{j=2}^{K} \sum_{y \in \Phi_b^j \setminus b_0^k} P_j h_{y,b_0^k} \beta \left| X_{y,b_0^k} \right|^{-\alpha_j}, \tag{5.16}$$

and

$$I_{u_{ul}^s,b_0^k} = \sum_{j=2}^{K} \sum_{z \in \Phi_u^j \setminus o} \rho_j \beta^{-\epsilon} |R_{z,b_z}|^{\epsilon\alpha_j} h_{z,b_0^k} \beta \left| X_{z,b_0^k} \right|^{-\alpha_j}, \tag{5.17}$$

respectively. In (5.15), $\left| X_{x,b_0^k} \right|$ is the distance between the typical SBS and interfering MBS and the approximation in (a) results as the small scale fading factor vanishes due to channel hardening effect. The distances between the typical SBS and the other SBSs, and the other UL small cell MUs are denoted as $\left| X_{y,b_0^k} \right|$ and $\left| X_{z,b_0^k} \right|$, respectively.

5.2.6 Interference Characterization

Characterizing the interference in proposed HCNs is the key challenge in evaluating the system performance. The reason is the difficulty to obtain exact characteristics of the interference from the UL small cell MUs to the DL macrocell MU, $I_{u_{ul}^s,u_0^{\mathrm{M}}}$ in (8), the interference from the UL small cell MUs to the DL small cell MU, $I_{u_{ul}^s,u_0^k}$ in (12), the interference from the MBSs in the DL to the SBSs in the UL, I_{M,b_0^k} in (14), and the interference from the SBSs in the DL to the SBSs in the UL, I_{S,b_0^k} in (15). These interferences have been characterized in Section 4.2.4 of Chapter 4, using similar approximation as in [69].

5.3 Performance Evaluation

In this section, the performance of the proposed HCNs is presented in terms of rate coverage probability and ASE. Since a typical MU can associate with at most one tier, the performance of each tier as well as per tier association probability determine the overall performance of HCNs in the DL and the UL as per the law of total probability. To facilitate the analysis, the per tier association probability is presented first.

DL Cell Association

The probability that a typical MU is associated with the MBS is derived as Lemma 4.3.1 in Chapter 4, given as

$$\Lambda_{\mathrm{M}} = 2\pi\lambda_{b^{\mathrm{M}}} \int_0^{\infty} r \exp\Big\{ -\pi\lambda_{b^{\mathrm{M}}} r^2 - \pi \sum_{j=2}^{K} \lambda_{\mathrm{b}^{\mathrm{j}}} \left(\frac{P_j}{\Psi P_{\mathrm{M}}}\right)^{2/\alpha_j} r^{2\alpha_{\mathrm{M}}/\alpha_j} \Big\} \mathrm{dr}, \tag{5.18}$$

where

$$\Psi = \frac{N - U_{\mathrm{M}} + 1}{U_{\mathrm{M}}}. \tag{5.19}$$

Similarly, the probability that a typical MU is associated with the kth tier SBS is derived as Lemma 4.3.3 in Chapter 4, given as

$$\Lambda_k^{\mathrm{DL}} = 2\pi\lambda_{b^k}\int_0^\infty r\exp\Big\{-\pi\sum_{j=2}^{K}\lambda_{b^j}(P_j r^{\alpha_k}/P_k)^{2/\alpha_j} - \pi\lambda_{b^{\mathrm{M}}}\left(\frac{P_{\mathrm{M}}\Psi}{P_k}\right)^{2/\alpha_{\mathrm{M}}} r^{2\alpha_k/\alpha_{\mathrm{M}}}\Big\}\mathrm{dr}, \tag{5.20}$$

where Ψ is given in (5.19).

(5.18) and (5.20) confirm the intuition that BS density is dominant in determining the tier association than the antenna gain and the transmit power because ($\alpha > 2$) both in practice and the considered network model. Moreover, higher antenna gain lead more MUs to connect to a macrocell when BS density and transmit power of each tier are equal or close.

UL Cell Association

In the UL transmission, a typical MUs can only associate with the nearest FD SBS. The probability that a typical MU is associated with the kth tier SBS is given as [117]

$$\Lambda_k^{\mathrm{UL}} = 2\pi\lambda_{b^k}\int_0^\infty r\exp\Big\{-\sum_{j=2}^{K}\pi\lambda_j r^{2\alpha_k/\alpha_j}\Big\}\mathrm{dr}, \tag{5.21}$$

which means that a MU prefers to associate with a tier having higher BS density. Furthermore, the BS density of each tier is the only factor in determining the UL cell association.

5.3.1 DL Rate Coverage Probability

In this section, the DL rate coverage probability of a typical MU in K-tier HCNs is derived. The DL rate coverage probability of a random MU in the K-tier HCNs is

given by

$$C^{\mathrm{DL}}(\mathrm{R}^{\mathrm{DL}}) = \Lambda_{\mathrm{M}}\mathrm{C}_{\mathrm{M}}(\mathrm{R}^{\mathrm{DL}}) + \sum_{\mathrm{k}=2}^{\mathrm{K}} \Lambda_{\mathrm{k}}^{\mathrm{DL}}\mathrm{C}_{\mathrm{k}}^{\mathrm{DL}}(\mathrm{R}^{\mathrm{DL}}), \tag{5.22}$$

where Λ_{M} and Λ_k^{DL} are given in (5.18) and (5.20), respectively, $C_{\mathrm{M}}(\mathrm{R}^{\mathrm{DL}})$ is the DL rate coverage probability of a typical macrocell MU, and $C_k^{\mathrm{DL}}(\mathrm{R}^{\mathrm{DL}})$ is the DL rate coverage probability of a typical small cell MU.

In (5.22), the DL rate coverage probability between a typical MU and its serving MBS is defined as

$$C_{\mathrm{M}}(\mathrm{R}^{\mathrm{DL}}) = \mathbb{E}_{\left|X_{o,u_0^{\mathrm{M}}}\right|}\left[\Pr\left[\mathrm{SINR}_{\mathrm{M}}^{\mathrm{DL}}\left(\left|X_{o,u_0^{\mathrm{M}}}\right|\right) \geq \gamma_{\mathrm{M}_{m\mathrm{M}}}^{\mathrm{DL}} \middle| \left|X_{o,u_0^{\mathrm{M}}}\right|\right]\right], \tag{5.23}$$

where $\mathrm{SINR}_{\mathrm{M}}^{\mathrm{DL}}$ is given in (5.6) and $\gamma_{\mathrm{M}_{m\mathrm{M}}}^{DL}$ is given as

$$\gamma_{\mathrm{M}_{m\mathrm{M}}}^{DL} = \frac{\gamma^{\mathrm{DL}}}{\Psi}, \tag{5.24}$$

In (5.24), Ψ is given in (5.19) and γ^{DL} is given as

$$\gamma^{\mathrm{DL}} = \mathrm{e}^{\mathrm{R}^{\mathrm{DL}}} - 1. \tag{5.25}$$

In (5.25), R^{DL} is the DL rate threshold. Similarly, the DL rate coverage probability of typical MU at a distance $\left|X_{o,u_0^k}\right|$ from its associated SBS in the kth tier is defined as

$$C_k^{\mathrm{DL}}(\mathrm{R}^{\mathrm{DL}}) = \mathbb{E}_{\left|X_{o,u_0^k}\right|}\left[\Pr\left[\mathrm{SINR}_k^{\mathrm{DL}}\left(\left|X_{o,u_0^k}\right|\right) \geq \gamma^{\mathrm{DL}} \middle| \left|X_{o,u_0^k}\right|\right]\right], \tag{5.26}$$

where $\mathrm{SINR}_{\mathrm{k}}^{\mathrm{DL}}$ and γ^{DL} are given in (5.10) and (5.25), respectively.

For massive multiuser MIMO at the MBSs, the DL rate coverage probability of a typical MU associated with the MBS and the kth tier SBS in Theorem 5.3.1 and Theorem 5.3.2, respectively.

Theorem 5.3.1. *For the massive multiuser MIMO regime, the DL rate coverage probability of a typical MU associated with the MBS is derived as*

$$C_{\mathrm{M}}(\mathrm{R}^{\mathrm{DL}}) = \frac{2\pi\lambda_{b^{\mathrm{M}}}}{\Lambda_{\mathrm{M}}}\int_0^\infty x\left[\frac{1}{2}-\frac{1}{\pi}\int_0^\infty \mathrm{Im}\Big[\exp\Big\{-\chi_1(x,\mathrm{w})-\pi\lambda_{b^{\mathrm{M}}}\chi_2(x,\mathrm{w}) - \sum_{j=2}^{K}2\pi\lambda_{b^j}\{\chi_3(x,\mathrm{w})+\chi_4(x,\mathrm{w})\}-\pi\lambda_{b^{\mathrm{M}}}x^2-\pi\sum_{j=2}^{K}\lambda_{b^k}\left(\frac{P_j}{\Psi P_{\mathrm{M}}}\right)^{2/\alpha_j} r^{2\alpha_{\mathrm{M}}/\alpha_j}\Big\}\Big]\right]\frac{\mathrm{dw}}{\mathrm{w}}\,\mathrm{d}x, \tag{5.27}$$

where

$$\chi_1(x,\mathrm{w}) = \mathrm{jw}\left(\frac{P_{\mathrm{M}}\beta}{\gamma^{DL}_{\mathrm{M}_{m\mathrm{M}}}x^{\alpha_{\mathrm{M}}}}-N_o\right), \tag{5.28}$$

$$\chi_2(x,\mathrm{w}) = \frac{\Gamma\left(1-\frac{2}{\alpha_{\mathrm{M}}}\right)+\frac{2}{\alpha_{\mathrm{M}}}\Gamma_u\left(-\frac{2}{\alpha_{\mathrm{M}}},\frac{-\mathrm{jw}P_{\mathrm{M}}\beta}{x^{\alpha_{\mathrm{M}}}}\right)}{(-\mathrm{jw}P_{\mathrm{M}}\beta)^{\frac{2}{\alpha_{\mathrm{M}}}}}-x^2, \tag{5.29}$$

$$\chi_3(x,\mathrm{w}) = \left(\frac{P_j^{\alpha_j/2}(-\mathrm{jw})\beta(\frac{x^{\alpha_{\mathrm{M}}}}{\Psi P_{\mathrm{M}}})^{2/\alpha_j-1}}{\alpha_j-2}\right){}_2F_1\left[1,1-\frac{2}{\alpha_j};2-\frac{2}{\alpha_j};\frac{\mathrm{jw}\Psi P_{\mathrm{M}}}{x^{\alpha_{\mathrm{M}}}}\right], \tag{5.30}$$

$$\chi_4(x,\mathrm{w}) = \int_0^\infty\int_0^{r^2}\frac{1}{1+(-\mathrm{jw}\rho_j\beta^{(1-\epsilon)})^{-1}u^{-\alpha_j\epsilon/2}r^{\alpha_j}}\Big(\pi\sum_{j=2}^{K}\lambda_{b^j}e^{-\pi\sum_{j=2}^{K}\lambda_{b^j}u}\Big)\lambda_{I_{\Phi^{\mathrm{UL}}_{bj}}}(r)\,\mathrm{d}u\,r\mathrm{d}r, \tag{5.31}$$

and Λ_{M}, $\gamma^{\mathrm{DL}}_{\mathrm{M}_{m\mathrm{M}}}$, Ψ, *and* $\lambda_{I_{\Phi^{\mathrm{UL}}_{bj}}}(r)$ *are given in* (5.18), (5.24), (5.19), *and* (C.6), *respectively.*

Proof. See Appendix C.1. □

Theorem 5.3.2. *For the massive multiuser MIMO regime, the DL rate coverage*

probability of a typical MU associated with the kth tier SBS is derived as

$$C_k^{\mathrm{DL}}(\mathrm{R}^{\mathrm{DL}}) = \frac{2\pi\lambda_{b^k}}{\Lambda_k^{\mathrm{DL}}} \int_0^\infty x \left[\frac{1}{2} - \frac{1}{\pi} \int_0^\infty \mathrm{Im}\Big[\exp\Big\{ \mathrm{j}\mathrm{w} N_o - \pi\lambda_{b^{\mathrm{M}}} \varpi_1(x,\mathrm{w}) - \sum_{j=2}^{K} 2\pi\lambda_{b^j} \{\varpi_2(x,\mathrm{w}) + \varpi_3(x,\mathrm{w})\} - \pi \sum_{j=2}^{K} \lambda_{b^j} \left(\frac{P_j x^{\alpha_k}}{P_k} \right)^{\frac{2}{\alpha_j}} - \pi\lambda_{b^{\mathrm{M}}} \left(\frac{P_{\mathrm{M}}\Psi}{P_k} \right)^{\frac{2}{\alpha_{\mathrm{M}}}} x^{\frac{2\alpha_k}{\alpha_{\mathrm{M}}}} \Big\} \left(1 + \frac{\mathrm{j}\mathrm{w} P_k \beta}{\gamma^{\mathrm{DL}} x^{\alpha_k}} \right)^{-1} \Big] \Big] \frac{dw}{\mathrm{w}} \, \mathrm{d}x, \tag{5.32}$$

where

$$\varpi_1(x,\mathrm{w}) = \frac{\Gamma\left(1 - \frac{2}{\alpha_{\mathrm{M}}}\right) + \frac{2}{\alpha_{\mathrm{M}}} \Gamma_u\left(-\frac{2}{\alpha_{\mathrm{M}}}, \frac{-\mathrm{j}\mathrm{w} P_M \beta}{(D_k^{\mathrm{M}}(x))^{\alpha_{\mathrm{M}}}} \right)}{(-\mathrm{j}\mathrm{w} P_{\mathrm{M}} \beta)^{\frac{2}{\alpha_{\mathrm{M}}}}} - \left(D_k^{\mathrm{M}}(x) \right)^2, \tag{5.33}$$

$$\varpi_2(x,\mathrm{w}) = \left(\frac{\left(\frac{P_j}{P_k}\right)^{2/\alpha_j} (-\mathrm{j}\mathrm{w}) \beta P_k (x^{\alpha_k})^{2/\alpha_j - 1}}{\alpha_j - 2} \right) {}_2F_1\Big[1, 1 - \frac{2}{\alpha_j}; 2 - \frac{2}{\alpha_j}; \frac{\mathrm{j}\mathrm{w}\beta P_j}{x^{\alpha_k}} (D_j^k(x))^{\alpha_k - \alpha_j} \Big], \tag{5.34}$$

$$\varpi_3(x,\mathrm{w}) = \int_0^\infty \int_0^{r^2} \frac{1}{1 + (-\mathrm{j}\mathrm{w}\rho_j \beta^{(1-\epsilon)})^{-1} u^{-\alpha_j \epsilon/2} r^{\alpha_j}} \Big(\pi \sum_{j=2}^{K} \lambda_{b^j} e^{-\pi \sum_{j=2}^{K} \lambda_{b^j} u} \Big) \lambda_{I_{\Phi_{b^j}^{\mathrm{UL}}}}(r) \, \mathrm{d}u \, r \mathrm{d}r, \tag{5.35}$$

and Λ_k^{DL}, γ^{DL}, Ψ, *and* $\lambda_{I_{\Phi_{b^j}^{\mathrm{UL}}}}(r)$ *are given in* (5.20), (5.25), (5.19), *and* (C.6), *respectively. In* (5.33), $D_k^{\mathrm{M}}(x)$ *is the distance between the closest interfering MBS and the typical small cell MU, and in* (5.34), $D_j^k(x)$ *is the distance between the closest interfering BS in the* j*th tier and the typical small cell MU, given respectively, as*

$$D_{\mathrm{M}}^k(x) = \left(\frac{\Psi P_{\mathrm{M}}}{P_k} \right)^{\frac{1}{\alpha_{\mathrm{M}}}} x^{\frac{\alpha_k}{\alpha_{\mathrm{M}}}}, \tag{5.36}$$

and

$$D_j^k(x) = \left(\frac{P_j}{P_k} \right)^{\frac{1}{\alpha_j}} x^{\frac{\alpha_k}{\alpha_j}}, \tag{5.37}$$

In (5.36), Ψ *is given in* (5.19).

Proof. The proof follows analogous steps to Theorem 5.3.1. □

5.3.2 DL Area Spectral Efficiency

The DL ASE measures the capacity of HCNs in the DL defined by [74, 139, 140]. In this section, we define the DL ASE of the proposed model as

$$\mathrm{ASE}^{\mathrm{DL}} = \underbrace{\lambda_{b^{\mathrm{M}}} U_{\mathrm{M}} C_{\mathrm{M}}(\mathrm{R}^{\mathrm{DL}}) \ln(1+\gamma^{\mathrm{DL}})}_{\mathrm{ASE}^{\mathrm{DL}}_{MBS}} + \underbrace{\sum_{k=2}^{K} \lambda_{b^k} C_k^{\mathrm{DL}}(\mathrm{R}^{\mathrm{DL}}) \ln(1+\gamma^{\mathrm{DL}})}_{\mathrm{ASE}^{\mathrm{DL}}_{SBS}}, \tag{5.38}$$

where $C_{\mathrm{M}}(\mathrm{R}^{\mathrm{DL}})$, $C_k^{\mathrm{DL}}(\mathrm{R}^{\mathrm{DL}})$, and γ^{DL} are given in (5.27), (5.32), and (5.25), respectively.

In the following, the UL performance metrics is presented which reflect the effect of the self-IC, the density of SBSs, the transmit power of SBSs, and the power control on the UL performance in the HCNs. The UL performance is characterized in terms of the UL rate coverage probability and the UL ASE.

5.3.3 UL Rate Coverage Probability

In this section, we derive the UL rate coverage probability using

$$C^{\mathrm{UL}}(\mathrm{R}^{\mathrm{UL}}) = \sum_{k=2}^{K} \Lambda_k^{\mathrm{UL}} C_k^{\mathrm{UL}}(\mathrm{R}^{\mathrm{UL}}), \tag{5.39}$$

where Λ_k^{UL} is given in (5.21), and C_k^{UL} is the UL rate coverage probability between a typical MU and its serving SBS defined as

$$C_k^{\mathrm{UL}}(\mathrm{R}^{\mathrm{UL}}) = \mathbb{E}_{\left|X_{o,b_0^k}\right|}\left[\Pr\left[\mathrm{SINR}_k^{\mathrm{UL}}\left(\left|X_{o,b_0^k}\right|\right) \geq \gamma^{\mathrm{UL}} \middle| \left|X_{o,b_0^k}\right|\right]\right], \tag{5.40}$$

where $\mathrm{SINR}_{\mathrm{k}}^{\mathrm{UL}}$ is given in (5.14) and γ^{UL} is given as

$$\gamma^{\mathrm{UL}} = \mathrm{e}^{\mathrm{R}^{\mathrm{UL}}} - 1, \tag{5.41}$$

and R^{UL} is the UL rate threshold.

Theorem 5.3.3. *For the massive multiuser MIMO regime, the UL rate coverage probability of a typical MU associated with the kth tier SBS is derived as*

$$\begin{aligned} C_k^{\mathrm{UL}}(\mathrm{R}^{\mathrm{UL}})\Big|_{m\mathrm{M}} =& \frac{2\pi\lambda_{b^k}}{\Lambda_k^{\mathrm{UL}}} \int_0^\infty x \Bigg[\frac{1}{2} - \frac{1}{\pi} \int_0^\infty \mathrm{Im}\Bigg[\exp\Big\{ \mathrm{j}\mathrm{w} N_o - \pi\lambda_{b^{\mathrm{M}}} \vartheta_1(x,\mathrm{w})) - \sum_{j=2}^{K} 2\pi\lambda_{b^j} \\ & \{\vartheta_2(x,\mathrm{w}+\vartheta_3(x,\mathrm{w})\} - \sum_{j=2}^{K} \pi\lambda_{b^j} x^{\frac{2\alpha_k}{\alpha_j}} \left(\frac{P_j}{P_k}\right)^{\frac{2}{\alpha_j}} \Big\} \left(1 + \frac{\mathrm{j}\mathrm{w}\rho_k x^{\alpha_k\epsilon}\beta^{-\epsilon}\beta}{\gamma^{UL} x^{\alpha_k}}\right)^{-1} \\ & \Bigg]\Bigg] \frac{\mathrm{d}\mathrm{w}}{\mathrm{w}}\, dx, \end{aligned} \tag{5.42}$$

where

$$\vartheta_1(x,\mathrm{w}) = (-\mathrm{j}\mathrm{w} P_{\mathrm{M}}\beta)^{\frac{2}{\alpha_{\mathrm{M}}}} \Gamma\left(1 - \frac{2}{\alpha_{\mathrm{M}}}\right), \tag{5.43}$$

$$\vartheta_2(x,\mathrm{w}) = (-\mathrm{j}\mathrm{w} P_j\beta) \frac{x^{2-\alpha_j}}{(\alpha_j - 2)} {}_2F_1\left[1, 1 - \frac{2}{\alpha_j}; 2 - \frac{2}{\alpha_j}; \frac{\mathrm{j}\mathrm{w}\beta P_j}{x^{\alpha_k}} x^{(\alpha_k - \alpha_j)}\right], \tag{5.44}$$

$$\vartheta_3(x,\mathrm{w}) = \int_0^\infty \int_0^{r^2} \frac{1}{1 + \left(-\mathrm{j}\mathrm{w}\rho_j\beta^{1-\epsilon}\right)^{-1} u^{-\alpha_j\epsilon/2} r^{\alpha_j}} \Big(\pi \sum_{j=2}^{K} \lambda_{b^j} e^{-\pi \sum_{j=2}^{K} \lambda_{bj} u}\Big) \mathrm{d}u\, r\mathrm{d}r, \tag{5.45}$$

and Λ_k^{UL} and γ^{UL} are given in (5.21) *and* (5.41)*, respectively.*

Proof. The proof follows analogous steps to Theorem 5.3.1. □

5.3.4 UL Area Spectral Efficiency

In this section, we derive the UL ASE in the K-tier HCNs. The UL ASE measures the capacity of HCNs in the UL, given as

$$\mathrm{ASE}^{\mathrm{UL}} = \sum_{k=2}^{K} \lambda_{b^k} C_k^{\mathrm{UL}}(\mathrm{R}^{\mathrm{UL}}) \ln(1+\gamma^{\mathrm{UL}}), \tag{5.46}$$

where $C_k^{\mathrm{UL}}(\mathrm{R}^{\mathrm{UL}})$ and γ^{UL} are given in (5.42) and (5.41), respectively.

5.4 Performance Comparison with the Conventional HD HCNs

In order to compare the performance of the proposed HCNs with FD SBSs with that of the conventional HD HCNs with HD SBSs, we define the total ASE of a random MU in HCNs as

$$\mathrm{ASE} = \mathrm{ASE}^{\mathrm{DL}} + \mathrm{ASE}^{\mathrm{UL}}, \tag{60}$$

where $\mathrm{ASE}^{\mathrm{DL}}$ and $\mathrm{ASE}^{\mathrm{UL}}$ are given in (5.38) and (5.46), respectively. Furthermore, we define the ASE of FD small cell MUs as

$$\mathrm{ASE}_{\mathrm{SBS}} = \mathrm{ASE}_{\mathrm{SBS}}^{\mathrm{DL}} + \mathrm{ASE}^{\mathrm{UL}}, \tag{61}$$

where $\mathrm{ASE}_{\mathrm{SBS}}^{\mathrm{DL}}$ and $\mathrm{ASE}^{\mathrm{UL}}$ are given in (5.38) and (5.46), respectively.

5.5 Numerical Results

In this section, the system performance in the DL and the UL is investigated in terms of the rate coverage probability and the ASE of HCNs with massive multiuser MIMO antennas at the MBSs and FD operation at the SBSs. The

Table 5.2: Parameter Values unless specified for Massive MIMO in HCNs with FD Small Cells

Parameter	Value	Parameter	Value
$\lambda_{b^{\mathrm{M}}}$	5×10^{-5}	μ	20
P_{M}	40 dBm	P_2	33 dBm
α_{M}	3.5	α_2	4
ρ_2	-40 dBm	ϵ	0.9
R^{DL}	0.5 nats/sec/Hz	R^{UL}	0.5 nats/sec/Hz
N_0	-100 dBm	$P_k h_{LI}$	0
N	128	U_{M}	5

performance of HCNs with multiuser MIMO at MBSs and FD at SBSs is compared with that of massive multiuser MIMO at MBSs and FD at SBSs. The DL rate coverage probability, the DL ASE, the UL rate coverage probability, and the UL ASE are plotted using (5.22), (5.38), (5.39), and (5.46), respectively. The accuracy of the derived expressions is validated for a two-tier HCNs with network radius $A_n = \pi(1000)^2$ km^2 consisting of HD macrocells with density $\lambda_{b^{\mathrm{M}}}$ and FD small cells with density λ_{b^2}, via Monte Carlo simulations. The interference approximations in Section II-H are not made in the simulation. The simulation is repeated and averaged over 10,000 iterations. The results presented in the figures of this section validate the accuracy of our approach to characterize the interferences and show that the assumptions made have a minor effect on the accuracy of the proposed analytical model. Unless specified, the parameter values used in this section are listed in Table 5.2.

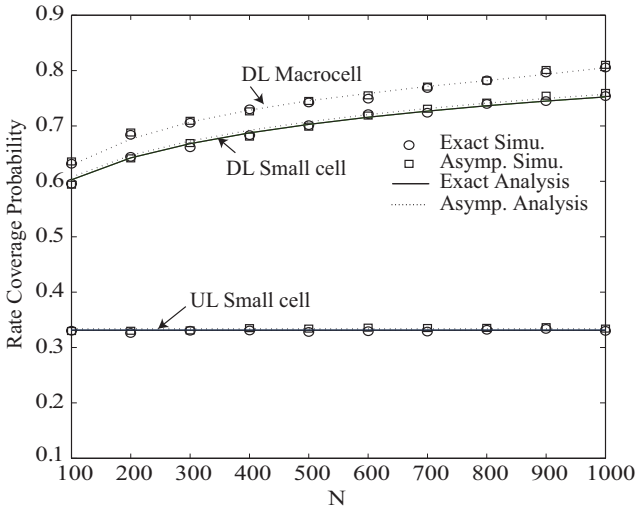

Figure 5.2: Rate coverage probability versus the number of MBS antennas.

5.5.1 Impact of number of massive multiuser MIMO antennas at the MBS on the DL and UL Rate Coverage Probability

Fig. 5.2 plots the DL and the UL rate coverage probability with massive multiuser MIMO at the MBS as a function of the number of antennas N at the MBS. As expected, the DL rate coverage probabilities of the macrocell MU and the small cell MU in massive multiuser MIMO case increases with N due to the large antenna array gain. However, the UL rate coverage probability of MU remains constant with increasing N due to that: 1) the UL MU can only associate with the SBSs, and 2) the interferences from N MBS antennas do not add coherently such that for the same total transmit power, the interference level from a MBS to an UL MU is the same, regardless of the number of N under i.i.d. Rayleigh fading channels.

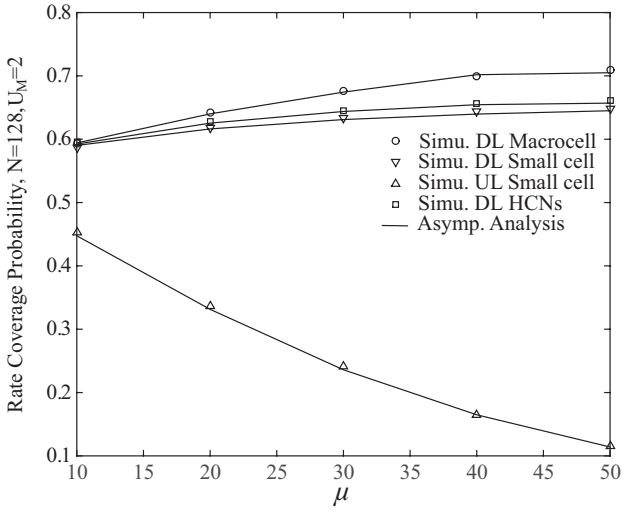

Figure 5.3: Rate coverage probability versus the ratio between SBSs density to MBSs density.

5.5.2 Impact of number of SBSs density on the DL and UL rate coverage probability

Fig. 5.3 compares the DL and the UL rate coverage probability with massive multiuser MIMO at the MBS as a function of the ratio between the SBSs density to the MBSs density ($\mu = \lambda_{b^2}/\lambda_{b^{\mathrm{M}}}$). The increase in λ_{b^2} improves the DL rate coverage probabilities of macrocell MU and small cell MU. This is according to the fact that increasing λ_{b^2} decreases the distance between the typical small cell MU and the serving SBS. Thus, the MUs transmit with less power due to distance-proportional fractional power control, which in turn reduces the UL interference for the macrocell MU and the small cell MU. However, increasing λ_{b^2} decreases the UL rate coverage probability due to the increased interference from larger number of SBSs.

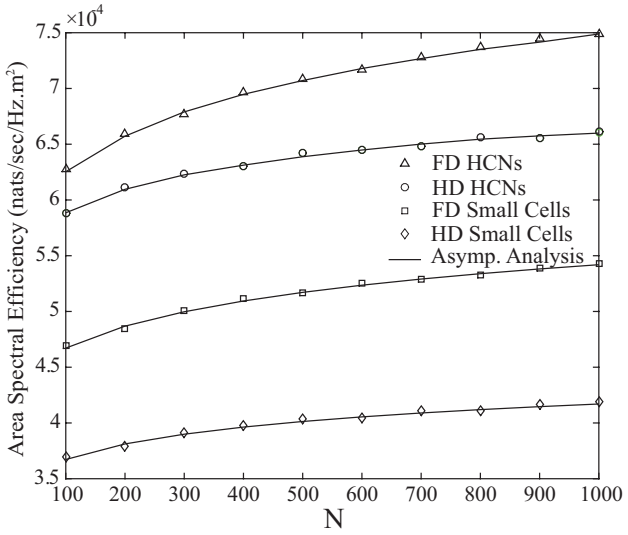

Figure 5.4: ASE versus the number of MBS antennas.

5.5.3 Performance comparison of the proposed HCNs with the conventional HCNs

Fig. 5.4 compares the ASE of the proposed HCNs with FD SBSs to that of the conventional HCNs with HD SBSs. The ASE of a random MU in the proposed HCNs is plotted using (60), and that in the conventional HCNs using ASE^{DL} in (5.38) with no UL interference from the MUs, i.e., $I_{u_{ul}^s,u_0^{\text{M}}} = 0$ in (5.6) and $I_{u_{ul}^s,u_0^k} = 0$ in (5.10). The ASE of a small cell MU of the proposed HCNs is plotted using (61), and that of conventional HCNs using $\text{ASE}_{\text{SBS}}^{\text{DL}}$ in (5.38) with no UL interference from the MUs, i.e., $I_{u_{ul}^s,u_0^k} = 0$ in (5.10). The ASE of the proposed HCNs is observed to be higher than that of the conventional HCNs. This suggests the ASE improvement brought by simultaneous transmission in DL and UL due to FD SBSs which dominates the resulting additional interferences. With the increase in the number of antennas at the MBSs, the ASE of the HCNs increases due to the increase in the rate coverage probability with larger N as shown in Fig. 5.2. Moreover, similar trends are observed for the small cell tier with improved ASE than that of the HCNs.

5.5.4 Impact of SBS density with different number of MBS antennas on the DL Performance

Fig. 5.5 (a) and Fig. 5.5 (b) examine the trade-off between the DL ASE and the DL rate coverage probability versus the ratio between density of SBSs to density of MBS ($\mu = \lambda_{b^2}/\lambda_{b^M}$) and the number of MBS antennas both for multiuser MIMO and massive multiuser MIMO at the MBSs. In Fig. 5.5 (a) and Fig. 5.5 (b), $\epsilon = 0$ and the transmit power at the MU P_u is taken as 23 dBm. Clearly, the DL ASE and rate coverage probability with massive multiuser MIMO at the MBS are higher as compared to those with multiuser MIMO at the MBSs due to sharp beamforming. The massive number of antennas at MBSs brings the higher DL rate coverage probability and ASE.

The DL ASE and the rate coverage probability of macrocell MU decreases with increasing the SBSs density due to the increased interference from SBSs. However, increasing the SBSs density λ_{b^k} increases the DL ASE, but decreases the DL rate coverage probability of small cell MU. With the increase in the SBSs density, the number of DL small cell transmissions and the aggregate interference from small cells increase, which results in a trade-off between DL ASE and rate coverage probability for the small cell MUs. It is shown that the UL interference can be reduced by employing UL power control in the UL, which improves the DL rate coverage probability in Fig. 5.3.

5.5.5 Impact of SBS density with different MBS and SBS transmit powers on the DL and UL Performance

Fig. 5.6 plots the DL and UL ASE and rate coverage probability as a function of the transmit powers at the MBSs and SBSs. In Fig. 5.6, $\epsilon = 0$ and the transmit power at the MU P_u is taken as 23 dBm. Increasing the MBS transmit power increases the DL ASE and the rate coverage probability of all tiers, which is due to the increase of $\mathrm{SINR}_{\mathrm{M}}^{\mathrm{DL}}$ in (5.6), and the reduced distance between the typical small cell MU

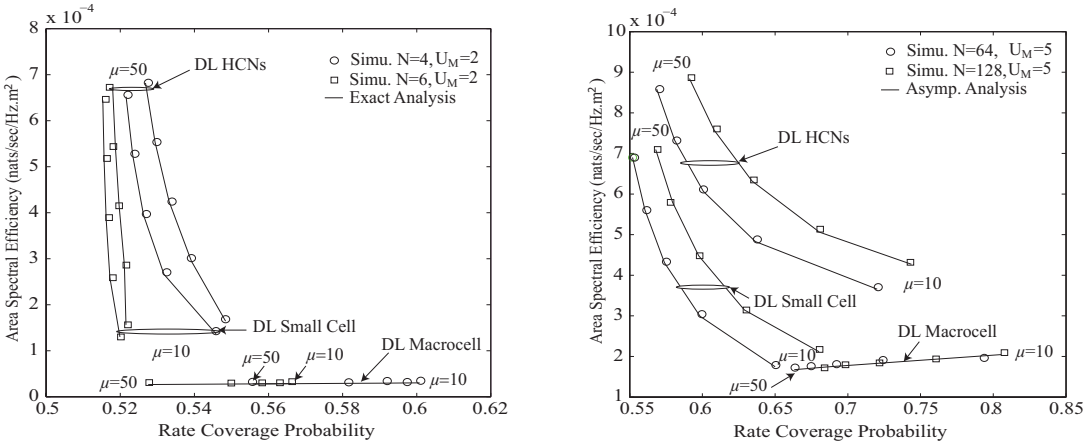

(a) ASE versus Rate Coverage Probability, multiuser MIMO.

(b) ASE versus Rate Coverage Probability, massive multiuser MIMO.

Figure 5.5: The tradeoff between the ASE and the rate coverage probability for various number of MBS antennas.

and the associated SBS. Moreover, the decrease in the UL ASE and the UL rate coverage probability is observed with the increase in P_{M} and P_k, which is due to the increased cross-tier and co-tier interferences as can be seen from (5.14). Furthermore, it is observed that the increase in the SBS density increases the UL rate coverage probability in contrast to the decreased DL rate coverage probability for small cell MU as shown in Fig. 5.5 (a) and Fig. 5.5 (b), which is due to the decreased distance between the UL small cell MU and the serving SBS. It can thus be concluded that the increase in the BS transmit power of each tier improves the DL performance in contrast to the degradation in the UL performance. On the other hand, the increase in the FD SBS density degrades the DL rate coverage probability whereas improves the UL rate coverage probability. However, both the DL and UL ASE are observed to be improved with the increase in FD SBSs density.

5.5.6 Impact of SI cancellation capability with different SBS transmit power on the DL and UL Performance

Fig. 5.7 examines the impact of the SI cancellation capability L_{dB} on the DL and UL rate coverage probabilities. As expected, increasing L_{dB} decreases the UL

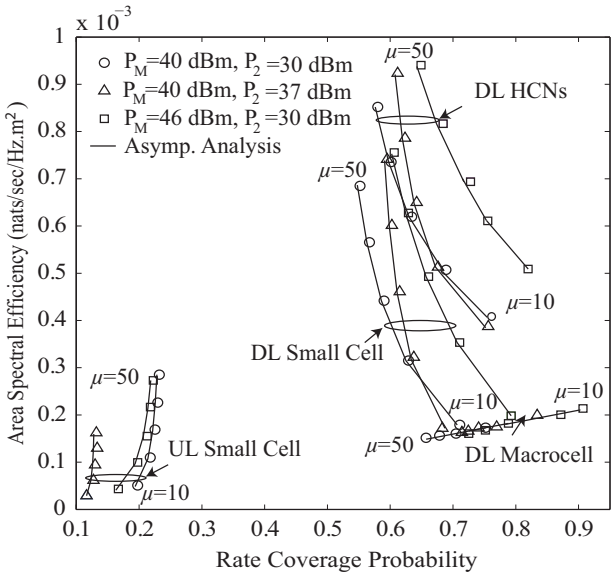

Figure 5.6: The tradeoff between the ASE and the rate coverage probability for various MBS and SBS transmit powers.

rate coverage probability of the small cell MU. Moreover, increasing the SBS transmit power decreases the UL rate coverage probability of the small cell MU, due to the increased self interference. However, increasing the SBS transmit power increases the DL rate coverage probability of a random MU, due to the increase of $\mathrm{SINR}_{\mathrm{k}}^{\mathrm{DL}}$ in (5.14).

5.5.7 Impact of receiver sensitivity at the SBS with different power control factors

Fig. 5.8 plots the DL and the UL rate coverage probability versus the receiver's sensitivity at SBSs ρ_2 for various power control factors ϵ. Increasing ρ_2 increases the UL rate coverage probability, and degrades the DL rate coverage probability. This is due to the reason that decreasing the the SBS receiver sensitivity (i.e., an increase in ρ_2) increases the transmit power required at each MU to perform channel inversion towards serving SBS, which in turn increases the useful signal power at the its associated SBS and the interference at the other BSs and MUs. Similarly,

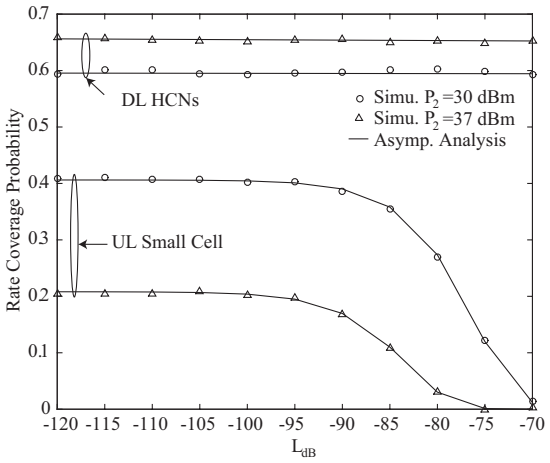

Figure 5.7: Rate coverage probability versus SI cancellation capability for various SBSs transmit powers.

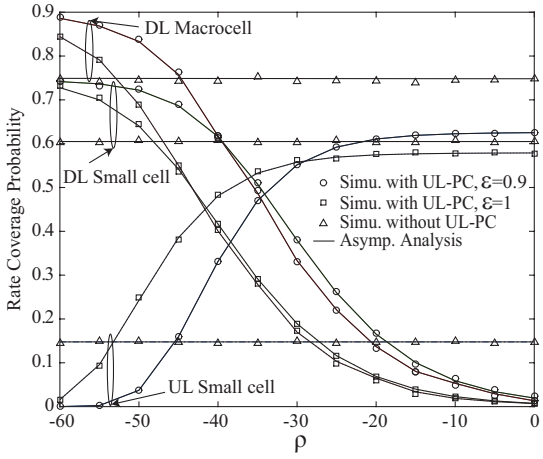

Figure 5.8: Rate coverage probability versus SBSs receivers sensitivity for various SBSs power control factors.

higher power control factor ϵ improves the UL performance, but degrades the DL performance. These results demonstrate that ρ_2 and ϵ can be optimized for joint DL and UL performance gain. The DL and UL performance of HCNs with UL power control is also compared to that without UL power control when the MUs transmit power is $P_u = 23$ dBm. The UL rate coverage probability in HCNs without UL power control is shown to be very small due to the increased inter-cell interference from the UL MUs.

5.6 Chapter Summary

In this chapter, a tractable model for massive multiuser MIMO-enabled HCNs with FD small cells and UL power control is investigated. Relying on stochastic geometry, the analytical expressions for DL rate coverage probability and ASE for macrocell and small cells, and UL rate coverage probability and ASE for small cells are derived. Numerical results demonstrated the benefits brought by massive multiuser MIMO in achieving high rate coverage probability and the benefits brought by of FD SBSs in achieving high ASE. It is shown that the SBSs density and the number

of antennas at the MBSs can be used as design parameters to target optimal DL ASE and DL rate coverage probability. The results also demonstrate that, to achieve similar performance in the DL and the UL, UL power control should be employed. With the advancements of massive multiuser MIMO and SI cancellation in FD, the proposed HCNs will prove to be a promising candidate for 5G systems.

Chapter 6

Conclusions and Future Work

In this chapter, the main conclusions of the works in this thesis are presented. Some interesting future research directions are also explored in Section 6.2.

6.1 Summary of Contributions

To cope with sheer volume of data for emerging future applications, such as smart cities, health monitoring devices, and driverless cars, and to meet with the escalating growth of the number of devices and the data rates, the next generation networks need to be a paradigm shift that includes dense base station and unprecedented numbers of antennas. Alongside, the energy efficiency of the communication network becomes even more critical consideration and will need to improve by at least the same amount as the data rate just to maintain the power consumption. This evokes the rise of efficient spectrum and energy utilization techniques for future wireless communications.

It is the aim of this thesis to investigate various heterogeneous network architectures with state-of-the-art spectral and energy efficient technologies. In this dissertation, the HCNs are modeled using random spatial models, where the locations of the BSs are assumed to form a realization of a spatial point process. The analysis presented is tractable which helps to gain system design insights using tools from stochastic geometry and spatial statistics. Since each chapter presents an independent network model, the main contributions of the thesis are summarized below with concluding remarks.

Chapter 3 is concerned with SWIPT in K-tier HCNs, where the information is

decoded and energy is harvested from the DL signal using power splitting protocol. The harvested energy is then utilized for UL information transmission. A tractable model using stochastic geometry was built to analyze the DL wireless power transfer and information transmission and UL information transmission with the NBS and the MRP cell associations. The average received power at MUs, the DL and the UL outage probabilities and average ergodic rates were derived to demonstrate the intrinsic relationship between the energy harvested from the BSs in the DL and the MUs performance in the DL and the UL. It is concluded that the small cell BS density improves the DL performance of macrocell and picocell MUs with the NBS cell association, whereas has little impact on that with the MRP cell association. Moreover, increasing the small cell BSs improves the UL performance of both macrocell and picocell MUs with the NBS cell association, whereas degrades that with the MRP cell association. By increasing the fraction of the received power used for harvesting energy, the UL performance is shown to be improved, whereas by increasing the SBSs density, the energy efficiency is improved.

Motivated by the recent advancements in SI cancellation capability of low-power wireless devices, FD SBSs in K-tier HCNs were considered in Chapter 4 with the benefits brought by FD communications. The FD small cell tier allows the use of same frequency spectrum for the DL as well as the UL transmissions of the small cells concurrently. The performance of the MU in the considered network is limited by several sources of interferences, such as the SBS in the DL to SBS in the UL interference and the SI, which were characterized in this work. A framework that models the DL and the UL average ergodic rates of a MU in the proposed HCNs with HD multiuser MIMO MBSs and FD SBSs is developed using tools from stochastic geometry. Numerical results compare the performance of the proposed HCNs with FD SBSs to that of the conventional HCNs with HD SBSs and the former is shown to outperform the later. It is also demonstrated that maintaining a correct density of FD small cells and appropriate SI cancellation value is crucial in achieving a desirable performance in both the DL and the UL.

Finally, Chapter 5 is built upon the K-tier HCNs with FD small cells proposed in Chapter 4, where massive multiuser MIMO are employed at the macrocells to improve the coverage performance that otherwise degrades by the DL, the UL, and the self interferences due to the FD small cells. It also considers the UL power control which benefits from maximizing the UL received signal power while limiting the generated interference. Using stochastic geometry analysis, the analytical expressions for the DL rate coverage probability, the DL ASE of the macrocells and small cells, the UL rate coverage probability, and the UL ASE of small cells are derived to evaluate the link reliability and spectral efficiency. Performance evaluation demonstrate the effectiveness of massive multiuser MIMO at the MBSs and the FD SBSs in enhancing the rate coverage probabilities and the ASEs. Additionally, one interesting conclusion is that the distance-proportional fractional power control can be tuned to achieve a desirable performance in both DL and UL, where decreasing the power control factor degrades the UL rate coverage probability, but improves the DL rate coverage probability.

6.2 Future Research

Several interesting future directions are highlighted as follows, which are deemed to be worthy of further investigation based on the results attained in this thesis.

6.2.1 Massive MIMO enabled SWIPT based HCNs

It would be interesting to investigate the potential gain in spectral and energy efficiency by considering massive MIMO technique to SWIPT based WPCNs. Massive MIMO employs a large number of antennas at the BS to exploit the high antenna array gain. The large antenna array improves the throughput by providing large degree of freedom, as well as enhances the received signal power by generating very sharp beams. Massive MIMO will thus boost the performance of WPCNs both in terms of spectrum and energy efficiency. Future work will also include the

analysis for a battery free MU with UL power control, where the probability that the instantaneous received power is sufficient to perform channel inversion power control need to be evaluated along with the coverage probability. Moreover, the network parameters, such as the time allocation factor, the power splitting factor could be optimized for the improved SWIPT based HCNs.

6.2.2 SI Channel Modeling

More recently, Rician fading model has been used for SI channel modeling in the stochastic geometry based analysis of FD communication networks, where the SI channel is treated as a random variable and the performance metric is obtained by averaging out over the SI channel distribution. An exciting area is to model and analyze SI aware fractional power control, where the MUs adjust their transmit power based on the distance-dependent path-loss, SI, and maximum available transmit power.

6.2.3 Pilot Contamination at massive MIMO BSs

Most of the literature assume no pilot contamination in massive MIMO enabled cellular networks, which might not be practical in reality. In Chapter 5, non-pilot contamination is assumed at massive MIMO MBSs, where each MU sends a pre-assigned orthogonal pilot sequence to the MBS, which is perfectly estimated by the MBS. It would be interesting to include the impact of pilot contamination, where additional interferences from those MBSs, which use the same pilot sequences would be considered.

6.2.4 Stochastic Geometry based Analysis of Distributed Antenna Systems

A distributed antenna system (DAS) is also one of the promising technologies to effectively improve spectral and energy efficiency of wireless communications. The

DAS is implemented with multiple distributed antennas through BSs located in different cells, thus can mitigate large-scale fading using many antennas distributed geographically. Since practical remote antennas in the DAS may be placed at arbitrary locations to cover the dead spots, therefore can be modeled as a spatial random process. Analysing the DAS using tools from stochastic geometry would be an interesting study. More interesting would be to compare the DAS with massive antenna ports (APs) to the co-located massive MIMO technique.

6.2.5 More Realistic Spatial Models for MU and BS/AP locations

With the exponential growth of mobile data traffic, the SBSs are deployed densely and there exists spatial coupling between MU and BS locations. Accordingly, modeling the HCNs with HPPP is not rich enough to capture the clustering of nodes that exists in real-world HCNs deployments. Recently, there has been great interest to reduce this ever-increasing gap between the PPP-based HCNs model and the real-world deployments by modeling a fraction of MUs and an arbitrary number of BS tiers using Poisson cluster processes (PCPs). In the next work, the distributed antenna ports within each cell in DASs will be modeled by PCP to account for the randomness in the topology of DAS.

Appendix A

Proofs from Chapter 3

A.1 Proof of Lemma 3.3.1

The average value of $I_{b_{\widehat{k}}}$ in (3.4) is derived as follows

$$\begin{aligned}\mathbb{E}[I_{b_{\widehat{k}}}] &= \mathbb{E}\left[P_{t,b_{\widehat{k}}}|h_{b_{\widehat{k}},u_0}|^2 L_0\big(\max\left\{\left\|\boldsymbol{x}_{b_{\widehat{k}},u_0}\right\|,d\right\}\big)^{-\ell_k}\right] \\ &\overset{(a)}{=} P_{t,b_{\widehat{k}}} L_0\left[\int_0^d d^{-\ell_k} f_{\left\|\boldsymbol{x}_{b_{\widehat{k}}}\right\|}(x)\mathrm{d}x + \int_d^\infty x^{-\ell_k} f_{\left\|\boldsymbol{x}_{b_{\widehat{k}}}\right\|}(x)\mathrm{d}x\right], \end{aligned} \tag{A.1}$$

where (a) follows from the fact that $|h_{b_{\widehat{k}}}|^2 \sim \exp(1)$. In (A.1), the PDF of $\left\|\boldsymbol{x}_{b_{\widehat{k}}}\right\|$ with the NBS cell association is given by [117]

$$f_{\left\|\boldsymbol{x}_{b_{\widehat{k}}}\right\|}(x)\big|_{\mathrm{NBS}} = 2\kappa x \exp\{-\kappa x^2\}, \tag{A.2}$$

where κ is given in (3.14).

Substituting (A.2) into (A.1), and simplifying the resulting equation using [119, eq. 3.381.1] and [119, eq. 3.381.6], $\mathbb{E}[I_{b_{\widehat{k}}}]$ is derived. Further, the average value of I_{b_x} is derived as

$$\mathbb{E}[I_{b_x}] = \sum_{j=1}^{K} \mathbb{E}_h\left[P_{t,b_j} L_0 |h_{b_j u_0}|^2\right] \mathbb{E}_x\left[\mathbb{E}_{\Phi_j}\Big[\sum_{b_j \in \Phi_j \setminus b_{\widehat{k}}} \big(\max\left\{\left\|\boldsymbol{x}_{b_j u_o}\right\|,d\right\}\big)^{-\ell_j}\Big]\right]. \tag{A.3}$$

The interfering BSs need to be located outside a disc of a radius $r_{min} = \left\|\boldsymbol{x}_{b_{\widehat{k}}}\right\| = x$ to satisfy the NBS cell association. Applying the Campbell's Theorem [23] to (A.3),

and utilizing the fact that $|h_{b_j u_0}|^2 \sim \exp(1)$ follows

$$\mathbb{E}[I_{b_x}] = \sum_{j=1}^{K} 2\pi P_{t,b_j} L_o \lambda_j \left[\int_0^{\infty} \Big[\int_{r_{min}}^{\infty} (max\{r,d\})^{-\ell_j} r dr \Big] f_{\left\|\boldsymbol{x}_{b_{\widehat{k}}}\right\|}(x) \mathrm{d}x \right]. \tag{A.4}$$

Inserting $r_{min} = x$ into (A.4) results as under

$$\begin{aligned} \mathbb{E}[I_{b_x}] = \sum_{j=1}^{K} 2\pi P_{t,b_j} L_o \lambda_j \Bigg[& \int_0^{d} \Big[d^{-\ell_j} \int_x^{d} r \mathrm{d}r + \int_d^{\infty} r^{-(\ell_j - 1)} \mathrm{d}r \Big] \\ & f_{\left\|\boldsymbol{x}_{b_{\widehat{k}}}\right\|}(x) dx + \int_d^{\infty} \Big[\int_x^{\infty} r^{-(\ell_j - 1)} \mathrm{d}r \Big] f_{\left\|\boldsymbol{x}_{b_{\widehat{k}}}\right\|}(x) \mathrm{d}x \Bigg]. \end{aligned} \tag{A.5}$$

Substituting the PDF of $\left\|\boldsymbol{x}_{b_{\widehat{k}}}\right\|$ with NBS cell association from (A.2) into (A.5), and solving the resulting equation by using [119, eq. 3.381.1] and [119, eq. 3.381.6], $\mathbb{E}[I_{b_x}]$ is obtained. Combining the equations of $\mathbb{E}[I_{b_{\widehat{k}}}]$ and $\mathbb{E}[I_{b_x}]$, the average received power at the typical kth tier MU with NBS cell association in (3.8) is obtained as Lemma 3.3.1.

A.2 Proof of Lemma 3.3.2

The PDF of $\left\|\boldsymbol{x}_{b_{\widehat{k}}}\right\|$ with the MRP cell association given by [117] is written as

$$f_{\left\|\boldsymbol{x}_{b_{\widehat{k}}}\right\|}(x)\big|_{\mathrm{MRP}} = \frac{x}{\Upsilon_k} \exp\Big\{ - \sum_{j=1}^{K} \mu_{k,j} x^{2\ell_k/\ell_j} \Big\}, \tag{A.6}$$

where Υ_k is given in (3.21) The average value of $I_{b_{\widehat{k}}}$ is derived by substituting the PDF of $\left\|\boldsymbol{x}_{b_{\widehat{k}}}\right\|$ with MRP cell association from (A.6) into (A.1). Further, the average value of I_{b_x} is derived as (A.4) with the interfering BSs located outside the disc of radius $r_{min} = {\delta_{j,k}}^{1/\ell_j} x^{\ell_k/\ell_j}$ to satisfy the MRP cell association. Combining the resulting equations of $\mathbb{E}[I_{b_{\widehat{k}}}]$ and $\mathbb{E}[I_{b_x}]$, and finally substituting the PDF of $\left\|\boldsymbol{x}_{b_{\widehat{k}}}\right\|$ with the MRP cell association from (A.6) the average received power at the typical kth tier

MU with the MRP cell association is derived as Lemma 3.3.2.

A.3 Proof of Theorem 3.4.1

According to (3.5) and (3.27), the DL outage probability of the typical MU in the kth tier is given as

$$P_{out,k}^{DL}(\beta) = 1 - \int_0^{\infty} \Pr\left[\frac{\left|h_{b_{\widehat{k}},\mathrm{u}_0}\right|^2 \left\|\boldsymbol{x}_{b_{\widehat{k}},\mathrm{u}_0}\right\|^{-\ell_k}}{(I_{b_{x_j}}^{DL} + \sigma^2)\Omega_k^{DL}} > \beta\right] f_{\left\|\boldsymbol{x}_{b_{\widehat{k}},\mathrm{u}_0}\right\|}(x)\mathrm{d}x, \tag{A.7}$$

where Ω_k^{DL} is given in (3.31), $I_{b_{x_j}}^{DL} = \sum_{b_j \in \Phi_j \setminus b_{\widehat{k}}} (1-\rho) P_{t,b_j} \left|h_{b_j,\mathrm{u}_0}\right|^2 L_0 \left\|\boldsymbol{x}_{b_j,\mathrm{u}_0}\right\|^{-\ell_j}$, and $f_{\left\|\boldsymbol{x}_{b_{\widehat{k}}}\right\|}(x)$ with the NBS cell association is given in (A.2).

In (A.8) the CCDF of a typical MU at a distance x from its associated BS in kth tier is given as

$$\begin{aligned}
&\Pr\left[\frac{\left|h_{b_{\widehat{k}},\mathrm{u}_o}\right|^2 \left\|\boldsymbol{x}_{b_{\widehat{k}},\mathrm{u}_o}\right\|^{-\ell_k}}{(I_{b_x}^{DL} + \sigma^2)\Omega_k^{DL}} > \beta\right] \\
&= \mathbb{E}_{I_{b_x}}\left[\Pr\left[\left|h_{b_{\widehat{k}},\mathrm{u}_o}\right|^2 > (I_{b_x}^{DL} + \sigma^2)\beta\Omega_k^{DL}\left\|\boldsymbol{x}_{b_{\widehat{k}},\mathrm{u}_o}\right\|^{-\ell_k}\right] \middle| I_{b_x}^{DL}\right] \\
&\overset{(a)}{=} \int_0^{\infty} \exp\left\{-\left(\Omega^{DL} + \sigma^2\right)\beta\Omega_k^{DL}\left\|\boldsymbol{x}_{b_{\widehat{k}},\mathrm{u}_o}\right\|^{-\ell_k}\right\} \mathrm{d}Pr\left(I_{b_x}^{DL} \le \Omega^{DL}\right) \\
&\overset{(b)}{=} \exp\left\{-\sigma^2\beta\Omega_k^{DL}\left\|\boldsymbol{x}_{b_{\widehat{k}},\mathrm{u}_o}\right\|^{\ell_k}\right\} \mathcal{L}_{I_{b_x}^{DL}}\left(\beta\Omega_k^{DL}\left\|\boldsymbol{x}_{b_{\widehat{k}},\mathrm{u}_0}\right\|^{-\ell_k}\right),
\end{aligned} \tag{A.8}$$

where (a) follows from the fact that $\left|h_{b_{\widehat{k}}u_0}\right|^2 \sim \exp(1)$, and (b) follows from the definition of Laplace transform of interference $\mathcal{L}_{I_{b_x}^{DL}}(s) = \int_x^{\infty} \exp\left(-s\Omega^{DL}\right) \mathrm{d}Pr\left(I_{b_x}^{DL} \le \Omega^{DL}\right)$, where the integration limit follows from the fact that the nearest interferer in jth tier is at least at $r_{min} = x$. Using generating

functional of HPPP in [23] $\mathcal{L}_{I_{b_x}^{DL}}(s)$ is given as

$$\mathcal{L}_{I_{b_x}^{DL}}(s) = \exp\Big\{2\pi\sum_{j=1}^{K}\lambda_j\int_{x}^{\infty}\Big(1-\mathbb{E}_h\big[-s(1-\rho)P_{t,b_j}\big|h_{b_j,\mathrm{u}_0}\big|^2 L_0\big\|\boldsymbol{x}_{b_j,\mathrm{u}_0}\big\|^{-\ell_j}\big]\Big)\,y\mathrm{d}y\Big\}$$

$$\stackrel{(a)}{=} \exp\Big\{2\pi\sum_{j=1}^{K}\lambda_j\int_{x}^{\infty}\big(1-\frac{1}{1+\mho_{k,j}y^{-\ell_j}}\big)y\mathrm{d}y\Big\} \tag{A.9}$$

$$= \exp\Big\{-\sum_{j=1}^{k}\pi\lambda_j\vartheta_{k,j}\Big\}, \tag{A.10}$$

where (a) follows from the fact that $|h_{b_j u_0}|^2 \sim 1$ and $\mho_{j,k}$ is given in (3.32). Simplifying (A.9) by employing change of variables $z = \mho_{k,j}^{-2/\ell_j}y^2$ (A.10) is derived, where $\vartheta_{k,j}$ is given in (3.30). Substituting (A.10) into (A.8) results as under

$$\Pr\left(SINR_k^{DL}\left(\big\|\boldsymbol{x}_{b_{\widehat{k}},\mathrm{u}_0}\big\|\right) > \beta\right) = \exp\Big\{-\sigma^2\beta\Omega_k^{DL}\big\|\boldsymbol{x}_{b_{\widehat{k}},\mathrm{u}_o}\big\|^{\ell_k} - \sum_{j=1}^{k}\pi\lambda_j\vartheta_{k,j}\Big\} \tag{A.11}$$

Finally plugging (A.11) and (A.2) into (A.7), Theorem 3.4.1 is obtained.

A.4 Proof of Theorem 3.4.2

For the MRP cell association, the Laplace transform in (A.8) is evaluated with lower integration limit $r_{min} = {\delta_{j,k}}^{1/\ell_j}x^{\ell_k/\ell_j}$ by utilizing the fact that the nearest interferer in the jth tier is at least at ${\delta_{j,k}}^{1/\ell_j}x^{\ell_k/\ell_j}$. Then following the similar steps as of Theorem 1 with the PDF of $\big\|\boldsymbol{x}_{b_{\widehat{k}}}\big\|$ for the MRP cell association given in (A.6), Theorem 3.4.2 is derived.

A.5 Proof of Theorem 3.4.3

Based on (3.54), the DL average ergodic rate of a typical MU associated with the kth tier using NBS cell association is derived as

$$\begin{aligned} R_k^{DL} &= \int_0^\infty \mathbb{E}_{SINR_k^{DL}}\left[\alpha \ln\left(1+SINR_k^{DL}(x)\right)\right] f_{\left\|\boldsymbol{x}_{b_{\widetilde{k}},\mathrm{u}_0}\right\|}(x)\mathrm{d}x \\ &= \int_0^\infty \int_0^\infty \Pr\left[SINR_k^{DL}(x) > (e^{t/\alpha}-1)\right] \mathrm{d}t f_{\left\|\boldsymbol{x}_{b_{\widetilde{k}},\mathrm{u}_0}\right\|}(x)\mathrm{d}x \end{aligned} \tag{A.12}$$

Simplifying (A.12) as of (A.11) and substituting (A.2), Theorem 3.4.3 is obtained.

A.6 Proof of Theorem 3.4.4

The DL average ergodic rate of a typical MU associated with the kth tier using MRP cell association is derived by simplifying (A.12) following the similar steps as of Theorem 3.4.2 for the MRP cell association and substituting (A.6).

Appendix B

Proofs from Chapter 4

B.1 Proof of Lemma 4.3.1

When $P_{r,\mathrm{M}} > P_{r,j}$ for all $j \in \{2, ..., K\}$, a typical MU is associated with the MBS. Therefore,

$$\begin{aligned}
\Lambda_{\mathrm{M}} &= \mathbb{E}_{R_M}\left[\Pr[P_{r,\mathrm{M}} > P_{r,j}]\right] \\
&= \mathbb{E}_{R_M}\left[\Pr[P_{r,\mathrm{M}}(R_m) > \max_j P_{r,j}]\right] \\
&\overset{(a)}{=} \mathbb{E}_{R_M}\left[\prod_{j=2}^{K} \Pr\left[R_j > \left(\frac{P_j}{\Psi P_{\mathrm{M}}}\right)^{1/\alpha_j} R_m^{\alpha_{\mathrm{M}}/\alpha_j}\right]\right] \\
&= \int_0^{\infty} \prod_{j=2}^{K} \Pr\left[R_j > \left(\frac{P_j}{\Psi P_{\mathrm{M}}}\right)^{1/\alpha_j} R_m^{\alpha_{\mathrm{M}}/\alpha_j}\right] f_{R_m}(r)\mathrm{d}r, \qquad \text{(B.1)}
\end{aligned}$$

where (a) is given using (4.3) and (4.4). $\Pr\left[R_j > \left(\frac{P_j}{\Psi P_{\mathrm{M}}}\right)^{1/\alpha_j} R_m^{\alpha_{\mathrm{M}}/\alpha_j}\right]$ and the PDF of R_m are derived using the null probability of a 2-D Poisson point process with density λ in an area A, which is $\exp(-\lambda A)$

$$\Pr\left[R_j > \left(\frac{P_j}{\Psi P_{\mathrm{M}}}\right)^{1/\alpha_j} R_m^{\alpha_{\mathrm{M}}/\alpha_j}\right] = e^{-\pi\lambda_{b^j}\left(\frac{P_j}{\Psi P_{\mathrm{M}}}\right)^{1/\alpha_j} R_m^{\alpha_{\mathrm{M}}/\alpha_j}}. \qquad \text{(B.2)}$$

and

$$f_{R_m}(r) = 1 - \frac{\mathrm{d}}{\mathrm{dr}}(\Pr[R_m > r]) = e^{-\pi\lambda_{b^{\mathrm{M}}} r^2} 2\pi\lambda_{b^{\mathrm{M}}} r. \qquad \text{(B.3)}$$

Combining (B.1), (B.2), and (B.3), Lemma 4.3.1 is obtained.

B.2 Proof of Lemma 4.3.2

Given the typical MU's association with the MBS, probability of $X_m > x$ can be given as

$$\Pr[X_{\mathrm{M}} > x] = \Pr[R_m > x | n = \mathrm{M}] = \frac{\Pr[\mathrm{R_m} > \mathrm{x}, \mathrm{n} = \mathrm{M}]}{\Pr[\mathrm{n} = \mathrm{M}]}, \tag{B.4}$$

where $\Pr[n = \mathrm{M}] = \Lambda_{\mathrm{M}}$ follows from Lemma 4.3.1, and the joint probability of $R_m > x$ and $n = \mathrm{M}$ is

$$\begin{aligned}
\Pr[R_m > x, n = M] &= \Pr\left[R_m > x, P_{r,\mathrm{M}}(R_m) > \max_j P_{r,j}\right] \\
&= \int_x^\infty \prod_{j=2}^{K} \Pr[P_{r,\mathrm{M}} > P_{r,j}] f_{R_m}(r)\mathrm{d}r \\
&\overset{(a)}{=} \int_x^\infty \prod_{j=2}^{K} \Pr\left[R_j > \left(\frac{P_j}{\Psi P_{\mathrm{M}}}\right)^{1/\alpha_j} R_m^{\alpha_{\mathrm{M}}/\alpha_j}\right] f_{R_m}(r)\mathrm{d}r \\
&\overset{(b)}{=} 2\pi\lambda_{b^{\mathrm{M}}} \int_x^\infty r \exp\left\{-\pi\lambda_{b^{\mathrm{M}}} r^2 - \pi \sum_{j=2}^{K} \lambda_{\mathrm{b^j}} \left(\frac{P_j}{\Psi P_{\mathrm{M}}}\right)^{2/\alpha_j} r^{2\alpha_{\mathrm{M}}/\alpha_j}\right\} \mathrm{d}r,
\end{aligned} \tag{B.5}$$

where (a) follows from (4.3) and (4.4), and (b) is given from (B.2) and (B.3). Substituting (B.5) into (B.4) gives

$$\Pr[X_{\mathrm{M}} > x] = \frac{2\pi\lambda_{b^{\mathrm{M}}}}{\Lambda_{\mathrm{M}}} \int_x^\infty r \exp\left\{-\pi\lambda_{b^{\mathrm{M}}} r^2 - \pi \sum_{j=2}^{K} \lambda_{\mathrm{b^j}} \left(\frac{P_j}{\Psi P_{\mathrm{M}}}\right)^{2/\alpha_j} r^{2\alpha_{\mathrm{M}}/\alpha_j}\right\} \mathrm{d}r, \tag{B.6}$$

The CDF of X_{M} is $F_{X_{\mathrm{M}}}(x) = 1 - \Pr[X_{\mathrm{M}} > x]$ and the PDF is given as

$$\begin{aligned}
f_{X_{\mathrm{M}}}(x) &= \frac{\mathrm{d}F_{X_M}(x)}{\mathrm{d}x} \\
&= \frac{2\pi\lambda_{b^{\mathrm{M}}}}{\Lambda_{\mathrm{M}}} x \exp\left\{-\pi\lambda_{b^{\mathrm{M}}} x^2 - \pi \sum_{j=2}^{K} \lambda_{\mathrm{b^j}} \left(\frac{P_j}{\Psi P_{\mathrm{M}}}\right)^{2/\alpha_j} x^{2\alpha_{\mathrm{M}}/\alpha_j}\right\},
\end{aligned} \tag{B.7}$$

B.3 Proof of Theorem 4.3.1

Based on (4.24), the DL average ergodic rate of the macrocell tier is defined as

$$R_M = \int_0^\infty \mathbb{E}_{\mathrm{SINR}_{\mathrm{M}}^{\mathrm{DL}}} \left[\ln \left(1 + SINR_M^{DL}|_{|X_{o,\mathrm{u}_0^M}|=x} \right) \right] f_{|X_{o,\mathrm{M}}|}(x)\, \mathrm{d}x$$

$$\overset{(a)}{=} \int_0^\infty \int_0^\infty \left(\frac{1}{\tau+1} \right) \underbrace{\Pr\left[SINR_M^{DL}(x) > \tau \right]}_{P_{Cov}^M(\tau)} f_{|X_{o,\mathrm{M}}|}(x)\, \mathrm{d}x \mathrm{d}\tau, \tag{B.8}$$

where $f_{|X_{o,\mathrm{M}}|}(x)$ is the PDF of the distance between a typical MU and its serving MBS given by (4.19). In (B.8), (a) follows by substituting $e^t - 1 = \tau$ and $P_{Cov}^M(\tau)$ is evaluated as

$$P_{Cov}^M(\tau) = \Pr\left(\frac{\frac{P_M}{U_M} \beta g_{0,u_0^M} x^{-\alpha_M}}{I_{u_0^M} + N_0} > \tau \right)$$

$$\overset{(a)}{=} \int_0^\infty e^{-\frac{\tau U_M x^{\alpha_M}(\gamma+N_0)}{P_M \beta}} \sum_{n=0}^{N-U_M} \frac{\left(\frac{\tau U_M x^{\alpha_M}(\gamma+N_0)}{P_M \beta} \right)^n}{n!} \mathrm{d}\Pr(I_{u_0^M} \leq \gamma), \tag{B.9}$$

where (a) follows from $g_{o,\mathrm{u}_0^M} \sim \Gamma(N - U_\mathrm{M} + 1, 1)$. After some mathematical manipulations, (B.9) can be written as

$$P_{Cov}^M(\tau) = \sum_{n=0}^{N-U_M} \frac{(x^{\alpha^M})^n}{n!(-1)!} \left. \frac{\mathrm{d}^n \left(e^{-\frac{\tau U_M q N_0}{P_M \beta}} \mathcal{L}_{I_{u_0^M}} \left(\frac{\tau U_M q}{P_M \beta} \right) \right)}{\mathrm{d}q^n} \right|_{q=x^{\alpha_M}}, \tag{B.10}$$

where $\mathcal{L}_{I_{u_0^M}}$ is the Laplace transform of the PDF of $I_{u_0^M}$ given as

$$\mathcal{L}_{I_{u_0^M}}(s) = \mathcal{L}_{I_{M,u_0^M}}(s) \mathcal{L}_{I_{S,u_0^M}}(s) \mathcal{L}_{I_{u_{ul}^S,u_0^M}}(s). \tag{B.11}$$

In (B.11), $\mathcal{L}_{I_{M,u_0^M}}(s)$ is the Laplace transform of the PDF of I_{M,u_0^M}, which is derived as

$$\begin{aligned}\mathcal{L}_{I_{M,u_0^M}}(s) &= \mathbb{E}\left[\exp\left\{-s\sum_{m\in\Phi_b^M\setminus 0}\frac{P_M}{U_M}h_{m,u_0^M}\beta|X_{m,u_0^M}|^{-\alpha_M}\right\}\right]\\ &\overset{(a)}{=}\exp\left\{-\int_0^\infty\left(1-\mathbb{E}_{h_{m,u_0^M}}\left\{\exp\left\{-s\frac{P_M}{U_M}h_{m,u_0^M}\beta r^{-\alpha_M}\right\}\right\}\right)2\pi r\lambda_M\mathrm{d}r\right\}\\ &\overset{(b)}{=}\exp\left\{-2\pi\lambda_M\sum_{\nu=1}^{U_M}\binom{U_M}{\nu}\int_x^\infty\frac{\left(\frac{P_M}{U_M}\beta\right)^\nu s^\nu(r^{-\alpha_M})^\nu}{\left(1+s\frac{P_M}{U_M}\beta r^{-\alpha_M}\right)^{U_M}}r\mathrm{d}r\right\},\end{aligned}\tag{B.12}$$

where (a) is obtained by using generating functional of PPP [141] and (b) follows from $h_{m,\mathrm{u}_0^M}\sim\Gamma(U_\mathrm{M},1)$ and using Binomial expansion. Likewise, $\mathcal{L}_{I_{S,u_0^M}}(s)$ is the Laplace transform of the PDF of I_{S,u_0^M}, which is evaluated as

$$\mathcal{L}_{I_{S,u_0^M}}(s)=\exp\left\{-\sum_{j=2}^K 2\pi\lambda_j\int_{D_j^M(x)}^\infty\left(\frac{sP_j\beta r^{-\alpha_j}}{1+sP_j\beta r^{-\alpha_j}}\right)r\mathrm{d}r\right\},\tag{B.13}$$

where $D_j^M(x)$ is the distance between a typical MU and the closest interfering BS in the jth tier. In (B.11), $\mathcal{L}_{I_{u_{ul}^S,u_0^M}}(s)$ is the Laplace transform of the PDF of $I_{u_{ul}^S,u_0^M}$. Due to difficulty in obtaining the exact characteristics of $I_{u_{ul}^S,u_0^M}$, we assume the distance between a typical macrocell MU and the UL MU of FD SBS can be approximated as the distance between a typical macrocell MU and the interfering FD SBS as in Section 4.2.4. Therefore, $I_{u_{ul}^S,u_0^M}$ is evaluated as follows

$$\mathcal{L}_{I_{u_{ul}^S,u_0^M}}(s)=\exp\left\{-\sum_{j=2}^K 2\pi\lambda_j\int_0^\infty\left(\frac{sP_u\beta r^{-\alpha_j}}{1+sP_u\beta r^{-\alpha_j}}\right\}r\mathrm{d}r\right),\tag{B.14}$$

where the integral has a lower limit of zero as the nearest UL MU of FD SBS can be arbitrarily close to the typical macrocell MU. Plugging (B.12), (B.13) and (C.5) into

(B.11), after some mathematical manipulations, $\mathcal{L}_{I_{u_0^M}}(s)$ is derived as

$$\mathcal{L}_{I_{u_0^M}}(s) = e^{-\zeta(s)}, \tag{B.15}$$

where $\zeta(s)$ is given by (4.29). Substituting (B.15) into (B.10), and using the Faa di Bruno's formula, we obtain $P_{Cov}^{M}(\tau)$. Finally, plugging $P_{Cov}^{M}(\tau)$ into (B.8), we obtain (4.27).

B.4 Proof of Theorem 4.3.2

Similar to (B.8), Theorem 4.3.1, the DL average ergodic rate of the small cell tier is defined from (4.26) as

$$R_k = \int_0^\infty \int_0^\infty \left(\frac{1}{\tau+1}\right) \underbrace{\Pr\left[SINR_k^{DL}(x) > \tau\right]}_{P_{Cov}^{k}(\tau)} f_{|X_{o,k}|}(x)\,\mathrm{d}x\mathrm{d}\tau, \tag{B.16}$$

where $f_{|X_{o,k}|}(x)$ is the PDF of the distance between a typical MU and its serving SBS given by (4.21). In (B.16), $P_{Cov}^{k}(\tau)$ is evaluated as

$$\begin{aligned} P_{Cov}^{k}(\tau) &= \Pr\left(\frac{P_k \beta g_{0,u_0^k} x^{-\alpha_k}}{I_{u_0^k} + N_0} > \tau\right) \\ &\overset{(a)}{=} \int_0^\infty e^{-\frac{\tau x^{\alpha_k}(\gamma+N_0)}{P_k\beta}}\,\mathrm{d}\Pr(I_{u_0^k} \le \gamma) \\ &\overset{(b)}{=} e^{-\frac{\tau x^{\alpha_k} N_0}{P_k\beta}} \mathcal{L}_{I_{u_0^k}}\left(\frac{\tau x^{\alpha_k}}{P_k\beta}\right), \end{aligned} \tag{B.17}$$

where (a) follows from $g_{o,\mathrm{u}_0^1} \sim \exp(1)$, and (b) follows from the definition of Laplace transform of interference $\mathcal{L}_{I_{u_0^k}}(s) = \int \exp(-s\gamma)\,\mathrm{d}\Pr\left(I_{u_0^k} \le \gamma\right)$. In (B.17), $\mathcal{L}_{I_{u_0^k}}(s)$ is given as

$$\mathcal{L}_{I_{u_0^k}}(s) = \mathcal{L}_{I_{M,u_0^k}}(s)\mathcal{L}_{I_{S,u_0^k}}(s)\mathcal{L}_{I_{u_{ul}^S,u_0^k}}(s). \tag{B.18}$$

In (B.18), $\mathcal{L}_{I_{M,u_0^k}}(s)$ is the Laplace transform of the PDF of I_{M,u_0^k}, which is derived as

$$\begin{aligned}\mathcal{L}_{I_{M,u_0^k}}(s) &= \mathbb{E}\left[\exp\left\{-s\sum_{m\in\Phi_b^M}\frac{P_M}{U_M}h_{m,u_0^M}\beta|X_{m,u_0^k}|^{-\alpha_M}\right\}\right] \\ &\overset{(a)}{=} \exp\left\{-\int_0^\infty\left(1-\mathbb{E}_{h_{m,u_0^k}}\left\{\exp\left\{-s\frac{P_M}{U_M}h_{m,u_0^k}\beta r^{-\alpha_M}\right\}\right\}\right)2\pi r\lambda_M \mathrm{d}r\right\} \\ &\overset{(b)}{=} \exp\left\{-2\pi\lambda_M\sum_{\nu=1}^{U_M}\binom{U_M}{\nu}\int_{D_{\mathrm{M}}^k(x)}^\infty\frac{\left(\frac{P_M}{U_M}\beta\right)^\nu s^\nu (r^{-\alpha_M})^\nu}{\left(1+s\frac{P_M}{U_M}\beta r^{-\alpha_M}\right)^{U_M}}r\mathrm{d}r\right\}, \end{aligned} \tag{B.19}$$

where (a) is obtained by using generating functional of PPP [141] and (b) follows from $h_{m,u_0^k}\sim\Gamma(U_{\mathrm{M}},1)$ and using Binomial expansion. In (B.19), $D_{\mathrm{M}}^k(x)$ is the distance between the closest interfering MBS and the typical MU given in (4.31). Likewise, $\mathcal{L}_{I_{S,u_0^k}}(s)$ is the Laplace transform of the PDF of I_{S,u_0^k}, which is evaluated as

$$\mathcal{L}_{I_{S,u_0^k}}(s) = \exp\left\{-\sum_{j=2}^K 2\pi\lambda_j\int_{D_j^k(x)}^\infty\left(\frac{sP_j\beta r^{-\alpha_j}}{1+sP_j\beta r^{-\alpha_j}}\right)r\mathrm{d}r\right\}, \tag{B.20}$$

where $D_j^k(x)$ is the distance between a typical MU and the closest interfering BS in the jth tier given in (4.32). In (B.18), $\mathcal{L}_{I_{u_{ul}^S,u_0^k}}(s)$ is the Laplace transform of the PDF of $I_{u_{ul}^S,u_0^k}$. Due to difficulty in obtaining the exact characteristics of $I_{u_{ul}^S,u_0^k}$, it is assumed that the distance between a typical DL small cell MU and the UL MU of FD SBS can be approximated as the distance between a typical DL small cell MU and the interfering SBS as in Section 4.2.4. Therefore, $I_{u_{ul}^S,u_0^k}$ is evaluated as follows

$$\mathcal{L}_{I_{u_{ul}^S,u_0^k}}(s) = \exp\left\{-\sum_{j=2}^K 2\pi\lambda_j\int_0^\infty\left(\frac{sP_u\beta r^{-\alpha_j}}{1+sP_u\beta r^{-\alpha_j}}\right\}r\mathrm{d}r\right), \tag{B.21}$$

where the integral has a lower limit of zero as the nearest UL MU of FD SBS can be arbitrarily close to the typical small cell MU. Substituting (B.19), (B.20) and (B.21)

into (B.18), after some manipulations, $\mathcal{L}_{I_{u_0^k}}(s)$ is derived as

$$\mathcal{L}_{I_{u_0^k}}(s) = e^{-\Xi(x,\tau)}, \tag{B.22}$$

where $\Xi(x,\tau)$ is given by (4.31). Plugging (B.22) into (B.17), we obtain $P^k_{Cov}(\tau)$. Finally, plugging $P^k_{Cov}(\tau)$ into (B.16), we obtain Theorem 4.3.2.

Appendix C

Proof from Chapter 5

C.1 Proof of Theorem 5.3.1

Based on (5.6), the DL rate coverage probability of the macrocell with massive multiuser MIMO at the BSs, can be given as

$$C_{\mathrm{M}}(\mathrm{R}^{\mathrm{DL}}) = \int_0^{\infty} F_{I_{u_0^{\mathrm{M}}}}\left(\frac{P_{\mathrm{M}}\beta}{\gamma^{\mathrm{DL}}_{\mathrm{M}_{m\mathrm{M}}}|X_{o,u_0^{\mathrm{M}}}|^{\alpha_{\mathrm{M}}}} - N_0\right) f_{|X_{o,\mathrm{M}}|}(x)\,\mathrm{d}x, \tag{C.1}$$

where we resort to apply the Gil-Pelaez inversion theorem [142] and the CDF of the interference $F_{I_{u_0^{\mathrm{M}}}}(.)$ can be derived as

$$F_{I_{u_0^{\mathrm{M}}}}(x) = \frac{1}{2} - \frac{1}{\pi}\int_0^{\infty} \mathrm{Im}\left[\frac{\mathcal{L}_{I_{\mathrm{M}_{m\mathrm{M}},u_0^{\mathrm{M}}}}(-\mathrm{jw})\mathcal{L}_{I_{S,u_0^{\mathrm{M}}}}(-\mathrm{jw})\mathcal{L}_{I_{u^s_{ul},u_0^{\mathrm{M}}}}(-\mathrm{jw})}{\exp\left(\mathrm{jw}\left(\frac{P_{\mathrm{M}}\beta}{\gamma^{\mathrm{DL}}_{\mathrm{M}_{m\mathrm{M}}} x^{\alpha_{\mathrm{M}}}} - N_0\right)\right)}\right]\frac{\mathrm{dw}}{\mathrm{w}}, \tag{C.2}$$

where Im(.) represents the imaginary part of the argument. In (C.2), the Laplace transform of $I_{\mathrm{M}_{m\mathrm{M}},u_0^k}$ can be derived as under

$$\mathcal{L}_{I_{\mathrm{M}_{m\mathrm{M}},u_0^k}}(-\mathrm{jw}) = \mathbb{E}\left[\exp\left\{-(-\mathrm{jw})\sum_{m\in\Phi_b^M} P_M\beta|X_{m,u_0^k}|^{-\alpha_M}\right\}\right]$$
$$\overset{(a)}{=} \exp\left\{-\int_x^\infty \left(1-\exp\left\{-(-\mathrm{jw})P_M\beta r^{-\alpha_M}\right\}\right)2\pi r\lambda_M \mathrm{d}r\right\}$$
$$= \exp\left\{-\pi\lambda_M\left(\frac{\Gamma\left(1-\frac{2}{\alpha_\mathrm{M}}\right)+\frac{2}{\alpha_\mathrm{M}}\Gamma_u\left(-\frac{2}{\alpha_\mathrm{M}},\frac{-\mathrm{jw}P_\mathrm{M}\beta}{x^{\alpha_\mathrm{M}}}\right)}{(-\mathrm{jw}P_\mathrm{M}\beta)^{-2/\alpha_\mathrm{M}}}-x^2\right)\right\}, \tag{C.3}$$

where (a) follows from the probability generating functional of PPP. In (C.3), Γ_u denotes the upper incomplete Gamma function. Similarly, $\mathcal{L}_{I_{S,u_0^M}}(-\mathrm{jw})$ is derived as

$$\mathcal{L}_{I_{S,u_0^M}}(-\mathrm{jw}) = \exp\left\{-\sum_{j=2}^K 2\pi\lambda_j \int_{D_j^M(x)}^\infty \left(\frac{(-\mathrm{jw})P_j\beta r^{-\alpha_j}}{1+(-\mathrm{jw})P_j\beta r^{-\alpha_j}}\right) r\mathrm{d}r\right\}, \tag{C.4}$$

where $D_j^M(x) = \left(\frac{P_j}{\Psi P_\mathrm{M}}\right)^{\frac{1}{\alpha_j}} x^{\frac{\alpha_\mathrm{M}}{\alpha_j}}$ is the distance between a typical MU and the closest interfering BS in the jth tier. In (C.2), $\mathcal{L}_{I_{u_{ul}^s,u_0^\mathrm{M}}}(-\mathrm{jw})$ is evaluated as

$$\mathcal{L}_{I_{u_{ul}^s,u_0^\mathrm{M}}}(-\mathrm{jw})$$
$$\overset{(a)}{=} \exp\left\{-\sum_{j=2}^K 2\pi\lambda_{b^j}\int_0^\infty \left(1-\exp(-\pi\frac{\lambda_{b^j}}{A_j^{UL}}r^2)\right)\mathbb{E}_R\left[\frac{(-\mathrm{jw})\rho_j\beta^{1-\epsilon}R^{\epsilon\alpha_j}r^{-\alpha_j}}{1+(-\mathrm{jw})\rho_j\beta^{1-\epsilon}R^{\epsilon\alpha_j}r^{-\alpha_j}}\right] r\mathrm{d}r\right\}, \tag{C.5}$$

where (a) follows from the probability generating functional of a PPP and the fact that the UL interference field is a non-homogeneous PPP with distance dependent density function given as

$$\lambda_{I_{\Phi_{b^j}^{\mathrm{UL}}}}(r) = \lambda_{b^j}\left(1-\exp\left(-\pi\frac{\lambda_{b^j}}{A_j^{UL}}r^2\right)\right) \tag{C.6}$$

where ($A_j^{UL} = \lambda_{b^j} / \sum_{i=2}^{K} \lambda_{b^i}$) is the repulsion parameter as in [143]. In (C.6), the integral has a lower limit of zero as the nearest UL MU of FD SBS can be arbitrarily close to the typical macrocell MU. Using the PDF of serving link distances given in (5.21), $\mathcal{L}_{I_{u_{ul}^s, u_0^{\mathrm{M}}}}(-\mathrm{jw})$ is derived.

Finally substituting $\mathcal{L}_{I_{\mathrm{M}_{m\mathrm{M}}, u_0^{\mathrm{M}}}}(-\mathrm{jw})$, $\mathcal{L}_{I_{S, u_0^{\mathrm{M}}}}(-\mathrm{jw})$, and $\mathcal{L}_{I_{u_{ul}^s, u_0^{\mathrm{M}}}}(-\mathrm{jw})$ into (C.2), and plugging (C.2) into (C.1), Theorem 5.3.1 is obtained.

References

[1] H. S. Dhillon, "Fundamentals of heterogeneous cellular networks," Ph.D. dissertation, The University of Texas at Austin, Dec. 2012.

[2] J. G. Andrews, F. Baccelli, and R. K. Ganti, "A tractable approach to coverage and rate in cellular networks," *IEEE Trans. Wireless Commun.*, vol. 59, no. 11, pp. 3122–3134, Nov. 2011.

[3] S. Bi, C. Ho, and R. Zhang, "Wireless powered communication: opportunities and challenges," *IEEE Commun. Mag.*, vol. 53, no. 4, pp. 117–125, Apr. 2015.

[4] A. Sabharwal, P. Schniter, D. Guo, D. W. Bliss, S. Rangarajan, and R. Wichman, "In-band full-duplex wireless: Challenges and opportunities," *IEEE J. Sel. Areas Commun.*, vol. 32, no. 9, pp. 1637–1652, Sept. 2014.

[5] D. Bharadia, E. McMilin, and S. Katti, "Full duplex radios," *SIGCOMM Comput. Commun. Rev.*, vol. 43, no. 4, pp. 375–386, Oct. 2013. [Online]. Available: http://doi.acm.org/10.1145/2534169.2486033

[6] D. Gesbert, M. Kountouris, R. W. H. Jr., C. b. Chae, and T. Salzer, "Shifting the MIMO paradigm," *IEEE Sig. Process. Mag.*, vol. 24, no. 5, pp. 36–46, Sept. 2007.

[7] P. Demestichas, A. Georgakopoulos, D. Karvounas, K. Tsagkaris, V. Stavroulaki, J. Lu, C. Xiong, and J. Yao, "5G on the horizon: Key challenges for the radio-access network," *IEEE Trans. Veh. Technol.*, vol. 8, no. 3, pp. 47–53, Sept. 2013.

[8] R. Hu and Y. Qian, "An energy efficient and spectrum efficient wireless heterogeneous network framework for 5G systems," *IEEE Commun. Mag.*, vol. 52, no. 5, pp. 94–101, May 2014.

[9] J. Andrews, S. Buzzi, W. Choi, S. Hanly, A. Lozano, A. Soong, and J. Zhang, "What will 5G be?" *IEEE J. Sel. Areas Commun.*, vol. 32, no. 6, pp. 1065–1082, June 2014.

[10] A. Gupta and R. K. Jha, "A survey of 5G network: Architecture and emerging technologies," *IEEE Access*, vol. 3, pp. 1206–1232, 2015.

[11] S. Parkvall, A. Furuskar, and E. Dahlman, "Evolution of LTE toward IMT-Advanced," *IEEE Commun. Mag.*, vol. 49, no. 2, pp. 84–91, Feb. 2011.

[12] A. Khandekar, N. Bhushan, J. Tingfang, and V. Vanghi, "LTE-Advanced: Heterogeneous networks," in *European Wireless Conference (EW)*, Apr. 2010, pp. 978–982.

[13] D. Liu, Y. Chen, K. K. Chai, T. Zhang, and M. Elkashlan, "Opportunistic user association for multi-service HetNets using nash bargaining solution," *IEEE Commun. Lett.*, vol. 18, no. 3, pp. 463–466, Mar. 2014.

[14] A. Ghosh, N. Mangalvedhe, R. Ratasuk, B. Mondal, M. Cudak, E. Visotsky, T. A. Thomas, J. G. Andrews, P. Xia, H. S. Jo, H. S. Dhillon, and T. D. Novlan, "Heterogeneous cellular networks: From theory to practice," *IEEE Commun. Mag.*, vol. 50, no. 6, pp. 54–64, June 2012.

[15] X. Lu, P. Wang, D. Niyato, D. I. Kim, and Z. Han, "Wireless networks with RF energy harvesting: A contemporary survey," *IEEE Commun. Surveys Tuts.*, vol. 17, no. 2, pp. 757–789, Secondquarter 2015.

[16] D. Mishra, S. De, S. Jana, S. Basagni, K. Chowdhury, and W. Heinzelman, "Smart rf energy harvesting communications: challenges and opportunities," *IEEE Commun. Mag.*, vol. 53, no. 4, pp. 70–78, Apr. 2015.

[17] H. Q. Ngo, E. G. Larsson, and T. L. Marzetta, "Energy and spectral efficiency of very large multiuser mimo systems," *IEEE Trans. Commun.*, vol. 61, no. 4, pp. 1436–1449, Apr. 2013.

[18] E. G. Larsson, O. Edfors, F. Tufvesson, and T. L. Marzetta, "Massive MIMO for next generation wireless systems," *IEEE Commun. Mag.*, vol. 52, no. 2, pp. 186–195, Feb. 2014.

[19] T. S. Rappaport, *Wireless Communications: Principles and Practice*, 2nd ed. Prentice-Hall, 2002.

[20] A. Wyner, "Shannon-theoretic approach to a gaussian cellular multiple-access channel," *IEEE Trans. Inf. Theory*, vol. 40, no. 6, pp. 1713–1727, Nov 1994.

[21] H. ElSawy, E. Hossain, and M. Haenggi, "Stochastic geometry for modeling, analysis, and design of multi-tier and cognitive cellular wireless networks: A survey," *IEEE Commun. Surveys and Tutorials*, vol. 15, no. 3, pp. 996–1019, 2013.

[22] A. Baddeley, *Spatial Point Processes and their Applications in Lecture Notes in Mathematics: Stochastic Geometry.* Springer Verlag, 2007.

[23] D. Stoyan, W. Kendall, and J. Mecke, *Stochastic geometry and its applications, vol.2.* Wiley New York, 1987.

[24] D. Daley and D. Vere-Jones, *An Introduction to the Theory of Point Processes, Volume II: General Theory and Structure*. Springer, 2008.

[25] D. Daley and D. Vere-Jones, *An Introduction to the Theory of Point Processes, Volume I: Elementary Theory and Methods*. Springer, 2003.

[26] M. L. Ku, W. Li, Y. Chen, and K. J. R. Liu, "Advances in energy harvesting communications: Past, present, and future challenges," *IEEE Commun. Surveys Tuts.*, vol. 18, no. 2, pp. 1384–1412, Secondquarter 2016.

[27] L. Xie, Y. Shi, Y. T. Hou, and A. Lou, "Wireless power transfer and applications to sensor networks," *IEEE Trans. Wireless Commun.*, vol. 20, no. 4, pp. 140–145, Aug. 2013.

[28] Y. Liu, L. Wang, S. A. R. Zaidi, M. Elkashlan, and T. Q. Duong, "Secure D2D communication in large-scale cognitive cellular networks: A wireless power transfer model," *IEEE Trans. Commun.*, vol. 64, no. 1, pp. 329–342, Jan. 2016.

[29] L. R. Varshney, "Transporting information and energy simultaneously," in *Proc. IEEE Intl. Symposium on Information Theory*, July 2008, pp. 1612–1616.

[30] P. Grover and A. Sahai, "Shannon meets tesla: Wireless information and power transfer," in *Proc. IEEE Intl. Symposium on Information Theory*, Jun. 2010, pp. 2363–2367.

[31] I. Krikidis, S. Timotheou, S. Nikolaou, G. Zheng, D. Ng, and R. Schober, "Simultaneous wireless information and power transfer in modern communication systems," *IEEE Commun. Mag.*, vol. 52, no. 11, pp. 104–110, Nov. 2014.

[32] K. Huang and E. Larsson, "Simultaneous information and power transfer for broadband wireless systems," *IEEE Trans. Signal Process.*, vol. 61, no. 23, pp. 5972–5986, Dec. 2013.

[33] S. Bi, Y. Zeng, and R. Zhang, "Wireless powered communication networks: An overview," *IEEE Wireless Communications*, vol. 23, no. 2, pp. 10–18, Apr. 2016.

[34] A. Gohil, H. Modi, and S. K. Patel, "5G technology of mobile communication: A survey," in *International Conference on Intelligent Systems and Signal Processing (ISSP)*, Mar. 2013, pp. 288–292.

[35] A. Sabharwal, P. Schniter, D. Guo, D. W. Bliss, S. Rangarajan, and R. Wichman, "In-band full-duplex wireless: Challenges and opportunities," *IEEE J. Sel. Areas Commun.*, vol. 32, no. 9, pp. 1637–1652, Sept. 2014.

[36] T. Snow, C. Fulton, and W. J. Chappell, "Transmit-receive duplexing using digital beamforming system to cancel self-interference," *IEEE Trans. Microw. Theory Tech.*, vol. 59, no. 12, pp. 3494–3503, Dec. 2011.

[37] M. Duarte and A. Sabharwal, "Full-duplex wireless communications using off-the-shelf radios: Feasibility and first results," in *Conf. Record of the Forty Fourth Asilomar Conf. on Signals, Systems and Computers*, Nov. 2010, pp. 1558–1562.

[38] T. Riihonen, S. Werner, and R. Wichman, "Mitigation of loopback self-interference in full-duplex MIMO relays," *IEEE Trans. Signal Process.*, vol. 59, no. 12, pp. 5983–5993, Dec. 2011.

[39] P. Lioliou, M. Viberg, M. Coldrey, and F. Athley, "Self-interference suppression in full-duplex MIMO relays," in *Proc. Asilomar Conf. Signals, Syst., Comput., Pacific Grove, CA*, Nov. 2010, pp. 658–662.

[40] L. Anttila, D. Korpi, E. Antonio-Rodrguez, R. Wichman, and M. Valkama, "Modeling and efficient cancellation of nonlinear self-interference in MIMO full-duplex transceivers," in *IEEE GLOBECOM Workshops*, Dec. 2014, pp. 777–783.

[41] T. Riihonen, S. Werner, and R. Wichman, "Hybrid full-duplex/half-duplex relaying with transmit power adaptation," *IEEE Trans. Wireless Commun.*, vol. 10, no. 9, pp. 3074–3085, Sep. 2011.

[42] D. W. K. Ng, E. S. Lo, and R. Schober, "Dynamic resource allocation in MIMO-OFDMA systems with full-duplex and hybrid relaying," *IEEE Trans. Commun.*, vol. 60, no. 5, pp. 1291–1304, May 2012.

[43] K. Hosseini, W. Yu, and R. S. Adve, "Large-scale MIMO versus network MIMO for multicell interference mitigation," *IEEE J. Sel. Areas Commun.*, vol. 8, no. 5, pp. 930–941, Oct. 2014.

[44] H. Ju and R. Zhang, "Throughput maximization in wireless powered communication networks," *IEEE Trans. Commun.*, vol. 13, no. 1, pp. 418–428, Jan. 2014.

[45] L. Liu, R. Zhang, and K.-C. Chua, "Multi-antenna wireless powered communication with energy beamforming," *IEEE Trans. Commun.*, vol. 62, no. 12, pp. 4349–4361, Dec. 2014.

[46] H. Ju and R. Zhang, "User cooperation in wireless powered communication networks," in *Proc. IEEE Global Commun. Conf. (GLOBECOM)*, Dec. 2014, pp. 1430–1435.

[47] X. Kang, C. Ho, and S. Sun, "Full-duplex wireless-powered communication network with energy causality," *IEEE Trans. Wireless Commun.*, vol. 14, no. 10, pp. 5539–5551, Oct. 2015.

[48] G. Yang, C. K. Ho, R. Zhang, and Y. L. Guan, "Throughput optimization for massive MIMO systems powered by wireless energy transfer," *IEEE J. Sel. Areas Commun.*, vol. 33, no. 8, pp. 1640–1650, Aug. 2015.

[49] S. Lee, R. Zhang, and K. Huang, "Opportunistic wireless energy harvesting in cognitive radio networks," *IEEE Trans. Wireless Commun.*, vol. 12, no. 9, pp. 4788–4799, Sept. 2013.

[50] A. H. Sakr and E. Hossain, "Cognitive and energy harvesting-based D2D communication in cellular networks: Stochastic geometry modeling and analysis," *IEEE Trans. Commun.*, vol. 63, no. 5, pp. 1867–1880, May 2015.

[51] K. Huang and V. K. N. Lau, "Enabling wireless power transfer in cellular networks: Architecture, modeling and deployment," *CoRR*, 2012. [Online]. Available: http://arxiv.org/abs/1207.5640

[52] A. Sakr and E. Hossain, "Analysis of multi-tier uplink cellular networks with energy harvesting and flexible cell association," in *Proc. IEEE Global Commun. Conf. (GLOBECOM)*, Dec. 2014, pp. 4525–4530.

[53] K. Huang and X. Zhou, "Cutting last wires for mobile communication by microwave power transfer," *CoRR*, vol. abs/1408.3198, 2014. [Online]. Available: http://arxiv.org/abs/1408.3198

[54] J. G. Andrews, "Seven ways that hetnets are a cellular paradigm shift," *IEEE Commun. Mag.*, vol. 51, no. 3, pp. 136–144, Mar. 2013.

[55] D. Liu, L. Wang, Y. Chen, M. Elkashlan, K. K. Wong, R. Schober, and L. Hanzo, "User association in 5G networks: A survey and an outlook," *IEEE Commun. Surveys Tuts.*, vol. PP, no. 99, pp. 1–1, 2016.

[56] A. Sakr and E. Hossain, "Analysis of K-tier uplink cellular networks with ambient RF energy harvesting," *IEEE J. Sel. Areas Commun.*, vol. 33, no. 10, pp. 2226–2238, Oct. 2015.

[57] K. Smiljkovikj, P. Popovski, and L. Gavrilovska, "Analysis of the decoupled access for downlink and uplink in wireless heterogeneous networks," *IEEE Commun. Lett.*, vol. 4, no. 2, pp. 173–176, Apr. 2015.

[58] S. Singh, X. Zhang, and J. G. Andrews, "Joint rate and sinr coverage analysis for decoupled uplink-downlink biased cell associations in hetnets," *IEEE Trans. Wireless Commun.*, vol. 14, no. 10, pp. 5360–5373, Oct. 2015.

[59] H. Elshaer, F. Boccardi, M. Dohler, and R. Irmer, "Downlink and uplink decoupling: A disruptive architectural design for 5g networks," in *Proc. IEEE Global Commun. Conf. (GLOBECOM)*, Dec. 2014, pp. 1798–1803.

[60] D. Kim, H. Lee, and D. Hong, "A survey of in-band full-duplex transmission: From the perspective of phy and mac layers," *IEEE Commun. Surveys Tuts.*, vol. 17, no. 4, pp. 2017–2046, Fourthquarter 2015.

[61] H. Alves, C. H. M. de Lima, P. H. J. Nardelli, R. D. Souza, and M. Latva-aho, "On the average spectral efficiency of interference-limited full-duplex networks," in *Proc. CROWNCOM*, Jun. 2014, pp. 550–554.

[62] A. AlAmmouri, H. ElSawy, O. Amin, and M. S. Alouini, "In-band α -duplex scheme for cellular networks: A stochastic geometry approach," *IEEE Trans. Wireless Commun.*, vol. 15, no. 10, pp. 6797–6812, Oct. 2016.

[63] A. H. Sakr and E. Hossain, "On cell association in multi-tier full-duplex cellular networks," *CoRR*, vol. abs/1607.01119, 2016. [Online]. Available: http://arxiv.org/abs/1607.01119

[64] G. Liu, F. R. Yu, H. Ji, V. C. M. Leung, and X. Li, "In-band full-duplex relaying: A survey, research issues and challenges," *IEEE Commun. Surveys Tuts.*, vol. 17, no. 2, pp. 500–524, Secondquarter 2015.

[65] S. Hong, J. Brand, J. I. Choi, M. Jain, J. Mehlman, S. Katti, and P. Levis, "Applications of self-interference cancellation in 5G and beyond," *IEEE Commun. Mag.*, vol. 52, no. 2, pp. 114–121, Feb. 2014.

[66] S. Kim and W. Stark, "Full duplex device to device communication in cellular networks," in *Int. Conf. on Comp., Net. and Commun. (ICNC)*, Feb. 2014, pp. 721–725.

[67] M. Duarte, "Full-duplex wireless: Design, implementation and characterization," Ph.D. dissertation, Rice University, Houston, TX, USA, Apr. 2012.

[68] D. Nguyen, L. N. Tran, P. Pirinen, and M. Latva-aho, "On the spectral efficiency of full-duplex small cell wireless systems," *IEEE Trans. Wireless Commun.*, vol. 13, no. 9, pp. 4896–4910, Sep. 2014.

[69] J. Lee and T. Q. S. Quek, "Hybrid full-/half-duplex system analysis in heterogeneous wireless networks," *IEEE Trans. Wireless Commun.*, vol. 14, no. 5, pp. 2883–2895, May 2015.

[70] S. Goyal, P. Liu, S. S. Panwar, R. Yang, R. A. DiFazio, and E. Bala, "Full duplex operation for small cells," *CoRR*, vol. abs/1412.8708, 2014. [Online]. Available: http://arxiv.org/abs/1412.8708

[71] S. Goyal, P. Liu, S. S. Panwar, R. A. Difazio, R. Yang, and E. Bala, "Full duplex cellular systems: will doubling interference prevent doubling capacity?" *IEEE Commun. Mag.*, vol. 53, no. 5, pp. 121–127, May 2015.

[72] S. Goyal, C. Galiotto, N. Marchetti, and S. Panwar, "Throughput and coverage for a mixed full and half duplex small cell network," in *Proc. IEEE ICC*, May 2016, pp. 1–7.

[73] C. Lim, T. Yoo, B. Clerckx, B. Lee, and B. Shim, "Recent trend of multiuser mimo in lte-advanced," *IEEE Commun. Mag.*, vol. 51, no. 3, pp. 127–135, Mar. 2013.

[74] H. S. Dhillon, M. Kountouris, and J. G. Andrews, "Downlink MIMO HetNets: Modeling, ordering results and performance analysis," *IEEE Trans. Wireless Commun.*, vol. 12, no. 10, pp. 5208–5222, Oct. 2013.

[75] A. K. Gupta, H. S. Dhillon, S. Vishwanath, and J. G. Andrews, "Downlink multi-antenna heterogeneous cellular network with load balancing," *IEEE Trans. Commun.*, vol. 62, no. 11, pp. 4052–4067, Nov. 2014.

[76] V. Jungnickel, K. Manolakis, W. Zirwas, B. Panzner, V. Braun, M. Lossow, M. Sternad, R. Apelfrojd, and T. Svensson, "The role of small cells, coordinated multipoint, and massive mimo in 5g," *IEEE Commun. Mag.*, vol. 52, no. 5, pp. 44–51, May 2014.

[77] E. G. Larsson, O. Edfors, F. Tufvesson, and T. L. Marzetta, "Massive mimo for next generation wireless systems," *IEEE Commun. Mag.*, vol. 52, no. 2, pp. 186–195, Feb. 2014.

[78] B. Li, D. Zhu, and P. Liang, "Small cell in-band wireless backhaul in massive MIMO systems: A cooperation of next-generation techniques," *IEEE Trans. Wireless Commun.*, vol. 14, no. 12, pp. 7057–7069, Dec. 2015.

[79] Y. Li, P. Fan, L. Anatolii, and L. Liu, "On the spectral and energy efficiency of full-duplex small cell wireless systems with massive MIMO," *IEEE Trans. Veh. Technol.*, vol. PP, no. 99, pp. 1–1, 2016.

[80] H. Tabassum, A. H. Sakr, and E. Hossain, "Analysis of massive MIMO-enabled downlink wireless backhauling for full-duplex small cells," *IEEE Trans. Commun.*, vol. 64, no. 6, pp. 2354–2369, Jun. 2016.

[81] T. K. Vu, M. Bennis, S. Samarakoon, M. Debbah, and M. Latva-aho, "Joint in-band backhauling and interference mitigation in 5G heterogeneous networks," in *European Wireless 2016; 22th European Wireless Conference*, May 2016, pp. 1–6.

[82] A. M. Hunter, J. G. Andrews, and S. Weber, "Transmission capacity of Ad Hoc networks with spatial diversity," *IEEE Trans. Wireless Commun.*, vol. 7, no. 12, pp. 5058–5071, Dec. 2008.

[83] N. Jindal, J. G. Andrews, and S. Weber, "Multi-antenna communication in Ad Hoc networks: Achieving MIMO gains with SIMO transmission," *IEEE Trans. Commun.*, vol. 59, no. 2, pp. 529–540, Feb. 2011.

[84] M. Kountouris and J. G. Andrews, "Downlink SDMA with limited feedback in interference-limited wireless networks," *IEEE Trans. Wireless Commun.*, vol. 11, no. 8, pp. 2730–2741, Aug. 2012.

[85] C. Li, J. Zhang, J. G. Andrews, and K. B. Letaief, "Success probability and area spectral efficiency in multiuser MIMO hetnets," *IEEE Trans. Commun.*, vol. 64, no. 4, pp. 1544–1556, Apr. 2016.

[86] J. D. Herdtner and E. K. P. Chong, "Analysis of a class of distributed asynchronous power control algorithms for cellular wireless systems," *IEEE J. Sel. Areas Commun.*, vol. 18, no. 3, pp. 436–446, Mar. 2000.

[87] D. Kim, "On the convergence of fixed-step power control algorithms with binary feedback for mobile communication systems," *IEEE Trans. Commun.*, vol. 49, no. 2, pp. 249–252, Feb. 2001.

[88] A. Agrawal, J. G. Andrews, J. M. Cioffi, and T. Meng, "Iterative power control for imperfect successive interference cancellation," *IEEE Trans. Wireless Commun.*, vol. 4, no. 3, pp. 878–884, May 2005.

[89] R. Mullner, C. F. Ball, K. Ivanov, J. Lienhart, and P. Hric, "Contrasting open-loop and closed-loop power control performance in UTRAN LTE uplink by UE trace analysis," in *2009 IEEE International Conference on Communications*, Jun. 2009, pp. 1–6.

[90] C. U. Castellanos, D. L. Villa, C. Rosa, K. I. Pedersen, F. D. Calabrese, P. H. Michaelsen, and J. Michel, "Performance of uplink fractional power control in UTRAN LTE," in *VTC Spring 2008 - IEEE Vehicular Technology Conference*, May 2008, pp. 2517–2521.

[91] T. D. Novlan, H. S. Dhillon, and J. G. Andrews, "Analytical modeling of uplink cellular networks," *IEEE Trans. Wireless Commun.*, vol. 12, no. 6, pp. 2669–2679, June 2013.

[92] H. ElSawy and E. Hossain, "On stochastic geometry modeling of cellular uplink transmission with truncated channel inversion power control," *IEEE Trans. Wireless Commun.*, vol. abs/1401.6145, 2014.

[93] M. K. Simon and M. S. Alouini, *Digital communication over fading channels, Vol. 95.* John Wiley & Sons, 2005.

[94] D. Tse and P. Viswanath, *Fundamentals of Wireless Communication.* Cambridge University Press, Cambridge, U.K., 2005.

[95] A. Lodhi, F. Said, M. Dohler, and A. H. Aghvami, "Closed-form symbol error probabilities of STBC and CDD MC-CDMA with frequency-correlated subcarriers over nakagami-m fading channels," *IEEE Trans. Veh. Technol.*, vol. 57, no. 2, pp. 962–973, Mar. 2008.

[96] M. Haenggi, J. G. Andrews, F. Baccelli, O. Dousse, and M. Franceschetti, "Stochastic geometry and random graphs for the analysis and design of wireless networks," *IEEE J. Sel. Areas Commun.*, vol. 27, no. 7, pp. 1029–1046, Sept. 2009.

[97] H. ElSawy, A. Sultan-Salem, M. S. Alouini, and M. Z. Win, "Modeling and analysis of cellular networks using stochastic geometry: A tutorial," *IEEE Commun. Surveys Tuts.*, vol. 19, no. 1, pp. 167–203, Firstquarter 2017.

[98] J. G. Andrews, A. K. Gupta, and H. S. Dhillon, "A primer on cellular network analysis using stochastic geometry," *CoRR*, vol. abs/1604.03183, 2016. [Online]. Available: http://arxiv.org/abs/1604.03183

[99] R. Zhang and C. K. Ho, "MIMO broadcasting for simultaneous wireless information and power transfer," *IEEE Trans. Wireless Commun.*, vol. 12, no. 5, pp. 1989–2001, May 2013.

[100] X. Zhou, R. Zhang, and C. K. Ho, "Wireless information and power transfer: Architecture design and rate-energy tradeoff," *IEEE Trans. Wireless Commun.*, vol. 61, no. 11, pp. 4754–4767, Nov. 2013.

[101] C. R. Anderson, S. Krishnamoorthy, C. G. Ranson, T. J. Lemon, W. G. Newhall, T. Kummetz, and J. H. Reed, "Antenna isolation, wideband multipath propagation measurements, and interference mitigation for on-frequency repeaters," in *Proc. IEEE SoutheastCon., Greensboro, NC, USA.*, Mar. 2004, pp. 110–114.

[102] H. Ju, E. Oh, and D. Hong, "Improving efficiency of resource usage in two-hop full duplex relay systems based on resource sharing and interference cancellation," *IEEE Trans. Wireless Commun.*, vol. 8, no. 8, pp. 3933–3938, Aug. 2009.

[103] I. E. Telatar, "Capacity of multi-antenna gaussian channels," *Europ. Trans. Telecommu.*, vol. 10, pp. 585–595, Nov./Dec. 1999.

[104] G. J. Foschini, "Layered space-time architecture for wireless communication in a fading environment when using multi-element antennas," *Bell Labs Technical Journal*, vol. 1, no. 2, pp. 41–59, Autumn 1996.

[105] V. Tarokh, H. Jafarkhani, and A. R. Calderbank, "Space-time block codes from orthogonal designs," *IEEE Trans. Inf. Theory*, vol. 45, no. 5, pp. 1456–1467, July 1999. [Online]. Available: https://doi.org/10.1109/18.771146

[106] G. J. Foschini, G. D. Golden, R. A. Valenzuela, and P. W. Wolniansky, "Simplified processing for high spectral efficiency wireless communication employing multi-element arrays," *IEEE J. Sel. Areas Commun.*, vol. 17, no. 11, pp. 1841–1852, Nov. 1999.

[107] R. Heath, Jr., and A. Paulraj, "Switching between multiplexing and diversity based on constellation distance," in *Proc. Allerton Conf. Communication, Control and Computing*, Oct. 2000.

[108] D. G. Brennan, "Linear diversity combining techniques," *Proceedings of the IRE*, vol. 47, no. 6, pp. 1075–1102, Jun. 1959.

[109] L. Zheng and D. N. C. Tse, "Diversity and multiplexing: A fundamental tradeoff in multiple-antenna channels," *IEEE Trans. Inf. Theory*, vol. 49, no. 5, pp. 1073–1096, May 2003.

[110] L. Lu, G. Y. Li, A. L. Swindlehurst, A. Ashikhmin, and R. Zhang, "An overview of massive MIMO: Benefits and challenges," *IEEE J. Sel. Top. Signal Process.*, vol. 8, no. 5, pp. 742–758, Oct. 2014.

[111] T. K. Y. Lo, "Maximum ratio transmission," *IEEE Trans. Commun.*, vol. 47, no. 10, pp. 1458–1461, Oct. 1999.

[112] N. Jindal, "MIMO broadcast channels with finite-rate feedback," *IEEE Trans. Inf. Theory*, vol. 52, no. 11, pp. 5045–5060, Nov. 2006.

[113] T. L. Marzetta, "Multi-cellular wireless with base stations employing unlimited numbers of antennas," in *Proc. UCSD Inf. Theory Applicat. Workshop*, Feb. 2010.

[114] T. L. Marzetta, "Noncooperative cellular wireless with unlimited numbers of base station antennas," *IEEE Trans. Wireless Commun.*, vol. 9, no. 11, pp. 3590–3600, Nov. 2010.

[115] J. Jose, A. Ashikhmin, T. L. Marzetta, and S. Vishwanath, "Pilot contamination and precoding in multi-cell TDD systems," *IEEE Trans. Wireless Commun.*, vol. 10, no. 8, pp. 2640–2651, Aug. 2011.

[116] H. Yin, D. Gesbert, M. Filippou, and Y. Liu, "A coordinated approach to channel estimation in large-scale multiple-antenna systems," *IEEE J. Sel. Areas Commun.*, vol. 31, no. 2, pp. 264–273, Feb. 2013.

[117] H.-S. Jo, Y. J. Sang, P. Xia, and J. G. Andrews, "Heterogeneous cellular networks with flexible cell association: A comprehensive downlink SINR analysis," *IEEE Trans. Wireless Commun.*, vol. 11, no. 10, pp. 3484–3495, Oct. 2012.

[118] F. Baccelli, B. Blaszczyszyn, and P. Muhlethaler, "An Aloha protocol for multihop mobile wireless networks," *IEEE Trans. Inf. Theory*, vol. 52, no. 2, pp. 421–436, Feb. 2006.

[119] I. S. Gradshteyn and I. M. Ryzhik, *Table of Integrals, Series and Products*, 7th ed. San Diego, C.A.: Academic Press, 2007.

[120] H. Ju and R. Zhang, "Throughput maximization in wireless powered communication networks," *IEEE Trans. Wireless Commun.*, vol. 13, no. 1, pp. 418–428, Jan. 2014.

[121] D. W. K. Ng, E. S. Lo, and R. Schober, "Wireless information and power transfer: Energy efficiency optimization in OFDMA systems," *IEEE Trans. Wireless Commun.*, vol. 12, no. 12, pp. 6352–6370, Dec. 2013.

[122] Q. Li, G. Li, W. Lee, M. i. Lee, D. Mazzarese, B. Clerckx, and Z. Li, "MIMO techniques in WiMAX and LTE: a feature overview," *IEEE Commun. Mag.*, vol. 48, no. 5, pp. 86–92, May 2010.

[123] C. Cox and E. Ackerman, "Demonstration of a single-aperture, full-duplex communication system," in *Proc. IEEE Radio and Wireless Symposium*, Jan. 2013, pp. 148–150.

[124] M. E. Knox, "Single antenna full duplex communications using a common carrier," in *Proc. IEEE WAMICON*, Apr. 2012, pp. 1–6.

[125] A. Ghosh, N. Mangalvedhe, R. Ratasuk, B. Mondal, M. Cudak, E. Visotsky, T. A. Thomas, J. G. Andrews, P. Xia, H. S. Jo, H. S. Dhillon, and T. D. Novlan, "Heterogeneous cellular networks: From theory to practice," *IEEE Commun. Mag.*, vol. 50, no. 6, pp. 54–64, June 2012.

[126] A. C. Cirik, Y. Rong, and Y. Hua, "Achievable rates of full-duplex MIMO radios in fast fading channels with imperfect channel estimation," *IEEE Trans. Signal Process.*, vol. 62, no. 15, pp. 3874–3886, Aug. 2014.

[127] M. Duarte, C. Dick, and A. Sabharwal, "Experiment-driven characterization of full-duplex wireless systems," *IEEE Trans. Wireless Commun.*, vol. 11, no. 12, pp. 4296–4307, Dec. 2012.

[128] J. I. Choi, M. Jain, K. Srinivasan, P. Levis, and S. Katti, "Achieving single channel, full duplex wireless communication," in *Proc. ACM Mobicom, Chicago, IL, USA*. ACM, Sept. 2010, pp. 1–12.

[129] J. I. Choi, M. Jain, K. Srinivasan, P. Levis, and S. Katti, "Practical, real-time, full duplex wireless," in *Proc. ACM Mobicom, Las Vegas, NV, USA*. ACM, Sept. 2011, pp. 301–312.

[130] P. Lioliou, M. Viberg, M. Coldrey, and F. Athley, "Self-interference suppression in full-duplex MIMO relays," in *Proc. Asilomar Conf. Signals, Syst., Comput., Pacific Grove, CA*, Nov. 2010, pp. 658–662.

[131] T. Riihonen and R. Wichman, "Analog and digital self-interference cancellation in full-duplex MIMO-OFDM transceivers with limited resolution in A/D conversion," in *Proc. Asilomar Conf. Signals, Syst., Comput., Pacific Grove, CA, USA*, Nov. 2012, pp. 45–49.

[132] A. AlAmmouri, H. ElSawy, O. Amin, and M. S. Alouini, "In-band full-duplex communications for cellular networks with partial uplink/downlink overlap," in *Proc. IEEE GLOBECOM*, Dec. 2015, pp. 1–7.

[133] E. Bjrnson, L. Sanguinetti, J. Hoydis, and M. Debbah, "Designing multi-user mimo for energy efficiency: When is massive MIMO the answer?" in *2014 IEEE Wireless Communications and Networking Conference (WCNC)*, April 2014, pp. 242–247.

[134] E. Björnson, M. Kountouris, and M. Debbah, "Massive MIMO and small cells: Improving energy efficiency by optimal soft-cell coordination," in *ICT 2013*, May 2013, pp. 1–5.

[135] D. Bharadia and S. Katti, "Full duplex MIMO radios," *Proc. 11th USENIX Symp. NSDI*, pp. 359–372, 2014.

[136] J. Hoydis, K. Hosseini, S. T. Brink, and M. Debbah, "Making smart use of excess antennas: Massive MIMO, small cells, and TDD," *Bell Labs Technical Journal*, vol. 18, no. 2, pp. 5–21, Sept. 2013.

[137] E. Björnson, J. Hoydis, M. Kountouris, and M. Debbah, "Massive MIMO systems with non-ideal hardware: Energy efficiency, estimation, and capacity limits," *IEEE Trans. Inf. Theory*, vol. 60, no. 11, pp. 7112–7139, Nov. 2014.

[138] T. L. Marzetta, "How much training is required for multiuser MIMO?" in *Proc. 40th Asilomar Conference on Signals, Systems and Computers, Pacific Grove, CA*, Oct. 2006, pp. 359–363.

[139] W. C. Cheung, T. Q. S. Quek, and M. Kountouris, "Throughput optimization, spectrum allocation, and access control in two-tier femtocell networks," *IEEE J. Sel. Areas Commun.*, vol. 30, no. 3, pp. 561–574, Apr. 2012.

[140] F. Baccelli, B. Blaszczyszyn, and P. Muhlethaler, "An Aloha protocol for multihop mobile wireless networks," *IEEE Trans. Inf. Theory*, vol. 52, no. 2, pp. 421–436, Feb. 2006.

[141] M. Haenggi, *Stochastic geometry for wireless networks*. Cambridge University Press, 2012.

[142] J. G. Wendel, "The non-absolute convergence of Gil-Pelaez' inversion integral," *Ann. Math. Statist.*, vol. 32, no. 1, pp. 338–339, Mar. 1961.

[143] S. Singh, X. Zhang, and J. G. Andrews, "Joint rate and SINR coverage analysis for decoupled uplink-downlink biased cell associations in hetnets," *IEEE Trans. Wireless Commun.*, vol. 14, no. 10, pp. 5360–5373, Oct. 2015.

List of Publications

Journal Publications

S. Akbar, Y. Deng, A. Nallanathan, M. Elkashlan, and G. K. Karagiannidis, "Massive Multiuser MIMO in Heterogeneous Cellular Networks with Full Duplex Small Cells," in *IEEE Trans. Commun.*, vol. PP, no.99, pp. 1-1, July. 2017.

S. Akbar, Y. Deng, A. Nallanathan, M. Elkashlan and A. H. Aghvami, "Simultaneous Wireless Information and Power Transfer in K -Tier Heterogeneous Cellular Networks," *IEEE Trans. Wireless Commun.*, vol. 15, no. 8, pp. 5804-5818, Aug. 2016.

Conference Publications

S. Akbar, Y. Deng, A. Nallanathan, M. Elkashlan, and G. K. Karagiannidis, "Massive MIMO-enabled HetNets with Full Duplex Small Cells," accepted for publication in *Proc. IEEE Global Communications Conference (GLOBECOM)*, Singapore, Dec. 2017.

S. Akbar, Y. Deng, A. Nallanathan and M. Elkashlan, "Downlink and Uplink Transmission in K-Tier Heterogeneous Cellular Network with Simultaneous Wireless Information and Power Transfer," in *Proc. IEEE Global Communications Conference (GLOBECOM)*, San Diego, CA, Dec. 2015, pp. 1-6.